Macroautophagy in Major Histocompatibility Complex (MHC) Class I-Restricted Antigen Presentation

---

Dissertation

zur

Erlangung der naturwissenschaftlichen Doktorwürde (Dr. sc. nat.)

vorgelegt der

Mathematisch-naturwissenschaftlichen Fakultät

der

Universität Zürich

von

Monica Loi

aus

Italien

Promotionskommission

Prof. Dr. rer. nat. Christian Münz (Vorsitz)

Prof. Dr. rer. nat. Lawrence Rajendran

Prof. Dr. rer. nat. Hangartner Lars

Zürich, 2017

Disclaimer

This thesis is based on the following manuscripts:

Loi M, Gannagé M, Münz C. ATGs help MHC class II, but inhibit MHC class I antigen presentation. Autophagy. 2016 Sep;12(9):1681-2

Loi M, Müller A, Steinbach K, Niven J, Barreira da Silva R, Paul P, Ligeon L, Caruso A, Albrecht RA, Becker A, Annaheim N, Nowag H, Dengjel J, García-Sastre A, Merkler D, Münz C and Gannagé M. Macroautophagy controls MHC class I levels on dendritic cells and shapes the anti-viral $CD8^+$ T cell response. Cell Rep. 2016 May 3;15(5):1076-87

Acknowledgement

I would like to express my deep gratitude to my supervisor, Christian Münz for his guidance, his patience, and his continuous support throughout my PhD path. I'm happy I had the chance to do my PhD with Christian as he is always in a good mood, always available for any issue I had to face, with a humble attitude despite his immense knowledge and his enthusiasm about science.

My sincere thanks go to the two other members of my PhD committee, Lawrence Rajendran and Lars Hangartner for their positive attitude, suggestions and helpful comments.

To every single person who gives in different ways their contribution to the development of my PhD project, thank you guys!

Thanks to Monique, who started the project on MHC-I internalization and suffered with me until the end to get our paper published.

Thanks to the autophagy team, Petra, Laure-Anne, Charlotte and Maria for your technical, scientific, sincere support also outside the lab. *I could not have imagined my PhD without you girls*!

Thanks to Anne, who helped Monique at the beginning of the project and provided me with a lot of technical assistance.

A special thank goes to Christian Keller for his support, technical help and his positive, humble attitude. *It has been a pleasure to work with you, Chris*.

Thanks also to Isaak for his input to my project and for his moral help during the revision time.

I would like to thank also former and current members of Münz lab for contributing to the nice atmosphere in the lab, and to Ani, Anita, Julia, my lab roommate, thanks for having endured my Italian chatty personality over my entire PhD.

Last but not least, thanks to my husband Andrea, my special friend Irene and my family who always stayed at my side and supported me especially in the toughest moments.

Summary

Autophagy is a physiological, conserved catabolic process by which cytoplasmic material is delivered for degradation into lysosomes. Autophagy plays a role in several cellular processes and in various aspects of immunity but its role in trafficking pathways and major histocompatibility complex (MHC) class I presentation has only been poorly described. Here, we show that molecular machinery of autophagy regulates MHC class I surface levels and intracellular antigen presentation *in vitro* and *in vivo*. Briefly, it has been found that MHC class I molecules are stabilized on the cell surface of murine antigen presenting cells deficient for core components of autophagy, such as ATG5 or ATG7. This stabilization seems to result from defective internalization of MHC class I molecules dependent on adaptor protein kinase 1 (AAK1), a member of clathrin-dependent endocytosis machinery. Indeed, AAK1 interacts with the cytosolic form of LC3 (Microtubule-associated protein 1A/1B-light chain 3), a pivotal molecule of autophagy, and it is recruited to the MHC class I internalization machinery upon LC3 lipidation. Therefore, when autophagy and specifically, LC3 lipidation is blocked, MHC class I molecules get stabilized on the surface of dendritic cells resulting in a more efficient stimulation of $CD8^+$ T cell responses *in vitro* and *in vivo*. Importantly, the absence of autophagy-dependent internalization during viral infections, such as influenza virus and lymphocytic choriomeningitis virus, leads to enhance virus-specific $CD8^+$T cell responses *in vivo* and a better immune control of influenza infection. Additionally, preliminary studies using B cells infected by Epstein Barr virus and deficient for the transporter-associated with antigen presentation (TAP), a key protein in the MHC class I presentation pathway, suggest a contribution of autophagy in the regulation of intracellular MHC class I antigen presentation. Indeed, preliminary data show that autophagy might contribute to deliver antigens as well as to supply MHC class I molecules to an endosomal compartment for an alternative MHC class I antigen processing and presentation as a consequence of the impairment of classical MHC class I antigen processing. These findings clearly show that the autophagy machinery

orchestrates T cell immunity by regulating MHC class I surface expression levels and it can also help to improve adaptive immune response against viral pathogens by circumventing viral immune escape mechanisms.

Zusammenfassung

Autophagie ist ein physiologischer, konservierter und katabolischer Prozess, durch den zytoplasmatisches Material zum Abbau in Lysosomen transportiert wird. Autophagy spielt eine Rolle in mehreren zellulären Prozessen und in verschiedenen Aspekten der Immunität, aber seine Rolle im Membrantransport und der Antigenpräsentation durch Major Histokompatibilität Komplex (MHC) Klasse I Moleküle wurde bisher nur ansatzweise beschrieben. Hier zeigen wir, dass die molekulare Maschinerie der Autophagie die Oberflächenexpression von MHC-Klasse-I-Molekülen und die intrazelluläre Antigenpräsentation *in vitro* und *in vivo* reguliert. Zusammenfassend wurde durch unsere Studien bestimmt, dass MHC-Klasse-I-Moleküle auf der Zelloberfläche von murinen Antigen-präsentierenden Zellen, die für Kernkomponenten der Autophagie, wie ATG5 oder ATG7, defizient sind, stabilisiert wird. Diese Stabilisierung resultiert aus einer defekten Internalisierung von MHC-Klasse-I-Molekülen, abhängig von der Adapterprotein-Kinase 1 (AAK1), einem Mitglied der Clathrin-abhängigen Endozytose-Maschinerie. In der Tat interagiert AAK1 mit der zytosolischen Form von LC3 (Microtubuli-assoziiertes Protein 1A / 1B-leichte Kette 3), einem zentrales Molekül der Autophagie, und diese Kinase wird zur MHC-Klasse-I-Internalisierungsmaschine bei LC3-Lipidierung rekrutiert. Daher werden, wenn Autophagie und insbesondere LC3-Lipidierung blockiert sind, MHC-Klasse-I-Moleküle auf der Oberfläche der dendritischen Zellen stabilisiert, was zu einer effizienteren Stimulation von $CD8^+$ T-Zellen *in vitro* und *in vivo* führt. Wichtig ist, dass das Fehlen einer autophagieabhängigen Internalisierung bei Virusinfektionen, wie durch den Influenzavirus und den lymphozytischen Choriomeningitisvirus, dazu führt, dass Virus-spezifische $CD8^+$ T-Zellreaktionen und eine bessere Immunkontrolle der Influenza-Infektion *in vivo* verstärkt werden. Darüber hinaus weisen vorläufige Studien mit B-Zellen, die durch das Epstein-Barr-Virus infiziert wurden und für den mit der Antigenpräsentation assoziierten Transporter (TAP), ein Schlüsselprotein im MHC-Klasse-I-Antigenpräsentationsweg, defizient sind, auf einen Beitrag der

Autophagie bei der Regulation der intrazellulären MHC-Klasse I vermittelten Antigenpräsentation hin. Tatsächlich zeigen vorläufige Daten, dass Autophagie dazu beitragen kann, Antigene für einen TAP unabhängigen MHC-Klasse I-Antigenpräsentationsweg zu liefern, sowie MHC-Klasse-I-Moleküle zu einem endosomales Kompartiment für eine alternative MHC-Klasse-I-Antigenpräsentation zu transportieren. Diese Ergebnisse zeigen deutlich, dass die Autophagie-Maschinerie die T-Zell-Immunität durch Regulierung der MHC-Klasse-I-Oberflächenexpression orchestriert und sie auch dazu beitragen kann, die adaptive Immunantwort gegen virale Pathogene zu verbessern, indem virale Immunabwehrmechanismen, wie TAP Inhibition, umgangen werden.

Table of Content

Chapter 1 – Introduction

Part I - Antigen processing and presentation

1.1.1 Principles and biological role of antigen presentation

Antigen presentation is a term used to describe a non-selective process of the immune system by which self and foreign material is presented by the cell to the specialized arm of the immune defences specifically to B and T cells, to induce highly specific mechanism to fight off the presented entity. Despite that such a process can be accomplished by all cells, three types of immune cells (macrophages, dendritic cells (DCs), and B cells) are categorized as professional antigen presenting cells. The antigen, any molecule able to trigger an immune response, can belong to either host or host-external components such as pathogens and it can be parts of proteins (peptides), lipids or sugars (polysaccharides). Physiologically, T cells against host antigens are negatively selected in the thymus and removed to ensure the host does not attack its own components. As peptide, antigen is presented at the surface of antigen presenting cells on molecules called Major Histocompatibility Complex (MHC) or human leukocyte antigen (HLA) molecules. Interestingly, T cells are able to recognize only some antigens and only if they are presented in the context of MHC molecules, phenomena known as peptide immunodominance and MHC restriction, respectively (Doherty and Zinkernagel 1975; Akram and Inman 2012). Moreover, different subclasses of T cells are activated based on which MHC complex presents the antigen. Classically, endogenous, cytosolic antigens are loaded on MHC class I molecules (MHC-I) and recognized by $CD8^+$ (cytotoxic) T lymphocytes. In contrast, exogenous, extracellular, antigens, taken up by endocytosis or phagocytosis, are then loaded on MHC class II molecules (MHC-II) and presented to $CD4^+$ T (helper) cells. However, there are exceptions to this distinction. Indeed, MHC-I molecules can present extracellular, endocytosed antigen in a process called cross-presentation, primarily by specialized antigen presenting cells, and similarly, peptides of intracellular origin can be loaded onto MHC-II molecules. The mechanism of antigen presentation has a central physiological role as it is responsible for the distinction between self/non-self-specific T cells and the consequent specific immune response to pathogen or to self-proteins causing autoimmune disorders. Moreover, it is the basis of vaccine development. In the following sections, biology of MHC-I molecules, MHC-I antigen

presentation pathways, and MHC-I trafficking will be presented. Finally, the role of MHC-I presentation as mechanism to provide immunological control against three viral infections will be described.

1.1.2 MHC class I biology and MHC class I polymorphism

MHC-I molecules are glycoproteins, members of the immunoglobulin superfamily displayed on the cell surface of all nucleated cells. They are heterodimers comprising a heavy chain and β2-microglobulin. Their structure is shown in **Figure 1.1**.

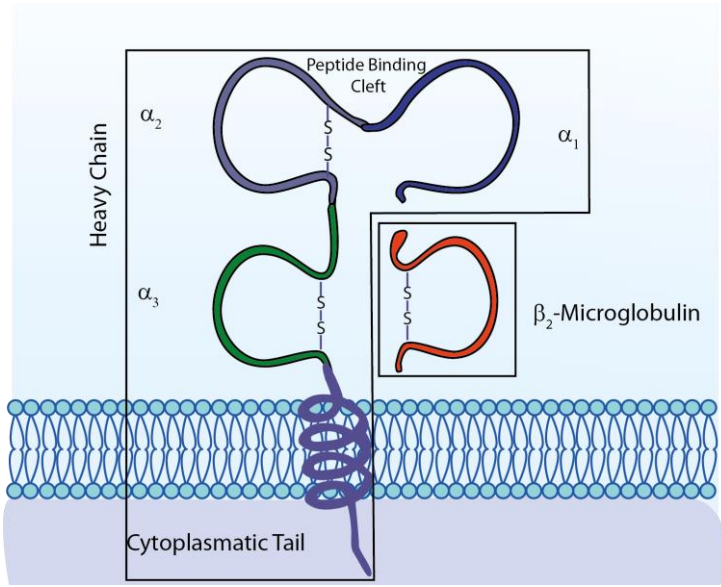

Figure 1.1 MHC class I structure
MHC-I molecules are heterodimers formed by the heavy chain α and β2-microglobulin. The heavy chain has three extracellular domains (α1, α2 and α3), a transmembrane section and a short cytoplasmic tail. The α1 and α2 domains create the antigen binding cleft. α3 and β2-microglobulin are Ig domains. *Figure adapted from what-when-how.com*

The MHC-I heavy chain locus comprises a group of different genes, which are expressed simultaneously by all cells. In humans, it encodes "classical MHC-I" (HLA-A, HLA-B and HLA-C) and "non-classical MHC-I" (HLA-E, HLA-F and HLA-G, Hfe, MHC-I polypeptide-related sequence A (MICA) and MHC-I polypeptide-related sequence B (MICB)). Similarly, in mice, the MHC-I locus, called also H2, encodes for H-2D, H-2K, and H-2L (classical) and H-2Q, H-2M and H-2T (non-classical). The non-classical MHC-I molecules are structurally highly related to the classical ones

and an increasing overlap of features with classical MHC-I has been observed (Kumanovics, Takada et al. 2003).

The ability of MHC-I molecules to bind a broad range of antigens, called antigen repertoire, is given by the high level of polymorphisms within the heavy chain. An elaborate nomenclature system, shown in **Figure 1.2,** has been developed to distinguish all the different alleles.

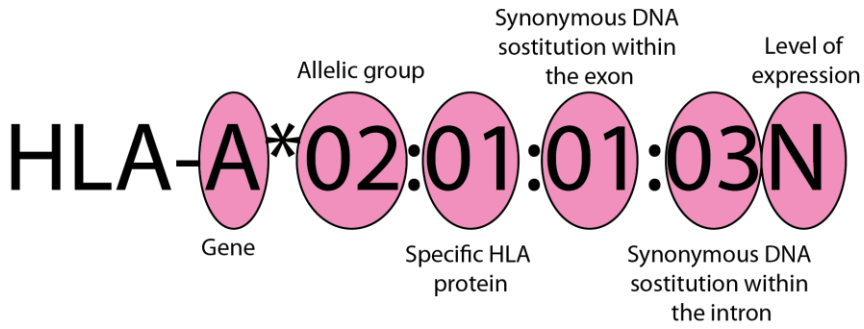

Figure 1.2 MHC-I nomenclature
Synonymous DNA mutation indicates a nucleotide change within the DNA sequence, which does not influence the protein sequence. Exon and intron indicate the coding and non-coding region of the DNA, respectively. The last field, the level of expression can be N, null allele; L, low expression; S, secreted form; A, aberrant expression; and Q, questionable.

1.1.3 Antigen processing and MHC-I presentation pathways

As mentioned, MHC-I molecules can present both endogenous and exogenous antigens by classical and cross-presentation pathway, respectively.

In the classical MHC-I pathway, the formation of peptide-MHC-I complex is the result of a highly regulated cascade of events that starts with antigen processing (**Figure 1.3**). Cytosol-derived proteins, mainly incomplete or misfolded proteins named DRiPs, for **D**efective **Ri**bosomal **P**roducts (Yewdell, Anton et al. 1996) are processed by the proteasome, a complex multisubunit proteolytic system in the cytosol. Proteins addressed to be degraded by the proteasome are marked by the addition of a chain of a small regulatory proteins called ubiquitin, to a lysine residue within the protein or its N-terminus. The proteasome-generated peptides range from 3 to 22 amino acids in length and among them only 15% are products of 8-9 residues available for being used for MHC-I presentation (Kisselev, Akopian et al. 1999). Interestingly, some peptides can derive from non-contiguous sequences in the original protein by splicing events mediated by

the proteasome (Liepe, Marino et al. 2016). Peptides are then translocated into the endoplasmic reticulum (ER) lumen by the transporter associated with antigen processing (TAP) in an ATP-dependant manner (van Endert, Saveanu et al. 2002). However, longer peptides may also be transported (Uebel and Tampe 1999). These peptides require additional N-terminal trimming in the ER before binding to MHC-I molecules by the ER aminopeptidase 1 (ERAP1 or ERAAP in mouse). In the ER, calnexin and ERp57 drive the formation of the MHC-I heterodimers, which subsequently associate with the peptide loading complex (PLC), which comprises TAP, tapasin, calreticulin, and ERp57. PLC stabilizes unloaded MHC-I molecules and facilitates peptide binding to MHC-I molecules (**Figure 1.3**).

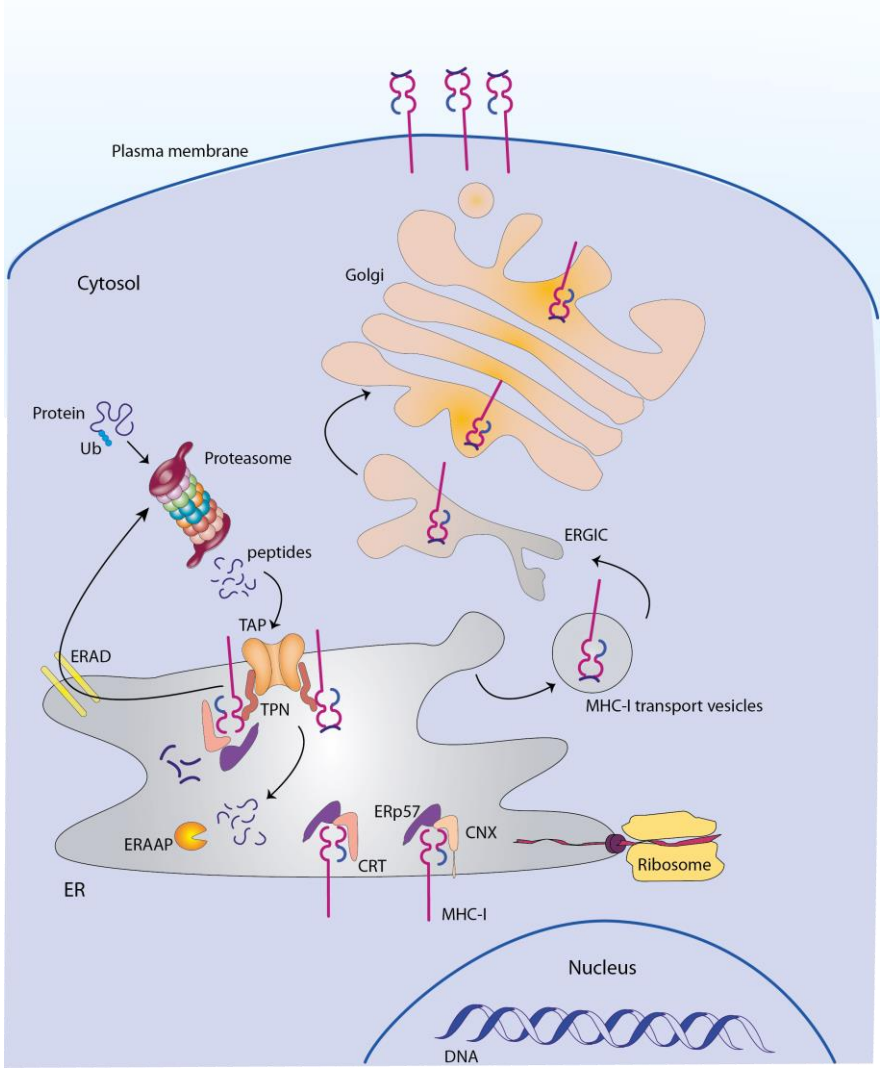

Figure 1.3 MHC class I pathway.

New synthetized, empty MHC-I molecules enter the ER immediately after their translation and they get assembled by calnexin (CNX) and stabilized by the peptide loading complex (PLC) that contains calreticulin

(CRT), ERp57, tapasin (TPN), and the transporter associated with antigen presentation (TAP). Ubiquitinated (Ub) cytosolic proteins are degraded by the proteasome and the resulting peptides are translocated into the ER via TAP, eventually subjected to further trimming by the ER-associated aminopeptidase (ERAAP), and then loaded into the MHC-I. Once loaded the complex peptide-MHC-I is then transported to the Golgi through the ER-Golgi intermediate compartment (ERGIC) and reaches the cell surface. Unstable MHC-I molecules are translocated back to the cytosol by retrograde translocation and degraded by the proteasome in a process called ER-associated degradation (ERAD).

If the peptide affinity is high, the MHC-I molecule dissociates from the PLC and can be transported from the ER to the ER-Golgi intermediate compartment (ERGIC) and then via the Golgi apparatus to the cell surface (Barlowe and Miller 2013). On the other hand, unstable MHC-I molecules are destroyed in the cytosol by the proteasome by a process called ER-associated degradation (Ahner and Brodsky 2004).

However, when the above-described MHC-I classical pathway is impaired, for example because of manipulation by pathogens or deficiency of cells for some components of the classical MHC-I pathway, alternative pathways exist to ensure MHC-I-restricted antigen presentation. The existence of alternative pathways for MHC-I antigen presentation has emerged from studies on cells with proteasome and TAP deficiencies. Indeed, individuals affected by bare lymphocyte syndrome-I, linked to TAP-deficiency, present a polyclonal repertoire of $CD8^+$ T cells and do not succumb to viral infections, supporting the hypothesis of alternative presentation pathways (de la Salle, Houssaint et al. 1997). Immunogenic peptides produced from alternative TAP-independent routes are named “T cell epitopes associated with impaired peptide processing” (TEIPP). The loading mechanism of TEIPP into MHC-I molecules is incompletely known. By studying latent membrane protein 2 (LMP2) of Epstein Barr virus (EBV), it has been suggested that after proteasome proteolysis, some peptides can access the ER thanks to their hydrophobicity overcoming the lack of the peptide transporter TAP (Lautscham, Mayrhofer et al. 2001). Additionally, several studies have suggested that the catabolic process of autophagy can play a role as an alternative pathway for MHC-I presentation, especially in absence of TAP (See **1.2.6**). The autophagy pathway will be introduced in the second part of the introduction, because the role of autophagy as alternative pathway in MHC-I-restricted antigen presentation is the main subject of the present PhD thesis.

MHC-I can also present peptides generated from exogenous proteins by cross-presentation. Three different pathways of cross-presentation have been identified so far. They are described in **Figure 1.4**. Upon internalization, proteins are degraded either by the proteasome in the cytosol or by proteases within phagosomes. Proteasome-produced peptides can then enter two ways: they can enter the classical MHC-I pathway via the ER where they are loaded on MHC-I (cytosolic pathway) or they are transported back into specialized compartments that have acquired ER-resident proteins after fusion with the ERGIC (ER-phagosome pathway). Differently, in a third pathway (vacuolar pathway) proteins are degraded and loaded within phagosomes onto MHC-I molecules of still unknown origin. It is indeed, under intense investigation whether the MHC-I molecules used in the vacuolar pathway are newly synthetized ones, coming from the ER, or are recycled from the plasma membrane.

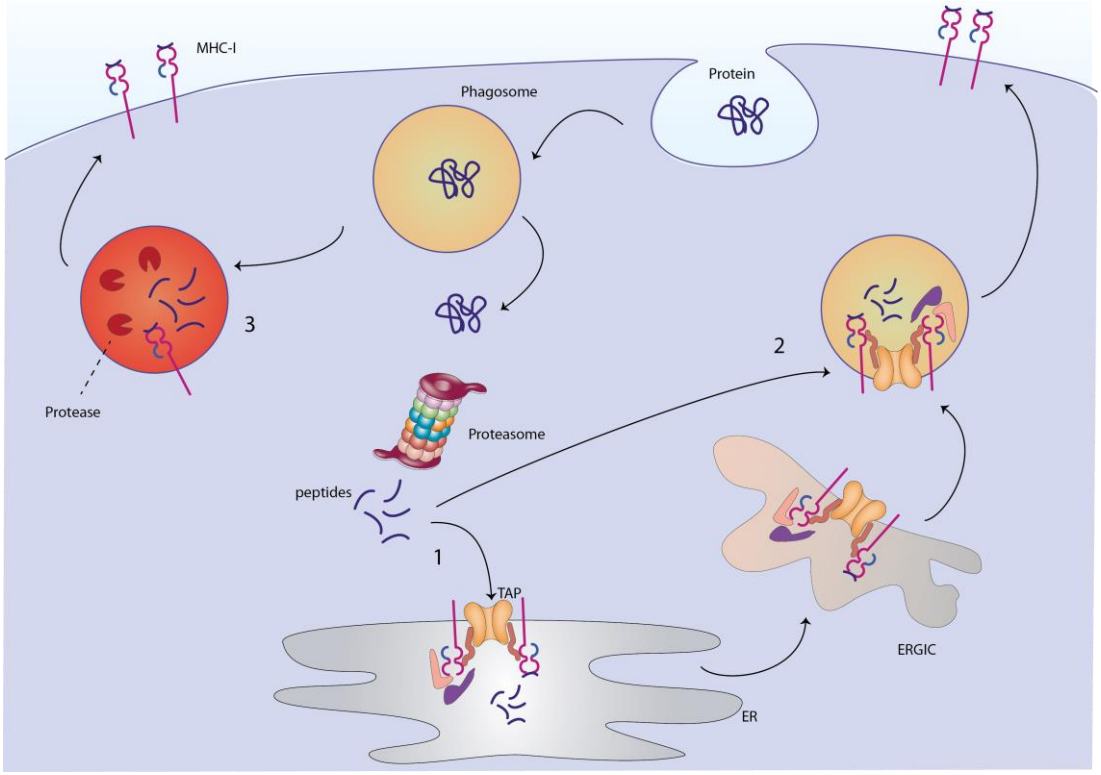

Figure 1.4 Cross-presentation pathways.

Three pathways for cross-presentation have been described. Once internalized, the protein is transported from the phagosome to the cytosol, degraded by the proteasome and loaded on MHC-I molecules either in the ER (1, The phagosome to cytosolic pathway) or in a compartment derived from the fusion of phagosomes with components of the ER, such as TAP (2, ER-phagosome pathway). (3) The vacuolar pathway: Antigens can be directly processed in the phagosome and the resulting peptides are loaded onto MHC-I.

1.1.4 MHC class I internalization and organization of endocytic pathway

Once at the plasma membrane, MHC-I are continuously removed by endocytosis and recycled back. Constitutive endocytosis of MHC-I molecules has been described for the first time almost 30 years ago in B and T lymphocytes and in non-lymphoid (i.e. fibroblast) cells, as a process requiring the MHC-I cytoplasmic tail (Capps, Van Kampen et al. 1989; Vega and Strominger 1989). Since kinetics of internalization, recycling, and the intracellular localization vary according to the cell type, MHC-I trafficking is still under intense debate. Nevertheless, MHC-I have been described to follow different pathways in professional and nonprofessional APCs: clathrin-dependent and clathrin-independent endocytosis, respectively. During clathrin-dependent endocytosis, cargoes carrying a specific tyrosine-based recognition motif in their cytoplasmic tail are specifically recognized by adaptor molecules (Bonifacino and Dell'Angelica 1999). Among them, the adaptor protein 2 (AP-2) is responsible for cargo selection and, upon phosphorylation by adaptor-associated kinase (AAK1), its affinity for the tyrosine motif within the target molecule increases (Honing, Ricotta et al. 2005) resulting in the invagination of the plasma membrane and formation of clathrin-coated vesicles. Such vesicles detach from the plasma membrane by the action of the GTPase dynamin and they fuse with early endosome upon clathrin removal by the heat shock cognate protein HSC70 and auxilin (Barouch, Prasad et al. 1997). The key role of the cryptic tyrosine motif within the cytoplasmic tail of MHC-I to drive their trafficking within the cells has been described in the context of cross-presentation in murine and human antigen-presenting cells (Lizee, Basha et al. 2003; Kulpa, Del Cid et al. 2013). Indeed, it has been shown that the tyrosine motif recognized also by the adaptor protein AP-1 is important for the trafficking of MHC-I molecules from the trans Golgi to a endolysosomal compartment important for cross-presentation of soluble antigens in antigen-presenting cells (Kulpa, Del Cid et al. 2013). In line, murine DCs lacking the cytosolic tyrosine motif have an impairment in cross-presentation with a subsequent negative impact on $CD8^+$T cell response against two viral antigens (Lizee, Basha et al. 2003). Some years after the same group showed that this was due to a slower internalization of MHC-I molecules from the surface when the tyrosine motif was deleted, impeding the MHC-I to reach the

endolysosomal compartment devote to cross-presentation (Basha, Lizee et al. 2008). On the other hand, clathrin-independent endocytosis is a less characterized process and allows the endocytosis and recycling of plasma membrane molecules that lack the tyrosine motif for the clathrin-dependent pathway. Clathrin-independent endocytosis consists of several pathways, and among them, it has been shown that ADP ribosyl factor 6 (Arf6)-dependent endocytosis plays a role in MHC-I internalization in HeLa and COS cells (Naslavsky, Weigert et al. 2004). As all GTPases, Arf6 cycles from an active state (GTP-bound form), mediate by guanine nucleotide exchange factors (GEFs) to an inactive state (GDP-bound form) upon hydrolysis of GTP to GDP by GTPase activating proteins (GAPs). The Arf6 cycle is important for its role in endosomal trafficking and actin remodelling (D'Souza-Schorey and Chavrier 2006). In non-professional antigen-presenting cells, MHC-I have been shown to be internalized by Arf6-dependent mechanism. Upon internalization, cargo-containing vesicles fuse with early endosome positive for the early endosomal marker, EEA-1, encountering the clathrin-mediated pathway. Next steps of the MHC-I trafficking require another small GTPase, Rab22a (Cebrian, Croce et al. 2016).

Upon internalization, MHC-I molecules, as any other molecule, enter the endocytic pathway, a dynamic cytosolic system of membrane compartments. Vesicles arising from different endocytosis pathways fuse with early endosomes, which are also called sorting endosomes due to their role as sorting station of the endocytic pathway (**Figure 1.5**). Indeed, from early endosomes, some receptors can recycle back to the cell surface in few minutes; some others are transported to the trans Golgi network entering a retrograde pathway; some, mainly ubiquitinated cargoes are usually delivered to late endosomes, multi-vesicular bodies (MVBs), and lysosomes for degradation; and finally, some proteins are sorted to the endosomal recycling compartment (ERC), a tubular structure which mediates a “slow” recycling.

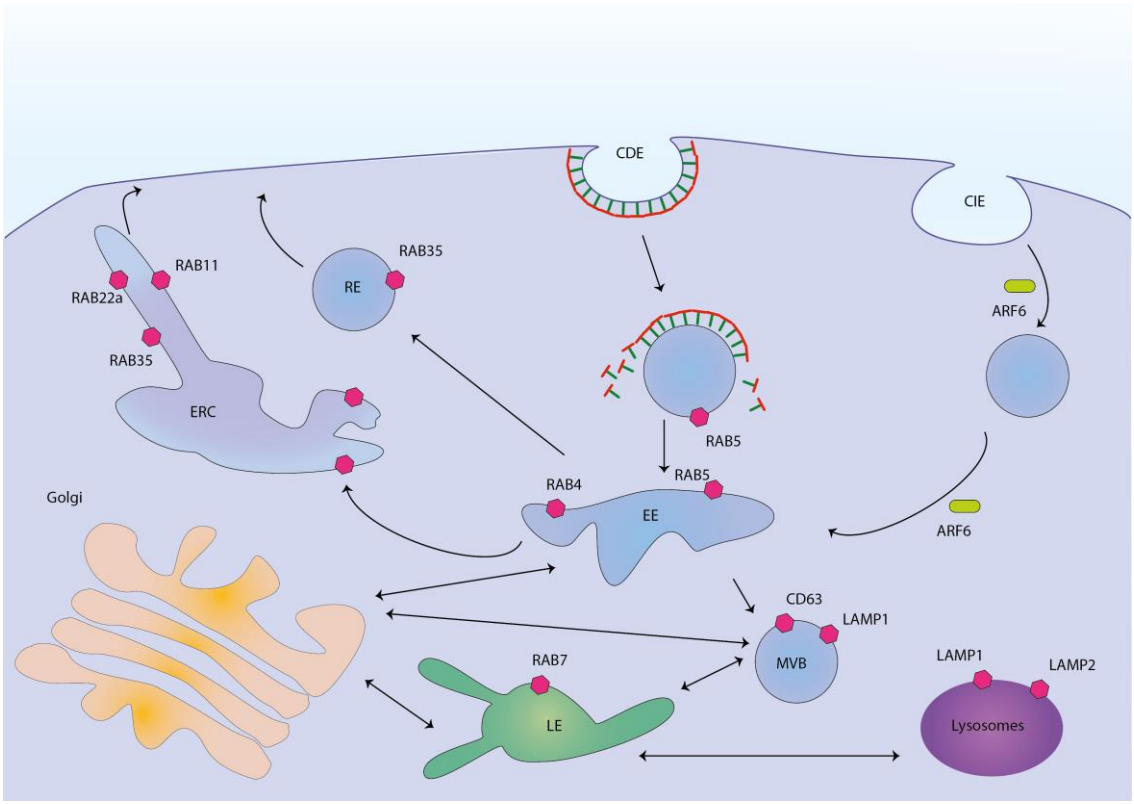

Figure 1.5 Endocytic pathways.

Proteins that are internalized through either clathrin-dependent or –independent pathways (CDE and CIE, respectively) are shuttled into early endosomes (EE) marked by the presence of RAB4, and RAB5. EEs regulate the sorting of the internalized cargoes. Some are rapidly or slowly recycled back to the plasma membrane in RAB35^{+} recycling endosomes (RE) or passing through the RAB11^{+} endosomal recycling compartment (ERC), respectively. Alternatively, mainly for endocytosed ubiquitinated proteins, EEs mature into multivesicular bodies (MVB) (CD63 and LAMP1^{+}), late endosomes (LE) (RAB7) and finally fuse with lysosome identified as LAMP1 and 2^{+} compartments responsible for degradation. Pink hexagons represent the proteins at the membrane of the different compartments.

Membrane compartments along the endocytic pathway are, in part, identified by composition of membrane markers such as Rab GTPase (**Figure 1.5**). Rab proteins recruit effector proteins, such as cargo adaptors, motor proteins to move the vesicles to its target membrane, as well as tethering complexes responsible for vesicles fusion by helping Soluble NSF Attachment Receptors (SNARE)(Hutagalung and Novick 2011).

To note, even though compartment within the endosomal network have their identity, they are not stable entities as they are dynamic structure and they can be altered when molecules and cargoes are exchanged in a process called endosomal maturation. During maturation, protein composition of early endosomes changes and various hydrolases are recruited as a result of vacuolar acidification. As early endosomes mature to become late endosomes/MVBs, they can

accumulate intraluminal vesicles in their vacuole to which cargo is transported by a multi subunit endosomal-sorting complex. When an endosome fuse with a lysosome, the intraluminal vesicles in the resulting endolysosome are degraded by lysosomal hydrolases. Finally, the classical lysosome is formed (Pryor and Luzio 2009).

1.1.5 Role of MHC class I antigen presentation for the immune control of influenza, LCMV and EBV

Influenza viruses are enveloped RNA viruses that belong to the Orthomyxoviridae family (Hampson and Mackenzie 2006). They are categorized based on the combination of haemagglutinin, responsible for the tropism of the virus, and neuraminidase glycoproteins. The knowledge that we have on the development of influenza A virus (IAV) infection *in vivo*, derived mainly from studies on mice which are confirmed by few studies in humans (Sridhar, Begom et al. 2013; Wang, Wan et al. 2015). It is clear that influenza-specific $CD8^+$T cells, activated upon peptide-MHC-I complex recognition, have an important role in fighting the virus resulting in a complete elimination of IAV by day 9 post infection (Bender, Croghan et al. 1992; Doherty, Topham et al. 1996). The presentation of IAV antigens starts at day 1-2 in the lung lymph nodes, leading to the activation of IAV-specific $CD8^+$ T cells (Yoon, Legge et al. 2007). The peak of antigen presentation within the lymph node is thought to occur from day 3 until at least day 9 post infection (Belz, Smith et al. 2004) but IAV-peptide-MHC complexes do not persist at later times (Mintern, Bedoui et al. 2009).

The prototypic herpesvirus Epstein Barr virus (EBV) is a ubiquitous human γ-herpesvirus that establishes persistent infection in more than 90% of the human adult population (Young and Rickinson 2004). The encounter of EBV during childhood results usually in asymptomatic infection, while during adolescence it causes infectious mononucleosis in 30-70% of cases (Auwaerter 1999; Tattevin, Le Tulzo et al. 2006). Additionally, EBV is the first virus discovered to be associated with human malignancies such as Burkitt lymphoma, Hodgkin lymphoma, and nasopharyngeal cancer (Ko 2015). Like other herpesviruses, EBV can undergo two infectious programs. During its latent state, EBV immortalized B are controlled by latent antigen-specific

CD8+T cells, and virus persistence is preserved. In the latent phase, 9 EBV genes are expressed as proteins: the EBV nuclear antigen family proteins (EBNA), which are comprised of EBNA1, -2, -3A, -3B, and -3C, the leader protein (LP), and latent membrane protein (LMP)-1, -2A, and -2B (Babcock, Hochberg et al. 2000; Thorley-Lawson 2001). However, herpesviruses occasionally undergo reactivation into their lytic cycle, where EBV expresses in a time-programmed manner a large number of lytic viral proteins (Miller, El-Guindy et al. 2007). The first genes to be transcribed are the immediate early lytic genes BZLF1 and BRLF1, which initiate the transcription of the more than 80 other lytic genes (Feederle, Kost et al. 2000). What exactly triggers the reactivation of the lytic cycle *in vivo* is not known yet. Nevertheless, it has been shown that differentiation of infected B cells into plasma cells could result in the latent-to-lytic switch (Babcock, Hochberg et al. 2000). Besides expression of different sets of genes, latent and lytic viral states also differ with respect to cells and their localization. Both latent and lytic antigens are expressed in B-lymphocytes within lymphoid tissue, but lytic antigens are mainly expressed in epithelial cells of the oropharynx tract (Hadinoto, Shapiro et al. 2009). Presentation of EBV in the context of MHC-I with the consequent activation of CD8+T cells plays an important role in controlling EBV infection and in deciding the outcome of the EBV infection. Indeed, restoration of T cell compartment in immunodeficient individuals, protect them from the high frequency of EBV-induced disease (Tangye, Palendira et al. 2017). During the latent phase, strong CD8+T cell response to immunodominant epitopes derive mainly from EBNA3 proteins, and with lesser extent from EBNA2 and LMP2. CD8+T cells specific for LMP1 and EBNA-LP antigens have been detected rarely (Hislop, Ressing et al. 2007; Brooks, Long et al. 2016). Additionally, in spite of the immune evasion ability, EBNA1 epitope-specific CD8+ T cell responses could be detected in virus-immune donors, and could be immunodominant in the context of certain HLA class I alleles, for example B*3501 (Blake, Haigh et al. 2000). As cells progressed through EBV's lytic cycle, the MHC-I levels and TAP function decrease due to specific immune escape mechanisms of EBV lytic cycle proteins targeting the HLA class I pathway (See **1.1.6**). CD8+T specific for lytic cycle proteins have been identified in infectious mononucleosis settings were the specificities were mainly directed against immediate-early proteins, BZLF1 or

BRLF1, or to early BZLF1-/BRLF1-induced proteins, such as BMLF1, BMRF1, BALF2, or BALF5 (Hislop and Taylor 2015). It is interesting to note that BZLF1 seems to be the most immunogenic protein, as it could be the result of an evolution of the immune system to ensure a proper control of the virus replication and of its spread within the host (Houssaint, Saulquin et al. 2001).

One of the best-characterized systems used to investigate $CD8^+$T cell function during both acute and chronic infection is lymphocytic choriomeningitis virus (LCMV). LCMV is a murine specific virus, which results in either acute or chronic infection, depending on the virus strain. Indeed, the Armstrong strain causes acute infections while its clone 13 variant is responsible for chronic infection. It has been shown that clearance of LCMV infection is dependent on $CD8^+$ T cells and β2-microglobulin as mice depleted for their $CD4^+$T cell compartment were still able to resolve LCMV infection as good as control mice, while β2-microglobulin knock-out mice were not (Matloubian, Concepcion et al. 1994). During acute infection, the majority of LCMV-specific $CD8^+$T cells found in the spleen were against the glycoprotein (GP_{33-41}) and the nucleoprotein ($NP_{396-404}$) presented on the MHC-I molecules H2-D^b and H2-K^b to $CD8^+$ T cells (Murali-Krishna, Altman et al. 1998). $CD8^+$ T cell specificities for other epitopes within those two proteins have been found as well (Appay, Nixon et al. 2000; Goepfert, Bansal et al. 2000). After resolution of infection, the effector T cell populations can either be eliminated via a cell death program called apoptosis, or become a pool of memory T cells ready to fight the virus again in case of a new infection (Kaech, Wherry et al. 2002). On the other hand, LCMV chronic infection persists for a maximum of 3 months. It causes suppression of $CD8^+$T cell response and relocalization of the virus-specific $CD8^+$T cells to non-lymphoid organs and bone marrow (Wherry, Blattman et al. 2003).

Thus, presentation of viral antigen by MHC-I molecules is indispensable for the host protection against viruses and for the efficient activation of $CD8^+$T cells. As counteracting mechanisms, viruses have evolved strategies to block the associated processes, as will be discussed in the next section.

1.1.6 Virus evasion of MHC class I presentation pathway

Viruses need a host for their life cycle, in order to replicate and spread. As discussed above, the host is equipped with defence mechanisms against viral infections such as viral antigen presentation on MHC-I. In turn, viruses have developed mechanisms of immune evasion by acquiring proteins able to alter the classical MHC-I biogenesis, trafficking and presentation. Indeed, some viral immunoregulatory proteins have been acquired from the host, while some others without sequence similarities to host genes have probably developed de novo as a result of evolutionary pressure (Alcami and Koszinowski 2000).

Viruses evade the MHC-I pathway at different levels (**Figure 1.6**). Some viruses, mainly herpesviruses, divert MHC-I molecules to degradation. For example, US2 and US11 proteins of the human cytomegalovirus as well as the mK3 protein of mouse herpesvirus 68 target the new MHC-I molecules to ER-associated degradation (Wiertz, Jones et al. 1996; Gewurz, Wang et al. 2001). On the other hand, endocytosed MHC-I degradation by lysosomal proteases results from their internalization induced by E3 ubiquitin ligases kK3 and kK5 of KSHV (Coscoy, Sanchez et al. 2001; Duncan, Piper et al. 2006) as well as new MHC-I molecules are redirected from the Golgi to lysosomes by the human immunodeficiency virus protein Nef (Schaefer, Wonderlich et al. 2008) and the murine cytomegalovirus protein gp48 (Reusch, Muranyi et al. 1999). A different strategy for viral immunoevasion is the inhibition of PLC components causing low peptide availability and an inefficient MHC-I loading. TAP activity is indeed inhibited by the action of several viruses such as the herpes simplex virus protein ICP47, the human cytomegalovirus protein US6 and the BNFL2a protein of Epstein Barr virus, which bind to and inhibit TAP activity (Lehner, Karttunen et al. 1997; Neumann, Kraas et al. 1997; Hislop, Ressing et al. 2007). Moreover, the human cytomegalovirus protein US3 inhibits tapasin-dependent peptide loading and peptide optimization (Park, Kim et al. 2004). Finally, the mature MHC-I molecules are retained within the ER by adenovirus E3-19K and cowpox CPXV203 proteins (Flomenberg, Szmulewicz et al. 1992; Byun, Wang et al. 2007).

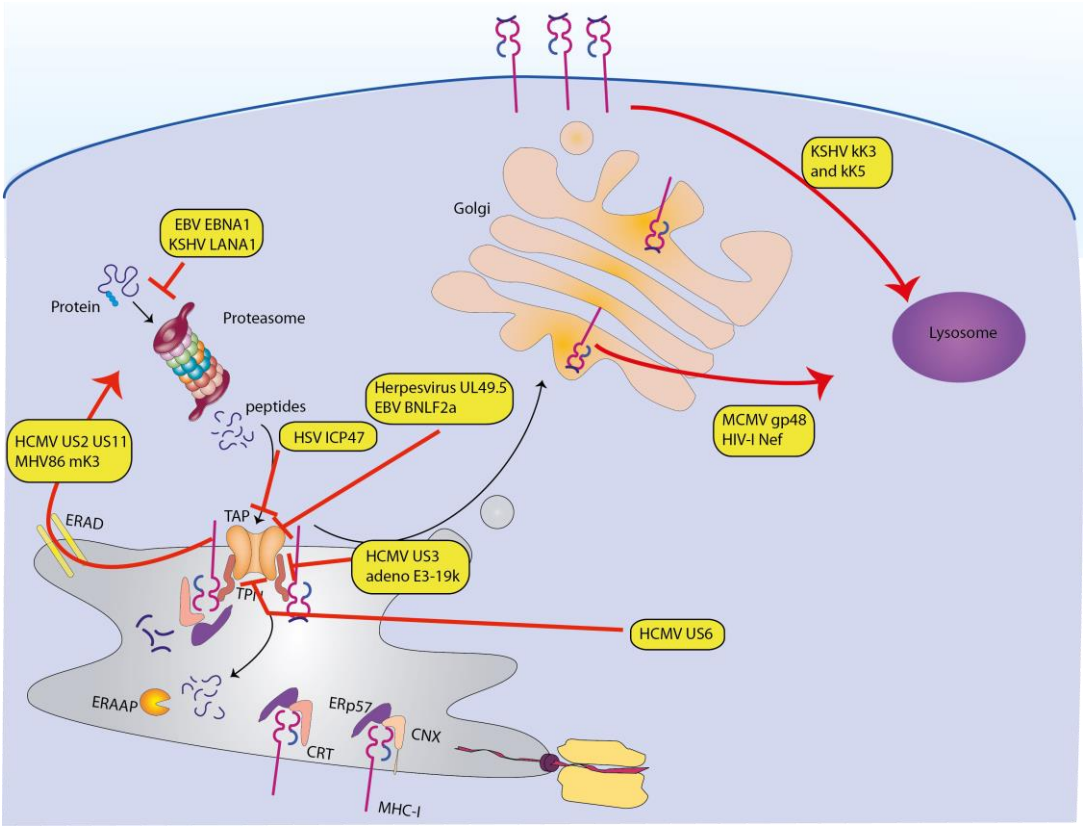

Figure 1.6 Viral Immunoevasion

Immune escape mechanisms for some viruses are depicted. Epstein-Barr nuclear protein 1 (EBNA1) and KSHV latency-associated nuclear antigen 1 (LANA1) inhibit their own degradation by the proteasome. US2 and US11 of human cytomegalovirus (HCMV), and mK3 of mouse herpesvirus 68 (MHV68) target new MHC-I molecules to ER-associated degradation (ERAD). Different steps of peptide transport by TAP are inhibited by herpes simplex virus (HSV) ICP47, HCMV US6, by the BNFL2a protein of Epstein Barr virus and by the UL49.5 proteins of bovine herpesvirus 1. Mature MHC-I molecules are retained in the ER by the adenovirus E3-19K and the HCMV US3. Differently, kK3 and kK5 of Kaposi' sarcoma-associated herpesvirus (KSHV), Nef of human immunodeficiency virus (HIV-1) and gp48 of murine cytomegalovirus (MCMV) target MHC-I to lysosomes for degradation.

However, down-regulation of MHC-I molecules has a drawback. While it offers protection from $CD8^+$T cells, it renders them susceptible to natural killer (NK) cells since MHC-I molecules expression inhibits NK cells. Nevertheless, viruses, such as human and mouse cytomegaloviruses, have evolved also NK cell recognition evasion, by encoding MHC-I-like ligands for inhibitory NK receptors (Voigt, Forbes et al. 2003; Prod'homme, Griffin et al. 2007).

Viruses can also target the proteasome degradation and the mRNA translation. Indeed, the EBV protein EBNA1 escapes processing by the proteasome due to the presence of glycine and alanine repeats (GAr) that interfere with the recognition and unfolding functions of the 26 S proteasome

(Daskalogianni, Apcher et al. 2008). Moreover, thanks to the same motif, EBNA1 inhibits translation of its own transcript by blocking the assembly of the EBNA1 translating ribosomes upon GAr synthesis (Yin, Manoury et al. 2003; Apcher, Komarova et al. 2009). Interestingly, the Kaposi' sarcoma-associated herpervirus latency-associated nuclear antigen 1 has a highly repetitive acidic sequence that is rich in glutamine, glutamic acid and aspartic acid residues with a similar inhibitory ability to that of EBNA1 (Kwun, da Silva et al. 2007; Apcher, Komarova et al. 2009).

Thus, it is important to understand how viruses evade the immune recognition by disrupting the classical MHC-I presentation in order to counteract such mechanisms and improve therapeutic approaches to boost the adaptive immune response against viral pathogens by allowing MHC-I-restricted viral antigen presentation via alternative pathways, and consequently thereby promoting $CD8^+$ cytotoxic T cell activity for effective viral clearance.

Part II - Autophagy

1.2.1 Autophagy pathways

Autophagy (form the Greek autóphagos, meaning "self-devouring") is a fundamental, evolutionary well conserved set of catabolic pathways that deliver cytoplasmic cargoes to the lysosome for degradation and recycling (Deter, Baudhuin et al. 1967; Deter and De Duve 1967). Originally, autophagy was described as a non-specific pathway, important during starvation to ensure supply of nutrients, while more recent evidence has shown that autophagy is also involved in the selective sequestration and degradation of cytoplasmic cargoes such as organelles, unfolded proteins, and pathogens. Furthermore, autophagy is involved in various cellular processes and a variety of disorders have been associated with dysfunctional autophagy in humans (Rubinsztein 2006; Qu, Zou et al. 2007; Cecconi and Levine 2008; Levine and Kroemer 2008; Saitoh, Fujita et al. 2008; Deretic and Levine 2009; Deegan, Saveljeva et al. 2013; Chhangani, Chinchwadkar et al. 2014).

Three different forms of classical (or canonical) autophagy can be distinguished in eukaryotic cells: microautophagy, chaperone-mediated autophagy (CMA), and macroautophagy. While microautophagy, known as endosomal microautophagy in mammals (Mukherjee, Patel et al. 2016), engulfs cytosolic proteins through invagination of the lysosomal or late endosomal membrane, during CMA, substrates containing a specific motif are recognized by the cytosolic heat shock protein 70 (HSP70) and translocated into lysosomes via lysosome-associated membrane protein 2a (LAMP2a). In both pathways the final stage is the degradation of the translocated material in lysosomes (**Figure 1.7**). Macroautophagy is the most studied form of autophagy, and as such often the term autophagy refers to macroautophagy. In this process, cytoplasmic substrate gets enclosed in a double-membrane vesicle, the autophagosome (Xie and Klionsky 2007), which fuses with the lysosome resulting in cargo degradation (Yang and Klionsky 2010) (**Figure 1.7**). In addition to the classical autophagy pathways, other pathways referred to as non-canonical autophagy that exploit sets of proteins of the autophagy machinery have been described. Examples are: LC3-associated phagocytosis (LAP)(Sanjuan, Dillon et al. 2007), Beclin

1-independent autophagy (Tian, Lin et al. 2010), Golgi-related autophagy (Nishida, Arakawa et al. 2009), and nuclear membrane-derived autophagy (English, Chemali et al. 2009).

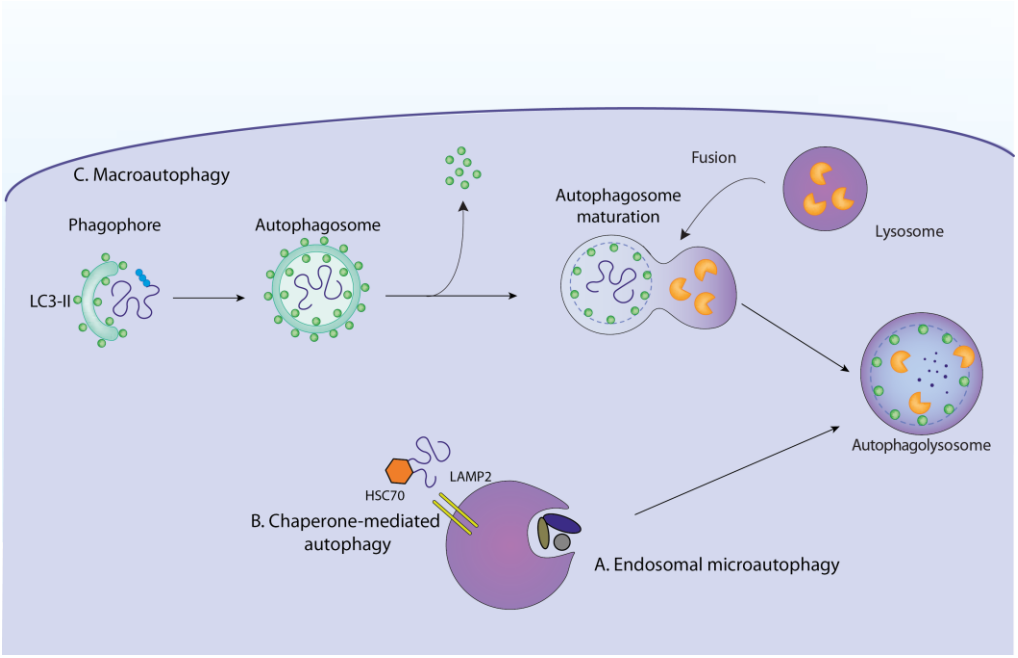

Figure 1.7 Schematic representation of the three forms of canonical autophagy.
During microautophagy or endosomal microautophagy in mammals (A) cytoplasmic material is taken up into the lysosome by membrane invagination. In chaperone-mediated autophagy (B) unfolded proteins are directly transported into lysosomes by the lysosomal chaperonin HSC70 and LAMP2a. (C) Macroautophagy involves the formation of a cup-shaped isolation membrane, also called phagophore, that encloses a portion of the cytoplasm. All forms of autophagy subsequently lead to the degradation of cytoplasmic constituents by lysosomal hydrolases.

1.2.2 Molecular mechanism of macrautophagy and its regulation

In mammals, a mature autophagosome forms in 5-10 minutes and it is about 0.5-1.5μm in diameter (Mizushima, Yamamoto et al. 2001; Fujita, Itoh et al. 2008). The formation of autophagosomes and its molecular machinery has been described first in yeast and requires a number of proteins called autophagy-related gene (*Atg*) products. More than 30 *Atgs* have been identified in yeast and many of them have orthologues in mammals (**Figure 1.8**). For the initial characterization of this machinery, Dr. Yoshinori Ohsumi has been awarded the Nobel Prize in physiology and medicine last year (Levine and Klionsky 2017). During the initiation of the autophagic process, the phagophore or isolation membrane is formed. The source of the membrane to form the autophagosome is under intense debate. Likely, it depends on the location of the substrates. The most probable sources are membranes derived from the ER,

Golgi, plasma membrane and mitochondria (Tooze and Yoshimori 2010). Autophagy is regulated by several mechanisms such as nutrient starvation, hypoxia and reactive-oxygen species (ROS) (He and Klionsky 2009). For example, the level of nutrients controls the phagophore formation by two energy-sensing kinases: the mammalian target of rapamycin (mTOR), and specifically the mTORC1 complex, functions as autophagy inhibitor, while the AMP-activated protein kinase (AMPK) triggers autophagy (Hardie 2011).

The formation of autophagosome is a complicated, highly regulated and specific interplay of different protein complexes. Conventionally, the autophagy process is divided into 5 steps: initiation, nucleation, elongation, closure and fusion. The initiation step occurs at the site of the isolation membrane formation, and starts with the assembly and activation of a serine-threonine kinase multiprotein complex called ULK complex containing ATG13, ATG101, FAK family kinase interacting protein of 200 kDa (FIP200) and unc-51-like autophagy activating kinase 1 (ULK1, the mammalian orthologue of yeast *Atg*1) or ULK2. The site of autophagy initiation is still under investigation. Recently, it has been described that ULK1 complexes are recruited to ER regions that are marked with ATG9 (Karanasios, Walker et al. 2016). The ULK complex recruits the multiprotein complex of the class III phosphatidylinositol 3-kinase (PI3K) for the nucleation step. This complex comprises beclin 1, vacuolar protein sorting (VPS) 34, VPS15, ATG14, which serves as sensor of membrane curvature, and the nuclear receptor-binding factor 2. The PI3K complex produces phosphatidylinositol 3-phospate (PI3P) which recruits and stabilizes some core autophagy proteins such as WD-repeat domain phosphoinositide-interacting (WIPI1-4) family and helps in the curvature of autophagosomes. Among WIPI proteins, WIPI-2 recruits the autophagy machinery responsible for the elongation phase, such as ATG16L1 (Proikas-Cezanne, Takacs et al. 2015). The elongation step is regulated by two ubiquitin-like protein conjugation systems: ATG16L1 complex and ATG8. The former complex comprises ATG16L1, ATG12 and ATG5. ATG12 is conjugated to ATG5 by ATG7 and ATG10 (Nakatogawa, Suzuki et al. 2009). ATG16L1 then associates with ATG5 and this complex mediates the elongation of the autophagosomal membrane and the incorporation of ATG8 into the autophagosomal membrane (Ohsumi 2001).

ATG8 is the yeast orthologue of a family of mammalian proteins that comprises LC3A-C, GABARAP, and GABARAPL1-3. LC3B is the principle ATG8 orthologue studied, and from now on I will refer to LC3B as LC3. LC3 undergoes different catalytic steps. First, the cytosolic precursor of LC3 is cleaved by the cysteine protease ATG4 to become LC3-I, known also as cytosolic LC3. Subsequently, ATG7 and ATG3 activate LC3-I in an ATP-dependent manner, making it a suitable substrate for the ATG16L1 complex. Indeed, the ATG16L1 complex conjugates the cytosolic LC3-I to the phospholipid phosphatidylethanolamine, resulting in the formation of the lipidated form of LC3, or LC3-II, which is integrated into the autophagosomal membrane (Fujita, Itoh et al. 2008). The role of LC3-II is still under discussion. It was believed to play a role in elongation and in the sealing of the autophagosome, while recently it has been shown that in absence of ATG3 and LC3 autophagosomes can close, even if smaller, and LC3 seems to be indispensable for fusion event (Nguyen, Padman et al. 2016) and proper degradation of the cargo (Tsuboyama, Koyama-Honda et al. 2016). LC3-II locates to both the outer and the inner membrane of the autophagosome. While LC3-II at the outer membrane gets cleaved from phosphatidylethanolamine by ATG4 upon autophagosome closure, LC3-II residing in the inner membrane gets degraded together with the cargo within lysosomes. Therefore, LC3 is widely used as autophagy marker and as indicator of the autophagic flux, indicating the rate of recruitment, segregation and degradation of autophagy substrates (Loos, du Toit et al. 2014).

Once autophagosomes close, they can fuse with late endosomes or lysosomes to form amphisomes or autolysosomes, respectively (Gordon and Seglen 1988; Klionsky, Eskelinen et al. 2014). Similar to other vacuole membrane fusion events, fusion of the autophagosome with the lysosome is thought to be mediated by Rabs and SNAREs but the exact mechanism is still under intense investigation.

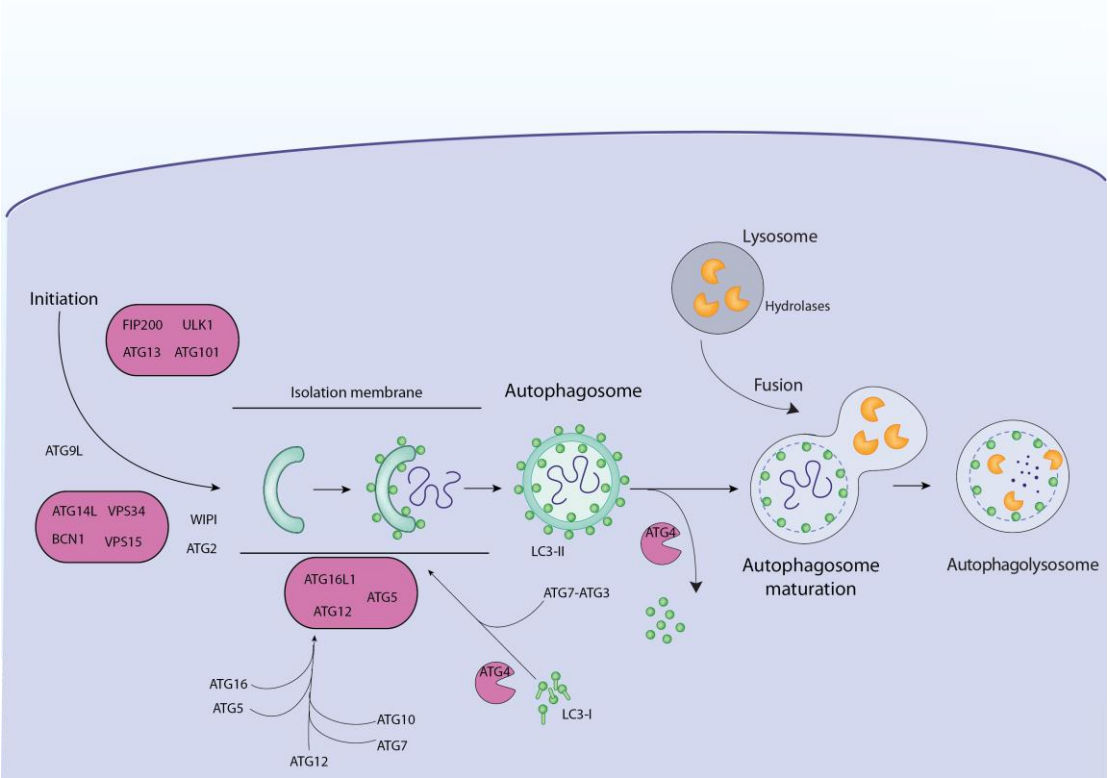

Figure 1.8 Macroautophagy

Upon signals for initiation of macroautophagy, the isolation membrane is formed followed by a cascade activation of the ULK1 complex and the PI3K complex. ATG12 is conjugated to ATG5 by ATG7 and ATG10. ATG16L1 then associates with ATG5 and this complex mediates the elongation of the autophagosomal membrane. In addition, LC3 is cleaved by cysteine protease ATG4 to become LC3-I. Subsequently, ATG7, ATG3 and the ATG16L1 complex conjugate free cytosolic LC3-I to phosphatidylethanolamine (PE) to become LC3-PE (LC3-II) that associates with autophagosomes. The resulting isolation membrane expands and engulfs a portion of the cytosol, including entire organelles. Upon closure of the double membrane surrounded autophagosome, the ATG12-ATG5-ATG16L1 complex dissociates and LC3 is cleaved by ATG4 from the outer autophagosomal membrane, while lipidated LC3 (LC3-II) remains bound to the inner autophagic membrane with which it is degraded, together with the cargo, after fusion with the lysosome.

It is worth noting that the study of the autophagy pathway is still challenging for the scientific community as autophagy is a dynamic and complex process, requiring interactions among several proteins. Moreover, selective pharmacological inducers and inhibitors of autophagy are lacking. The main accepted drugs are Bafilomycin A and chloroquine, which inhibit lysosomal fusion and acidification, respectively, causing an accumulation of LC3-II. On the other hand, as inducers, rapamycin, which inhibits mTOR, and starvation are the most widely used. Molecular biology-based approaches could overcome the lack of specificity in these approaches, even if they might induce compensatory mechanisms in the affected cellular or animal systems. Indeed, the silencing or the genetic removal of components of the different autophagy complexes has been developed for both *in vitro* and *in vivo* applications.

1.2.3 Selective autophagy and LIR motif

As mentioned above, despite autophagy being initially described as a non-selective process, it is now clear that selected cargo can be specifically degraded by autophagy. Indeed, the term selective autophagy refers to the degradation of targeted organelles or pathogens and each type of selective autophagy has been named after the targeted substrate (*e.g.* mitophagy for mitochondria degradation, xenophagy for bacteria and virus degradation). Moreover, autophagy substrates can be selectively recognized by specific receptors (Farre and Subramani 2016). By definition, autophagy receptors are "proteins that recognize and bind autophagy substrates, allowing their engulfment within the autophagic vesicles, and become degraded within lysosomes in the course of functional autophagic responses" (Galluzzi, Baehrecke et al. 2017). Most autophagy receptors are characterized by the presence of a specific motif called LC3-interacting region (LIR) (**Table 1.1**) and some, for instance p62, have an ubiquitin-binding domain allowing engulfment of ubiquitinated substrates (Khaminets, Behl et al. 2016). Interestingly, some receptors not only target autophagy substrates to form autophagosomes upon LC3 binding, but have also regulatory functions (Kimura, Jain et al. 2015; Verlhac, Gregoire et al. 2015).

LIRs have been recently characterized (Jacomin and Nezis 2016) as a consensus sequence of 6 amino acid residues in length. Within the sequence, the aromatic and the hydrophobic residues in position 3 and 6, respectively, are the most crucial determinants (Alemu, Lamark et al. 2012). In addition, a non-conventional LIR, lacking the aromatic residue, has been identified within the autophagy receptor nuclear dot protein 52 (NDP52), and can specifically interact with LC3C (von Muhlinen, Akutsu et al. 2012). An additional mechanism by which cells regulate selective autophagy-mediated degradation could be the phosphorylation status of LIR motifs, since such modifications impair the interaction between LC3 and autophagy receptors (Rogov, Suzuki et al. 2017).

Protein	LIR position	LIR sequence
ATG19	406-415	NEKALT**WEEL**
ATG32	80-91	DSISGS**WQAI**QP
ATG34	402-412	TLSRPFT**WEEL**
BNIP3L	30-44	AGLNSS**WVEL**PMNSS
FUNDC1	6-26	YESDDQS**YEVL**DLTEY
NBR1	724-738	QSSASSED**YIIL**PE
NDP52	126-140	RPENEED**ILVV**TTQG
OPTN	169-184	NSSGSSEDS**FYE**IRMA
p62	330-345	NCSGGDDD**WTHL**SSKE
TAX1BP	135-147	EGENSD**VLVV**TTKA

Table 1.1 List of LC3-interacting regions (LIRs).
Positions from 3 to 6 of the LIR motif are in bold. ATG, autophagy-related protein; BNIP3L BCL2 interacting protein 3-like; FUNDC1, FUN14 domain containing 1; NBR1, neighbour of BRCA1 gene 1; NDP52, nuclear dot protein 52 kDa; OPTN, Optineurin; p62 or sequestosome 1; TAX1BP, Tax1 Binding Protein 1.

Presence of LIR motifs has been reported also within components of the receptor internalization machinery linking autophagy to internalization process of plasma membrane molecules.

1.2.4 ATGs in receptor internalization

Links between autophagy and the clathrin-mediated internalization machinery have been reported. Indeed, clathrin contains a LIR motif and clathrin-mediated endocytosis has been shown to support autophagosome formation (Ravikumar, Moreau et al. 2010). Moreover, the adaptor protein 2 (AP2), a component of the machinery implied in clathrin-mediated endocytosis, was shown to function as autophagy receptor for the trafficking of the Alzheimer's amyloid protein precursor from the plasma membrane to the autophagosomes for degradation (Tian, Chang et al. 2013). Moreover, recently, the non-classical MHC-I molecules, CD1d, has been shown to be internalized by a clathrin-mediated endocytosis process dependent on *Atg5* (Keller, Loi et al. 2017). Interestingly, the tyrosine motif recognized during clathrin-dependent endocytosis has been found within the MHC-I sequence and studies have reported its importance for proper internalization and trafficking during cross-presentation (Lizee, Basha et al. 2003; Basha, Lizee et al. 2008). Thus, it is tempting to speculate about a role of the autophagy machinery in the regulation of MHC-I internalization via its interactions with the clathrin-dependent endocytosis machinery.

1.2.5 ATGs in antigen presentation

Among the various roles of autophagy, several studies have shown that autophagy is also involved in both innate and adaptive immune responses. Autophagy has been identified as a regulator of antigen presentation of cytosolic (Paludan, Schmid et al. 2005; Schmid, Pypaert et al. 2007) and extracellular proteins (Romao, Gasser et al. 2013) for MHC-II presentation. On the contrary, the role of autophagy in MHC-I presentation has only been poorly described.

As mentioned earlier, MHC-II molecules serve classically as platform to present extracellular antigens to $CD4^+$T cells, but biology does not lack exceptions. Indeed, MHC-II can also present cytosolic antigens via alternative pathways, such as autophagy. It has been shown that autophagosomes fuse with the MHC-II loading compartments (MIICs) in human B cells, DCs and epithelial cell lines, as well as in mouse thymic epithelial cells, and that fusing proteins to the N-terminus of LC3 enhances MHC-II presentation of viral and tumour antigens up to 20 fold (Schmid, Pypaert et al. 2007; Kasai, Tanida et al. 2009). Processing of endogenous MHC-II antigens via macroautophagy promotes presentation of intracellular antigens to $CD4^+$T cells contributing to the thymic selection of the $CD4^+$ T cell repertoire (Nedjic, Aichinger et al. 2008). In contrast, exogenous antigen processing for MHC-II presentation benefits from the autophagy machinery via LAP, a non-canonical form of autophagy. During LAP, phagosomes get coated with LC3 and require ROS production by NADPH oxidase, NOX2, to acquire or maintain this coat (Martinez, Malireddi et al. 2015). Depending on the cellular context, phagosome-associated LC3 seems to accelerate fusion with lysosomes in mouse macrophages (Sanjuan, Dillon et al. 2007), or preferentially fuse with compartments containing pathogen-associated molecular pattern receptors (Henault, Martinez et al. 2012). In contrast, in human macrophages and DCs, LAP vesicles seem to be stabilized and maintain antigen, resulting in prolonged MHC-II presentation (Romao, Gasser et al. 2013). Thus, the autophagy pathways seem to support both endogenous as well as exogenous antigen processing for MHC-II presentation via canonical and non-canonical autophagy, respectively. A role of autophagy in MHC-II via its fusion with the endosomal-loading compartment is not surprising as autophagosomes fuse with late endosomes to form amphisomes before the final

fusion with lysosomes (Berg, Fengsrud et al. 1998). In contrast to this supportive role for MHC-II restricted antigen presentation, a role for autophagy in classical MHC-I antigen presentation is not obvious given that the endogenous MHC-I antigen presentation pathway does not seem to intersect with the autophagosomal route. Therefore, the role of autophagy in MHC-I antigen presentation is still controversial. Despite the large body of evidence that suggests autophagy does not play a role in MHC-I antigen presentation, there are some reports supporting its involvement. Indeed, it has been shown that autophagy's contribution to MHC-I presentation become important when the classical MHC-I pathway is impaired by viral proteins, as described in section **1.1.6**, for example by herpesviruses. It has been shown that during herpes simplex virus 1 infection, the viral envelope glycoprotein B is presented on MHC-I in an autophagy-dependent manner at late time points during infection (English, Chemali et al. 2009). Moreover, in cells defective for the TAP protein responsible for the translocation of peptides from the cytosol to the ER in the classical MHC-I pathway (See **1.1.3**), the latent viral protein pUL138 of human cytomegalovirus was presented to $CD8^+$ T cells by an autophagy-dependent pathway (Tey and Khanna 2012). In the same condition, the autophagy pathway CMA has been shown to play a role in the presentation of endogenous antigen such as the truncated forms of the Simian virus 40 (SV40) large T antigen (Schirmbeck, Bohm et al. 1997). Therefore, autophagy clearly serves to overcome viral immune escape mechanisms, providing an alternative pathway to alert the immune system about the presence of viruses within cells.

In other contexts, further evidence supports a possible role of autophagy in MHC-I presentation of endogenous antigens. For example, the induction of autophagy during mycobacterium tuberculosis infection increases the proliferation of $CD8^+$ T cells (Jagannath, Lindsey et al. 2009). Similarly, autophagy degradation of tumour antigen aggregates enhances MHC-I presentation of a melanoma-derived peptide, resulting in $CD8^+$ T lymphocyte proliferation and decreased tumour growth *in vivo* (Fu, Tao et al. 2010). Thus, besides being a valid strategy to fight viruses, autophagy enhances the immune defence mechanisms against bacterial pathogens and tumours.

Under debate is also the role of autophagy in cross-presentation. Some studies have shown that in professional antigen presenting cells, autophagy can provide antigens for cross-presentation and helps in their packaging for their delivery to antigen presenting cells (Li, Wang et al. 2008; Uhl, Kepp et al. 2009). Interestingly, in cross-presenting subsets of DCs, autophagic membrane formation is most pronounced and ATG7 is required for efficient presentation of soluble protein, but not of antigen targeted to the endocytic receptor DEC-205 on DCs or of antigen incorporated into apoptotic cell debris (Mintern, Macri et al. 2015). In line with this, the involvement of autophagy in the cross-presentation of the soluble human cytomegalovirus antigen pp65 has also been demonstrated (Dasari, Rehan et al. 2016).

Thus, autophagy actively supports and provides alternative mechanisms to ensure immune cell control of infections that compromise classical antigen processing for MHC-I presentation. It is therefore not surprising that in turn, viruses have evolved mechanism to manipulate autophagy.

1.2.6 Regulation of autophagy by viruses

Autophagy is an anti-viral mechanism and as such viruses have evolved mechanisms to manipulate it. The interplay between autophagy and viruses is still under investigation as viruses can in some cases block autophagy or use it for their own benefits. Autophagy, playing a role in the process of antigen presentation, contributes, indeed, to help the host immune system to fight viruses. For example, for some herpes viruses it has been suggested that the inhibition of autophagy by viruses is required for their efficient replication (A. Orvedahl, et al, 2011; G.H. Jang et al. 2016) and also for the development of viral oncogenesis for EBV (Deretic and Levine 2009) as the inhibition of autophagy further limit adaptive immune response of the host. Therefore, it is important to understand how viruses interfere with autophagy to develop strategies to block them. Viruses have evolved several ways to manipulate autophagy mainly at two levels. As depicted in **Figure 1.9**, some viruses have been found to interfere with autophagosome formation, while others mainly regulate autophagosome fusion with lysosomes (Paul and Munz 2016).

At initial phases of autophagy the protein mainly targeted by herpesviruses is beclin1 but many viruses have usually more than one mechanism to evade the same or different steps of the autophagy pathway. For example, herpes simplex virus 1 blocks beclin1 via both ICP34.5 and US11 (Orvedahl, Alexander et al. 2007; Lussignol, Queval et al. 2013). On the other side, Kaposi' sarcoma-associated herpes virus uses its Bcl-2 orthologue and the viral FLICE-like inhibitory protein to inhibit beclin1 and the LC3 lipidation step by targeting ATG3, respectively (Lee, Li et al. 2009).

Interestingly, the two viruses used in the present PhD thesis, the Influenza A virus (IAV) and EBV provide example of the dual manipulation of autophagy. More specifically, IAV ion-channel protein M2 interacts with LC3 thanks to its LIR motif. This binding causes on one hand the accumulation of autophagosomes by inhibiting their fusion with the lysosome (Gannage, Dormann et al. 2009) and on the other hand results in the re-localization of LC3 at the plasma membrane of the infected cells rendering virus particles more stable and thus, enhancing virus transmission (Beale, Wise et al. 2014).

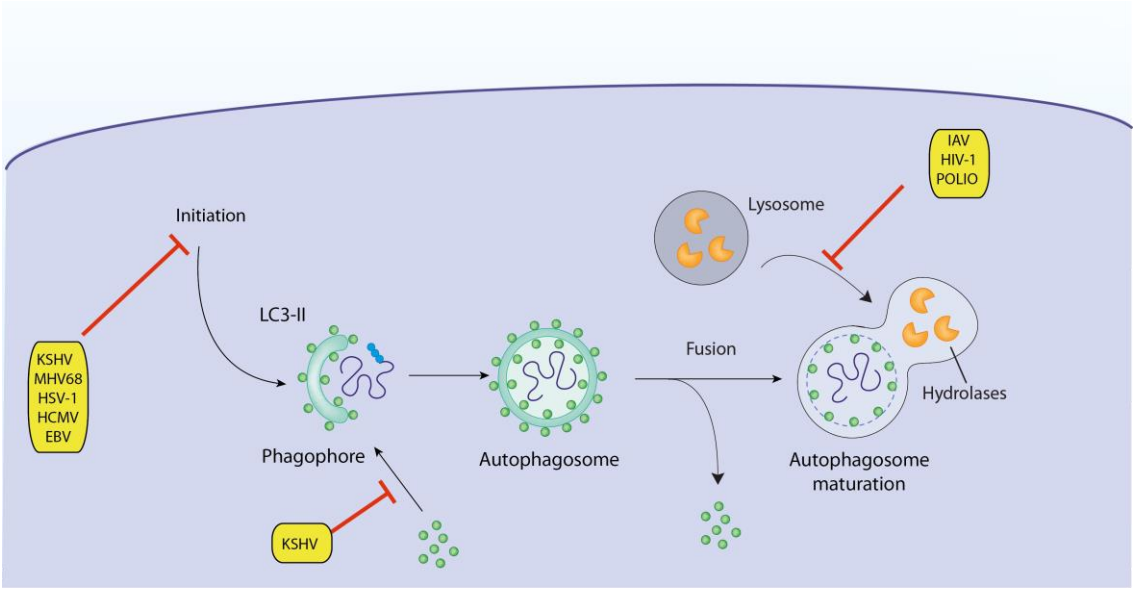

Figure 1.9 Viral inhibition of autophagy.
Viruses can inhibit autophagy mainly at two stages: the formation of autophagosomes (such as Kaposi's sarcoma associated herpesvirus (KSHV), murine γ-herpesvirus 68 (MHV68), herpes simplex virus-1 (HSV-1), human cytomegalovirus (HCMV), and Epstein Barr virus (EBV)) and the fusion of autophagosome with lysosomes (influenza A virus (IAV), polio, and HIV).

Similarly, the Bcl-2 homologues, BamHI rightward fragment 1 (BHRF1) and BamH1 A leftward fragment 1 (BALF1) of EBV might be responsible for blocking autophagy by inhibiting beclin1 (Coleman, McGraw et al. 2014; De Leo, Colavita et al. 2015). At the same time, EBV exploits the autophagic membranes for its exocytosis from infected cells (Nowag, Guhl et al. 2014). Moreover, LMP1 and LMP2 protein of EBV prevent cell death by inducing autophagy (Lee and Sugden 2008; Fotheringham and Raab-Traub 2015; McFadden, Hafez et al. 2016).

Thus, it is clear that autophagy plays an important role in the life cycle of some viruses. As such, it is of great importance to understand how to exploit the molecular machinery of autophagy, as alternative mechanism against viruses, especially for those that are invisible to the immune system thanks to their ability to inhibit the classical MHC-I pathway.

Chapter 2 - Aim and Outline of the PhD thesis

This study aims at elucidating how autophagy influences antigen processing, vesicular MHC-I loading and trafficking. Since knowledge on the mechanism of viral antigen presentation is crucial for rational vaccine design, these studies might help to improve the adaptive immune response against viral pathogens via manipulation of autophagy proteins. In addition, understanding how autophagy regulates antigen presentation to T cells could facilitate the generation of therapeutic approaches that promote $CD8^+$ cytotoxic T cell activity against pathogens. The gained information will allow the regulation of $CD8^+$ T cell stimulation via autophagy and they may open an interesting perspective for application of innovative strategies for vaccination.

With the above-mentioned purpose, the proposed thesis deals with the role of the molecular machinery of autophagy in the regulation of MHC-I surface levels and antigen presentation both *in vitro* and *in vivo*. In particular, the role of the autophagy machinery in MHC-I stabilization on antigen presenting cells (Results part I) and in endogenous antigen presentation by MHC-I molecules I *in vitro* (Results part II) have been investigated.

Chapter 3 - Results

Part I- Autophagy in MHC class I internalization

3.1.1 Increased MHC class I levels on autophagy-deficient *Atg5*$^{-/-}$ or *Atg7*$^{-/-}$ DCs and macrophages *in vitro* and *in vivo*

The catabolic process of autophagy has been linked to the process of antigen presentation for MHC-II but its role in the context of MHC-I is under investigation and still under debate. In order to address whether MHC-I presentation could be affected by autophagy deficiency we made use of Cre technology to obtain mice in which specific autophagy key genes, namely *Atg5* or *Atg7,* were deleted in antigen presenting cells. *Atg5* is a component of the ATG16L1 complex required for autophagosome formation, while *Atg7* is required for the formation of the ATG16L1 complex as well as for LC3 lipidation. Specifically, in our mouse model Cre is under the control of the CD11c promoter, a marker expressed by all dendritic cells (DCs). Cre is a recombinase enzyme able to recognize and recombine floxed gene sequences. In our mice such sequences were at the flanking region of *Atg5* or *Atg7* gene leading to deletion of the gene of interest upon Cre expression by DCs. These mice are referred to as *Atg5*$^{-/-}$ or *Atg7*$^{-/-}$ DC mice, respectively.

In the above-described animal model, we first analysed the surface levels of the MHC-I molecules H2-K^{b} and H2-D^{b} on *Atg5* deficient DCs from lung, spleen and bone marrow-DCs (BM-DCs) by flow cytometry. Different subsets of DCs have been distinguished based on their surface markers such as CD11b, for both lung and spleen, CD103 and CD8 for lung and spleen, respectively. We found that in the lung *Atg5*$^{-/-}$ alveolar macrophages, CD11b^{+} and CD103^{+} DCs displayed higher MHC-I cell surface expression at steady state than in their *Atg5*$^{flox/flox}$ littermates (**Figure 3.1 A-B**).

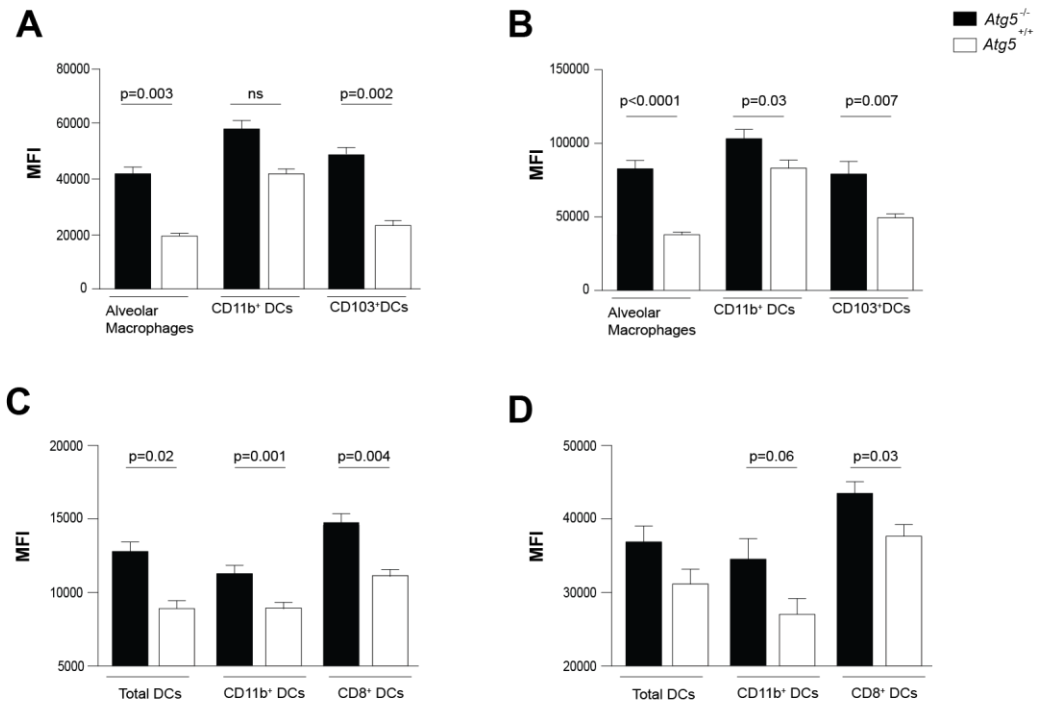

Figure 3.1 Elevated MHC class I expression on *Atg5* deficient DCs and macrophages.
Expression of H2-D^b and H2-K^b on lung and splenic *Atg5*$^{-/-}$ and *Atg5*$^{+/+}$ DCs and macrophages. Lung DCs were gated as live CD11c MHC-II^{high} cells. DC subsets were further subdivided on the basis of CD11b and CD103expression, and alveolar macrophages as double negative CD11b$^-$CD103$^-$ cells. Inflammatory DCs and monocytes were gated out using Ly6C staining. Similarly, splenic DCs were gated as live CD11c$^+$ MHC class II^{high} cells, excluding inflammatory DCs and macrophages by using both Ly6C and F4/80 staining. Graphs summarize mean fluorescence intensity (MFI) values and SEM of H2-D^b in the lung **(A)** and in the spleen **(C)** from 3 independent experiments, each with 3 mice per group. Surface expression of H2-K^b in lung **(B)** and in the spleen **(D)** *Atg5*$^{-/-}$ and *Atg5*$^{+/+}$ DCs and macrophages. Three experiments are summarized. P values are derived from unpaired non-parametric two tailed t test.

Accordingly, in the spleen, both H2-K^b and H2-D^b molecules of CD11c$^+$ cells and specifically on both CD11b$^+$ and CD8$^+$ subsets of splenic DCs were expressed at significantly higher surface levels in *Atg5*$^{-/-}$ DC mice (**Figure 3.1 C-D**). Importantly, C57BL/6 wild-type and CD11c-cre transgenic C57BL/6 mice did not display the same phenotype (**Figure 3.2**).

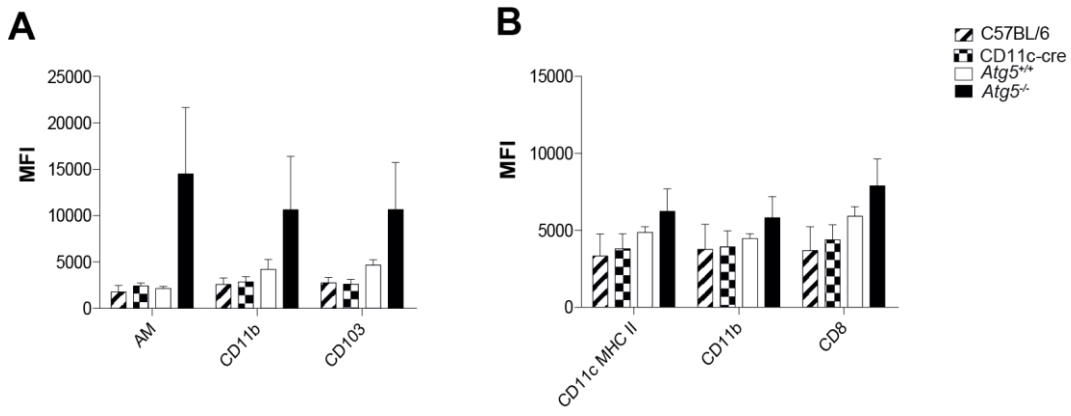

Figure 3.2 Elevated MHC class I expression is detected on *Atg5* deficient DCs.

(A) Surface expression of H2- D^b on lung DC subsets for C57BL/6 wild type, CD11c-Cre, CD11c-cre x *Atg5*$^{fl/fl}$ and *Atg5*$^{fl/fl}$ mice. **(B)** Surface expression of H2- D^b on splenic DC subsets for C57BL/6 wild type, CD11c-Cre, CD11c-cre x *Atg5*$^{fl/fl}$ and *Atg5*$^{fl/fl}$ mice. P values are derived from unpaired non-parametric two tailed t test.

Moreover, *Atg5* deficient BM-DCs displayed higher MHC-I levels than their wild-type counterparts (**Figure 3.3A**). In contrast, MHC-I surface expression was unchanged on B and T cells (**Figure 3.3B**).

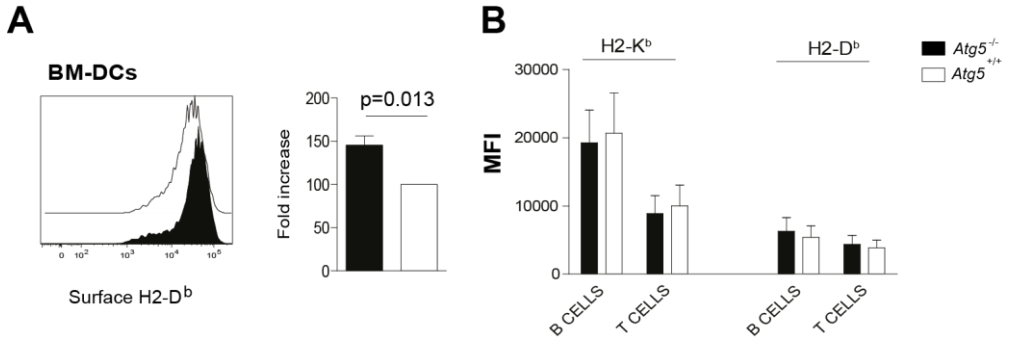

Figure 3.3 Elevated MHC class I expression on *Atg5* deficient BM-DCs.
Expression of H2-D^b on *Atg5*$^{+/+}$ and *Atg5*$^{-/-}$ BM-DCs. **(A)** Representative flow cytometric staining (left) and all summarized results (right) are derived from 5 independent experiments and are summarized as fold increase compared to *Atg5*$^{+/+}$ DCs set as 100%. **(B)** MHC class I surface expression on B and T cells for the experiments of 3.1 and 3.2. Mean and SEM were plotted.

These data were confirmed in *Atg7*$^{-/-}$ DC mice where MHC-I levels were elevated on *Atg7* deficient alveolar macrophage and DC populations, but not B or T cells (**Figure 3.4**).

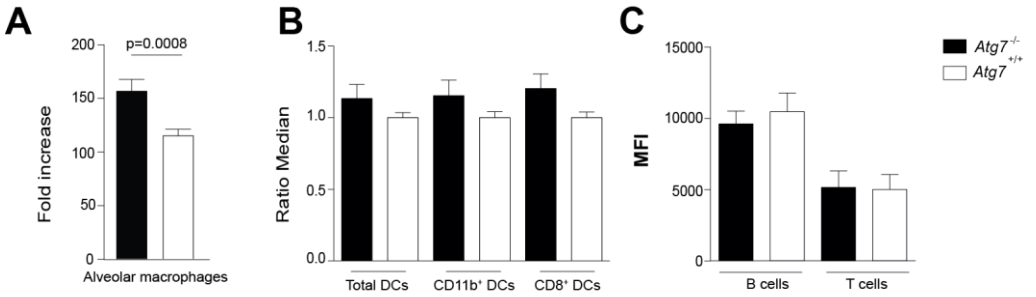

Figure 3.4 Elevated MHC class I expression on *Atg7* deficient lung and splenic DCs and macrophages.
(A) Expression of MHC-I on *Atg7*$^{+/+}$ and *Atg7*$^{-/-}$ alveolar macrophages. Results are from 6 independent experiments and are summarized as fold increase compared to *Atg7*$^{+/+}$ macrophages. Unpaired non-parametric two tailed t tests were performed to obtain the indicated p values. **(B)** Surface expression of MHC-I on splenic *Atg7*$^{+/+}$ and *Atg7*$^{-/-}$ DC subsets. **(C)** Surface expression of MHC-I on splenic *Atg7*$^{+/+}$ and *Atg7*$^{-/-}$ B and T cells. 5 experiments are summarized.

These findings suggest that deficiency in the core machinery of autophagy, which is required for LC3 lipidation, increases MHC-I levels on myeloid antigen presenting cells.

3.1.2 MHC class I transcription and transport to the cell surface are not altered in absence of autophagy

In order to address the mechanisms that could lead to MHC-I up-regulation in the absence of autophagy, we tested four hypotheses (**Scheme 3.1**).

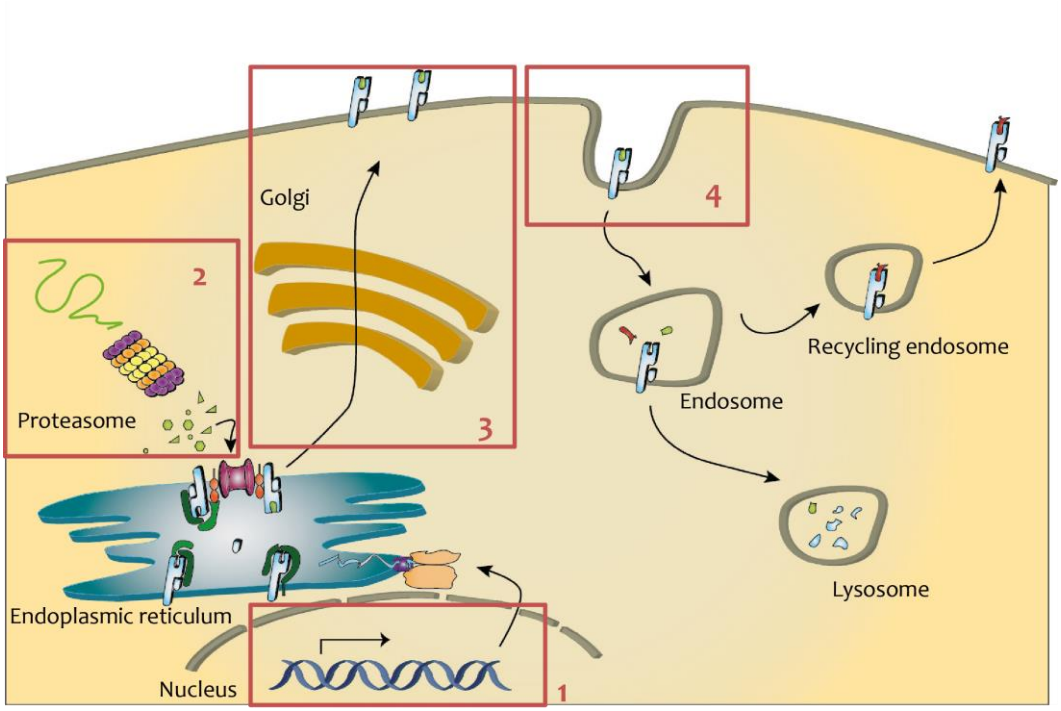

Scheme 3.1 Four hypotheses tested
Schematic representation of the 4 hypotheses tested to investigate by which mechanism autophagy deletion result in an increased MHC-I surface level on murine CD11c-expressing cells. **1**. Investigation on transcription levels of MHC-I genes; **2**. Evaluation of proteasomal degradation; **3**. Analysis on the rate of assembly and trafficking to the cell surface of newly synthetized MHC-I molecules; **4.** Quantification of the rate of internalization of MHC-I molecules.

First, we ruled out a difference in MHC-I gene expression, by quantifying MHC-I transcript levels in flow cytometrically sorted splenic *Atg5*$^{+/+}$ and *Atg5*$^{-/-}$ DCs (**Figure 3.5A**). Except for CD8^{+} splenic DCs that show a tendency towards increased H2-K^{b} transcription levels, no difference in MHC-I transcription was confirmed in the investigated lung and splenic DC and macrophage subpopulations (**Figure 3.5B**). These data indicate that the increased MHC-I surface expression of macroautophagy deficient DCs is not due to altered MHC-I gene transcription. We therefore addressed as the second hypothesis a difference in the availability of ubiquitinated substrates for proteasomal degradation and MHC-I loading. We could not detect any difference in the total amount of polyubiquitinated proteins in *Atg5*$^{-/-}$ DCs compared to *Atg5*$^{+/+}$ DCs by Western blot quantification (data not shown). As the third hypothesis, we

hypothesized the existence of a compensatory mechanism in the absence of degradation by autophagy. We considered an increased proteasome activity with a subsequent increase of MHC-I ligand production that could result in a faster assembly or transport to the cell surface of new peptide-MHC-I complexes (Dengjel, Hoyer-Hansen et al. 2012; Marshall, Li et al. 2015). However, we did not see any difference in the rate of *de novo* expression of MHC-I molecules on the cell surface as assessed after acid stripping, which denatures surface MHC-I molecules, followed by measuring the kinetics of MHC-I recovery at the cell surface (**Figure 3.5C-D**). As acid stripping influences MHC-I recovery at the surface by four different pathways, namely MHC class I synthesis, peptide loading in the ER, trafficking through the ER-Golgi secretory route and recycling through endosomes, these could be excluded as significant contributors to the described phenotype. These results taken together suggest that the higher surface expression of MHC-I molecules on *Atg5*$^{-/-}$ DCs is not related to enhanced gene transcription, increased availability of antigenic peptides, elevated synthesis or trafficking of *de novo* formed peptide-MHC-I complex.

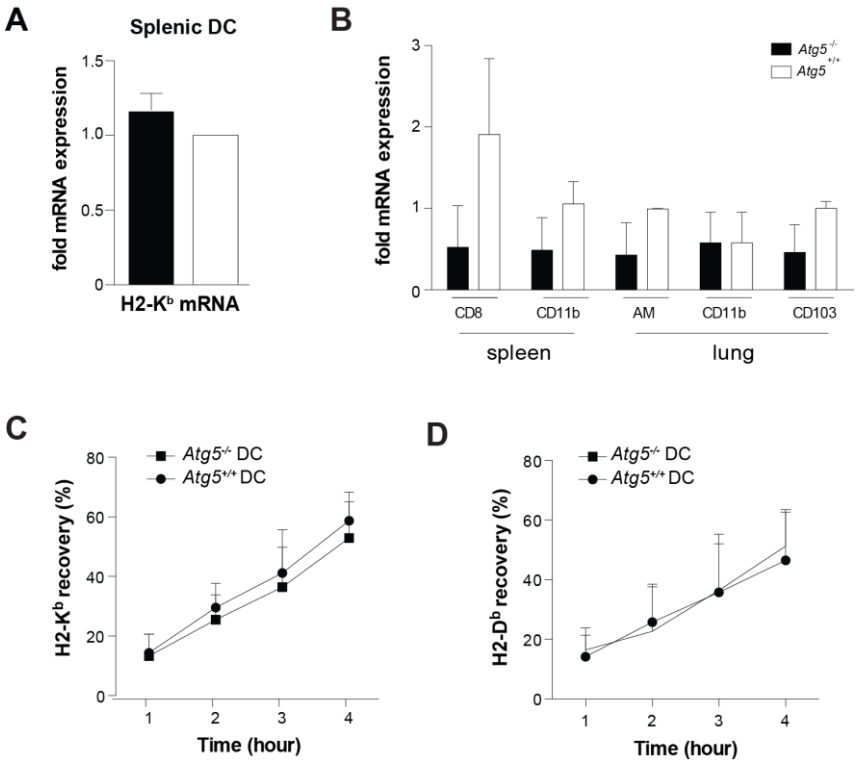

Figure 3.5 Similar MHC class I transcription and transport to the cell surface in *Atg5*$^{-/-}$deficient DCs.
(A) Quantification of MHC-I transcript levels in splenic *Atg5*$^{+/+}$ and *Atg5*$^{-/-}$ DCs. H2-K^{b} mRNA levels were determined by qRT-PCR in FACS sorted splenic DCs. Fold change in H2-K^{b} mRNA of *Atg5*$^{-/-}$ cells compared to *Atg5*$^{+/+}$

cells is represented (values are calculated using the 2exp-ΔΔct formula). Data combine 3 independent experiments. **(B)** H2-K^b transcript levels in the indicated lung and splenic DC and macrophage populations. Data are from three mice per indicated experimental group. **(C)** and **(D)** Restoration of H2-K^b and H2-D^b surface expression over time, in *Atg5*$^{-/-}$ and *Atg5*$^{+/+}$ DCs after acid stripping of surface molecules. Graphs represent the mean of 3 independent experiments.

3.1.3 Deficiency in the autophagy machinery compromises MHC class I internalization by DCs

The fourth hypothesis explored a potentially attenuated internalization of MHC-I molecules in the absence of the autophagy core machinery. Indeed, we found that antibody labelled MHC-I molecules were internalized at a slower rate in *Atg5*$^{-/-}$ compared to *Atg5*$^{+/+}$ DCs (**Figure 3.6A-D**), increasing the difference in surface labelled H2-D^b and H2-K^b molecules between *Atg* deficient and sufficient DCs over time (**Figure 3.6A-B**). Therefore, we concluded that a reduced internalization rate is responsible for higher surface expression of MHC-I molecules in *Atg5*$^{-/-}$ DCs and increased stability of MHC-I complexes on the cell surface. In good agreement with these findings, the total amount of MHC-I molecules was nearly two-fold higher in extracts of *Atg5*$^{-/-}$ splenic DCs than in the respective *Atg5*$^{+/+}$ controls as determined by immunoblot quantification (**Figures 3.6E**), suggesting enhanced degradation of MHC-I molecules after internalization in the presence of the autophagy core machinery. Moreover, these data further exclude a possible role of a more efficient recycling in absence of autophagy and strengthen our conclusions on the central role of MHC-I internalization in our model, leading both to decreased internalization and degradation of MHC class I molecules.

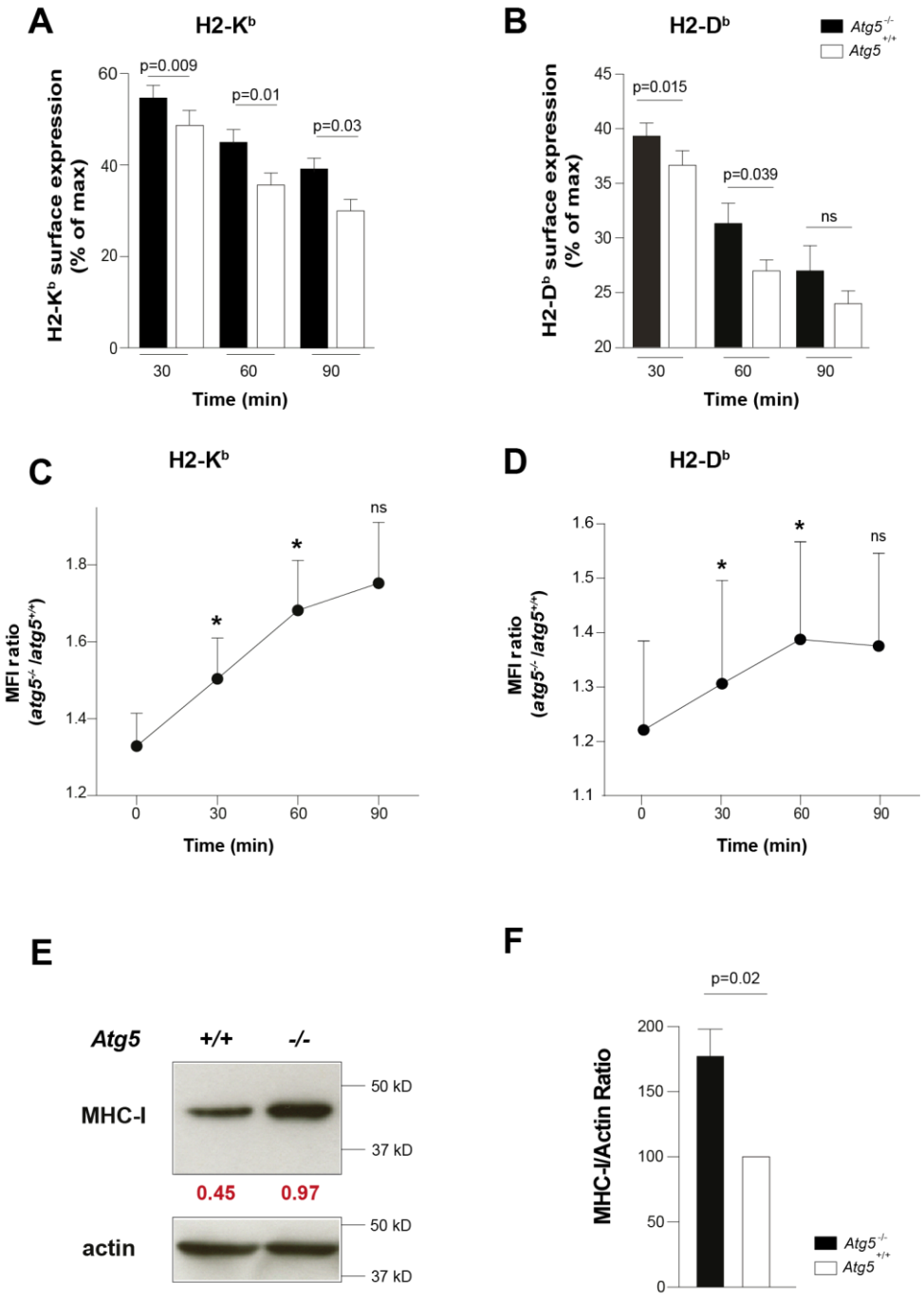

Figure 3.6 *Atg* deficiency compromises MHC class I internalization

Internalization of MHC-I molecules over time in *Atg5*$^{-/-}$ and *Atg5*$^{+/+}$ DCs. Cells were labelled with anti-H2-K^b **(A)** or anti-H2-D^b **(B)**, specific antibodies and incubated at 37°C for the indicated times. The rate of internalization at 37°C of H2-K^b molecules was evaluated by the decrease of MFI intensity compared to the MFI of control DCs incubated at 4°C and set as a reference to 100%. P values are from paired non-parametric two tailed t tests. Graphs (A and B) are the summary of 3 independent experiments. **(C)** and **(D)** The MFI ratio of H2-K^b surface staining on *Atg5*$^{-/-}$ compared to *Atg5*$^{+/+}$ DCs increases over time during incubation at 37°C. Statistics were performed using paired non parametric two tailed t tests to compare the H2-K^b MFI ratio (log values) of time 0 to 30 min (p=0.015), to 60 min (p=0.01) and to 90 min (ns, not significant) **(C)** or the H2-D^b MFI ratios (log values) of time 0 to 30 min (p=0.04), to 60 min (p=0.025) and to 90 min (ns, not significant)**(D)**. **(E)** Immunoblot analysis of MHC-I protein content in *Atg5*$^{-/-}$ and *Atg5*$^{+/+}$ splenic DCs. One representative immunoblot out of 5 is shown. Numbers below bands represent the ratio of normalized intensity of the MHC-I band compared to actin. **(F)** Summary of the MHC-I quantification, normalized to actin, for all five immunoblots as described in (E).

In order to determine if this loss of internalization in the absence of *Atg5* also affected other surface receptors we tested the expression of CD29, CD44, transferrin receptor (TfR), the co-stimulatory molecules CD80 and CD86, and MHC-II **(Figure 3.7**). Only CD80 seemed to be regulated in a similar fashion as MHC-I, as it showed a tendency towards stabilization on the cell surface of some *Atg5*$^{-/-}$ DC populations (mainly CD8^{+} splenic DCs, which could be in part due to an up-regulation of gene transcription as for MHC-I (**Figure 3.5**)), while the surface expression of the other investigated receptors was unchanged during steady-state as well as infection (**Figure 3.7**).

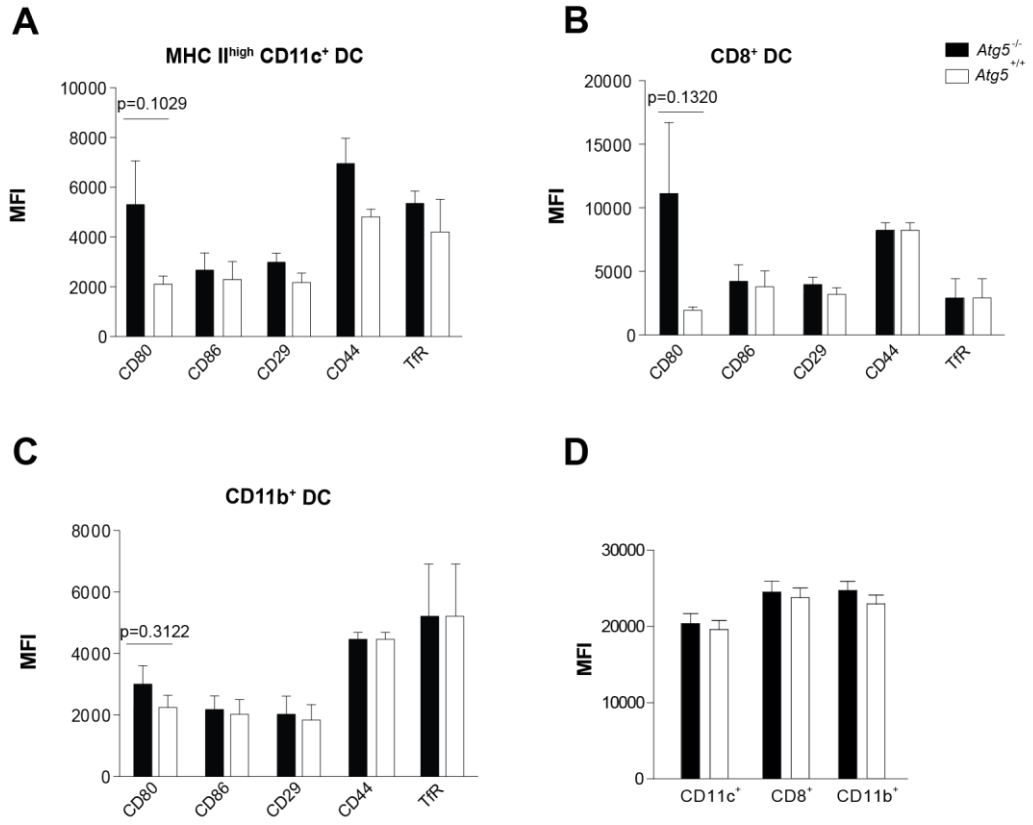

Figure 3.7 Expression of most others surface receptors is not affected by the absence of *Atg5*.
(A) Expression of surface receptors in splenic *Atg5*$^{+/+}$ and *Atg5*$^{-/-}$ DCs. Splenic DCs were gated as live CD11c^{+} MHC-II^{high} cells (GFP^{+} for *Atg5*$^{-/-}$ cells) and analysed for the expression of CD80, CD86, CD29, CD44 and transferrin receptor (TfR). Splenic DCs subsets were further divided on the basis of CD8 **(B)** and CD11b **(C)** expression. **(D)** MHC-II expression of the respective splenic DC subsets. Graphs represent the summary of MFI values from 7 independent experiments for CD80, CD86, CD29, MHC-II and 3 independent experiments for CD44 and transferrin receptor (TfR). Unpaired non-parametric two tailed t tests were used to obtain the displayed p values.

Furthermore, we also observed that vesicular MHC-I pools could not be efficiently formed in alveolar macrophages and DCs of *Atg5*$^{-/-}$ and *Atg7*$^{-/-}$ DC mice (**Figure 3.8**). These data suggest that in absence of the autophagy machinery the MHC-I molecules are not efficiently internalized

and, in agreement with previous studies (Basha, Lizee et al. 2008; Nair-Gupta, Baccarini et al. 2014), they are not efficiently shuttled to the endosomal compartment appropriate to cross-presentation.

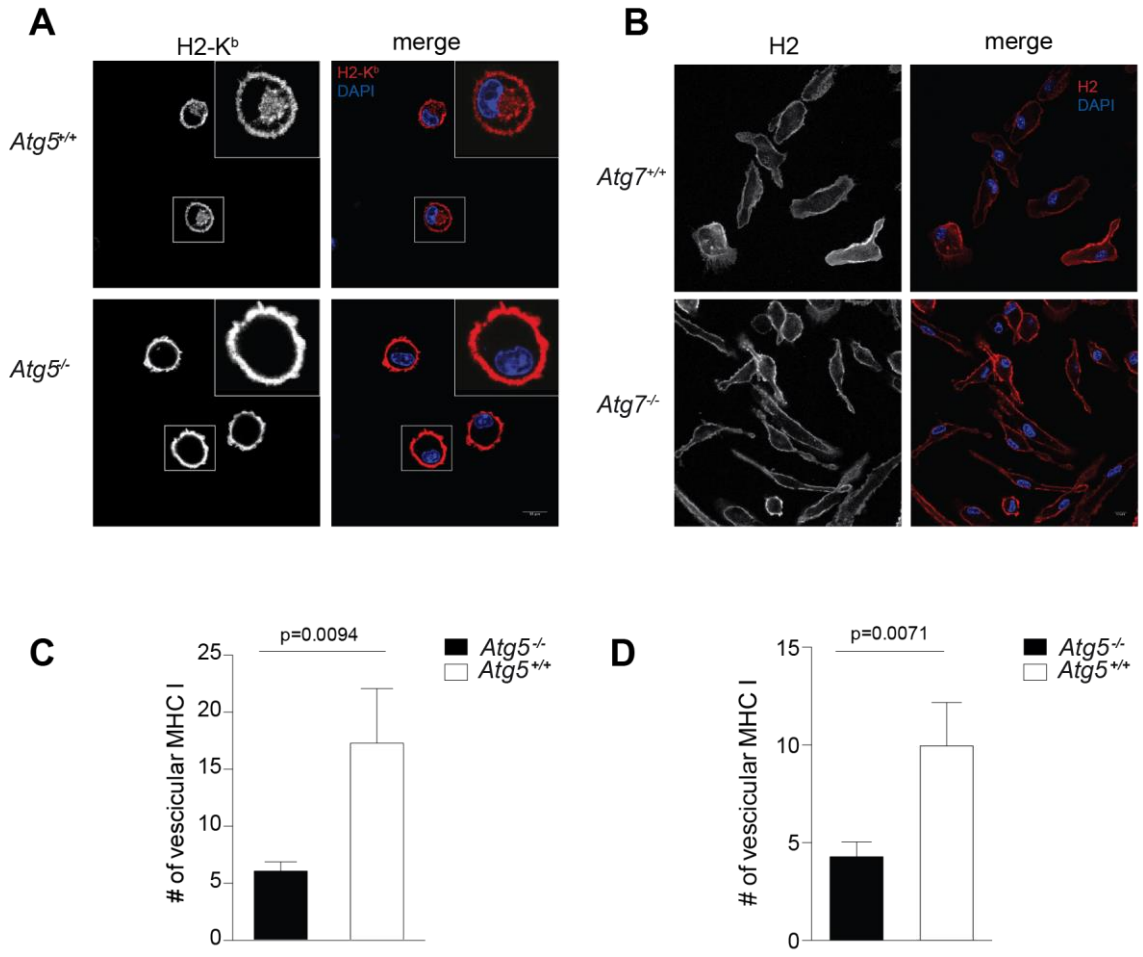

Figure 3.8 Deficiency in autophagy machinery depletes intracellular pools of MHC class I molecules
Immune fluorescence staining for H2-K^b on *Atg5*$^{+/+}$ and *Atg5*$^{-/-}$ lung CD11c$^+$ cells **(A)** and MHC-I of *Atg7*$^{+/+}$ and *Atg7*$^{-/-}$ BM-DCs **(B)**. Counterstaining for nuclear DNA was performed with DAPI. One representative experiment is shown. Scale bar indicates 10 μm. **(C)** and **(D)** Quantification of vesicular (intracellular) MHC-I staining in *Atg5*$^{+/+}$ and *Atg5*$^{-/-}$ lung CD11c$^+$ cells and BM-DCs, respectively. The presented data summarize 4 independent experiments. P values are derived from unpaired non-parametric two tailed t tests.

Finally, lysosomal degradation of MHC-I was also attenuated in *Atg5* deficient BM-DCs (**Figure 3.9**). Indeed, upon treatment with chloroquine, a lysosomotrophic agent able to inhibit lysosomal degradation, MHC-I molecules accumulate in wild type cells but not in their autophagy deficient counterpart. In parallel LC3-II also accumulated only in *Atg5* positive DCs. Thus, the autophagy machinery assists in internalization and it might help in the degradation of a subset of surface receptors, including MHC-I molecules, in DCs.

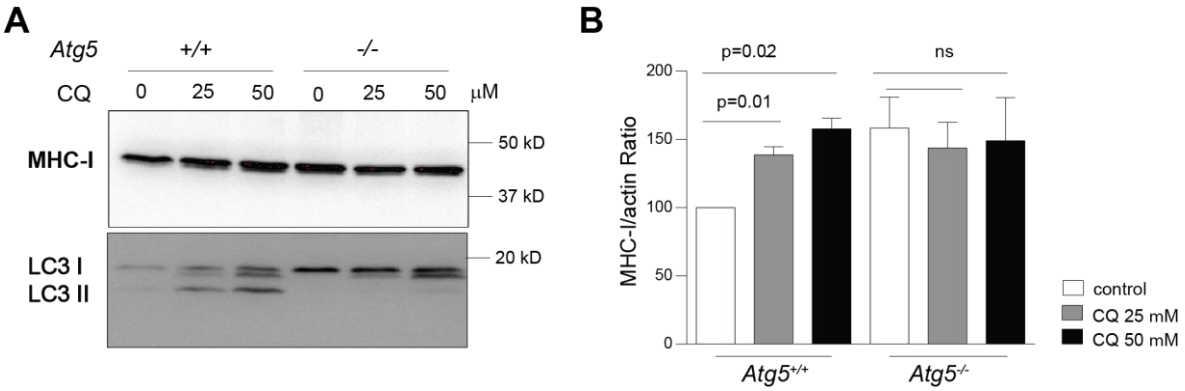

Figure 3.9 Lysosomal degradation of MHC class I is attenuated in absence of *Atg5*
(A) Immunoblot analysis of MHC -I protein content in *Atg5*$^{-/-}$ and *Atg5*$^{+/+}$ BM-DCs with and without chloroquine (CQ) treatment for 20 hours at concentrations of 25 and 50µM. One representative immunoblot out of 3 is shown. **(B)** Summary of the MHC-I quantification, normalized to actin, for all three immunoblots as described in (A). P values were determined by unpaired non- parametric two tailed t tests.

3.1.4 *Atg* deficiency compromises MHC class I association with AAK1, which regulates MHC class I internalization

In order to analyse the molecular mechanism by which the autophagy machinery assists MHC-I internalization and degradation, we immunoprecipitated MHC-I molecules from *Atg5*$^{+/+}$ murine embryonic fibroblasts (MEFs) and analysed the results by mass spectrometry. We found two molecules that were previously reported to be involved in receptor-mediated endocytosis and degradation: the AAK1 (Conner and Schmid, 2002) and the Ral A binding protein 1 (RALBP1) (Nakashima et al., 1999).

First, we confirmed the mass spectrometry results by immunoprecipitation and Western blot analysis. We were able to identify both AAK1 and RALBP1 in MHC-I immune precipitates of both *Atg5*$^{-/-}$ and *Atg5*$^{+/+}$ BM-DCs (**Figure 3.10 A-B**). However, only the association of AAK1 with MHC-I was significantly reduced in *Atg5*$^{-/-}$ BM-DCs, compared to their wild type counterparts (**Figure 3.10 A**). In good agreement, AAK1 association with MHC -I molecules was also reduced in *Atg7* deficient BM-DCs (**Figure 3.10 C**).

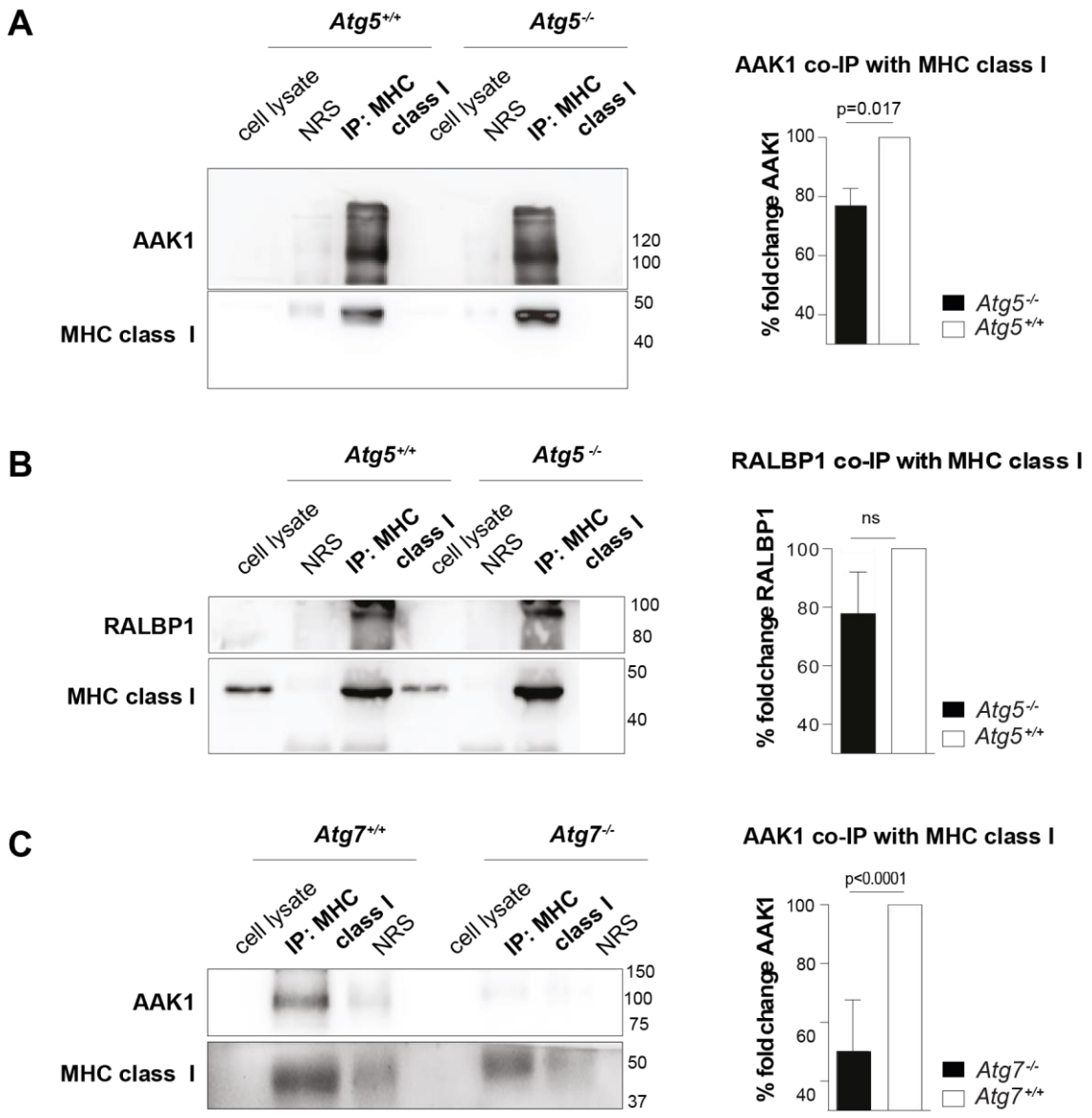

Figure 3.10 AAK1 but not RALBP1 does not efficiently associate with MHC class I in the absence of LC3 lipidation.
(A) AAK1 co-immunoprecipitation with MHC-I. Lysates of *Atg5*$^{-/-}$ and *Atg5*$^{+/+}$ BM-DCs were used to immunoprecipitate MHC -I. On the left: representative immunoblot analysis showing the co-immunopreciptation (co-IP) of AAK1 with MHC-I. On the right: quantification of 5 independent experiments. Co-immunoprecipitation intensity of AAK1 was normalized to MHC-I intensity. The AAK1 amount co-immunoprecipitated from the *Atg5*$^{-/-}$ samples (n=5 mean= 76.8%, Standard error 5.9) and the *Atg5*$^{+/+}$ samples (set to 100% as a reference) were compared. P value shown is from an unpaired non-parametric two tailed t test. (B) RALBP1 co-immunoprecipitation (co-IP) with MHC -I: lysates of *Atg5*$^{-/-}$ and *Atg5*$^{+/+}$ BM-DCs were used to immune precipitate MHC -I. On the left: representative immunoblot analysis showing the co-immunoprecipitation of RALBP1 with MHC-I. On the right: quantification of 3 independent experiments. The co-immunoprecipitation intensity of RALBP1 was normalized to MHC-I. The amount of RALBP1 co-immunoprecipitated from the *Atg5*$^{-/-}$ samples and the *Atg5*$^{+/+}$ samples (set to 100% as a reference) were compared and the indicated p value was determined by performing an unpaired non-parametric two tailed t test. **(C)** Lysates of *Atg7*$^{-/-}$ and *Atg7*$^{+/+}$ BM-DCs were used to immunoprecipitate MHC-I. On the left: representative immunoblot analysis showing the co-immunopreciptation (co-IP) of AAK1 with MHC-I. On the right: quantification of 3 independent experiments. Co-immunoprecipitation intensity of AAK1 was normalized to MHC-I intensity. The AAK1 amount co- immunoprecipitated from the *Atg7*$^{-/-}$ samples and the *Atg7*$^{+/+}$ samples (set to 100% as a reference) were compared. P value shown is from an unpaired non-parametric two tailed t test of the non- normalized values.

RNA silencing of AAK1 stabilized MHC-I levels at the plasma membrane on both MEFs and BM-DCs (**Figure 3.11**), confirming its previously published role during receptor internalization (Ricotta, Conner et al. 2002).

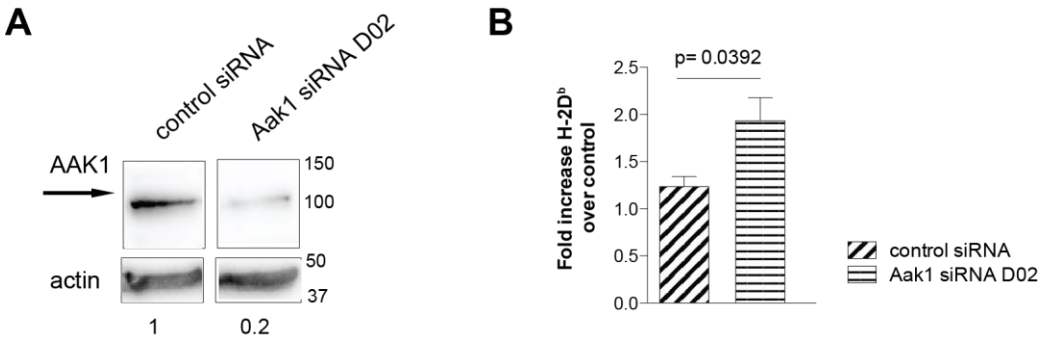

Figure 3.11 AAK1 silencing stabilized MHC class I on the cell surface
Immunoblot for AAK1 on lysates from MEFs **(A)**. One representative of 3 experiments is shown. **(B)** H2–D^b surface expression levels on MEFs after AAK1 silencing with AAK1 specific siRNA as well as control siRNA. 4 experiments are summarized. P values were obtained from unpaired non-parametric two tailed t tests.

Additionally, using the iLIR platform (Kalvari, Tsompanis et al. 2014); http://repeat.biol.ucy.ac.cy/iLIR/), we predicted two and one LIR (LC3-interacting region) motifs in the murine AAK1 and RALBP1 proteins, respectively (**Scheme 3.2**)

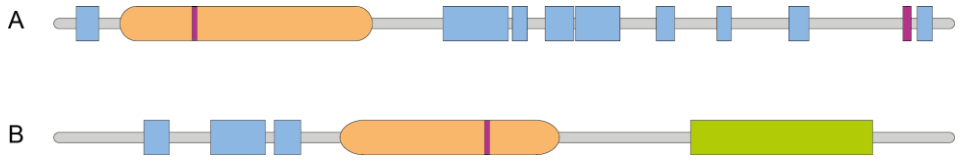

Scheme 3.2 Predicted LIR motifs on AAK1 and RALBP1
Representation of the domains of AAK1 **(A)** and RALBP1 **(B).** Purple lines represent the predicted LIR motifs. AAK1118-123: DVWEVL [score 18], AAK1914-919: DEFDPI [score 15], RALBP1318-323: LSWLIV [score 16].

Interestingly, the LIR sequences are conserved in the human AAK1 protein, but not in human RALBP1. We validated the interactions of LC3 with AAK1 and RALBP1 by co-immunoprecipitations. Indeed, we found that both, AAK1 (**Figure 3.12A**) and RALBP1 (**Figure 3.12B**) could be co-immunoprecipiated with LC3, but this association did not seem to be influenced by the autophagy core machinery. These data suggest that LC3 lipidation via the autophagy core machinery is required to efficiently localize AAK1 to MHC-I molecules for optimal internalization and degradation.

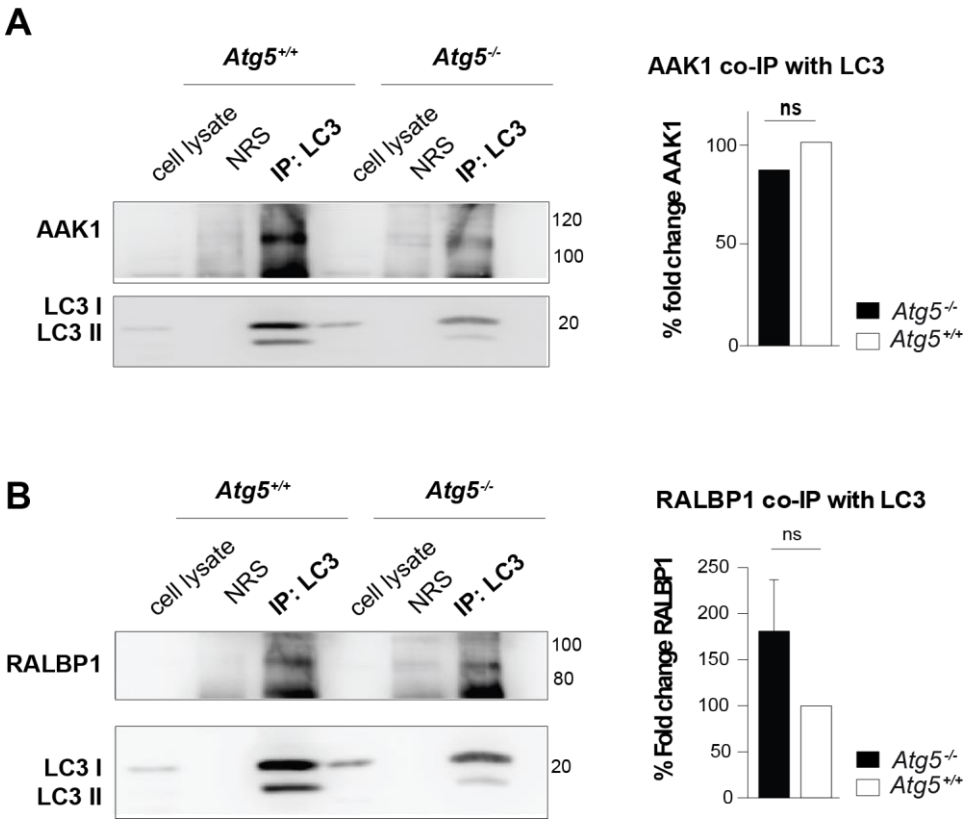

Figure 3.12 AAK1 and RALBP1 association with LC3 is not influenced by autophagy machinery.
(A) AAK1 co-immunoprecipitate with LC3. Lysates from *Atg5*$^{-/-}$ and *Atg5*$^{+/+}$ BM-DCs were used to immune precipitate LC3. On the left: representative immunoblot analysis showing the co-immunoprecipitation (co-IP) of AAK1 with LC3. On the right: quantification of 3 independent experiments. The co-immunoprecipitation intensity of AAK1 was normalized to the total LC3 (I and II). The amount of AAK1 co- immunoprecipitated from the *Atg5*$^{-/-}$ samples (n=3) and the *Atg5*$^{+/+}$ samples (set to 100% as a reference) were compared. Statistical analysis was performed with an unpaired non-parametric two tailed t test (ns, not significant). **(B)** RALBP1 co-immunoprecipitates with LC3: lysates from *Atg5*$^{-/-}$ and *Atg5*$^{+/+}$ BM-DCs were used to immune precipitate LC3. On the left: representative immunoblot analysis showing the co-immunoprecipitation (co-IP) of RALBP1 with LC3. On the right: quantification of 3 independent experiments. The co-immunoprecipitation intensity of RALBP1 was normalized to the total LC3 (I and II). The amount of RALBP1 co-immunoprecipitated in the *Atg5*$^{-/-}$ samples (n=3) and the *Atg5*$^{+/+}$ samples (set to 100% as a reference) was compared and the indicated p value was determined by performing unpaired non-parametric two tailed t tests (ns, not significant).

3.1.5 Enhanced antigen presentation on stabilized MHC class I molecules by autophagy deficient DCs *in vitro*

In order to correlate the enhanced MHC-I expression on *Atg5*$^{-/-}$ DCs with better antigen presentation we tested the ability of DCs deficient in the autophagy machinery to restimulate anti-viral CD8^{+} T cell responses *in vitro*. We co-cultured influenza A virus (IAV) infected *Atg5*$^{+/+}$ or *Atg5*$^{-/-}$ DCs with virus specific polyclonal memory T cells isolated from IAV infected wild-type animals. We found that infected *Atg5*$^{-/-}$ DCs were able to expand IAV specific memory CD8^{+} T cells more efficiently than *Atg5*$^{+/+}$ DCs (**Figure 3.13A-B**). This applied to both influenza NP specific and overall CD8^{+} T cell populations. In contrast, IAV CD4^{+} T cell expansion was not

significantly different when stimulating with *Atg5*$^{-/-}$ or *Atg5*$^{+/+}$ influenza infected DCs (**Figure 3.13C**).

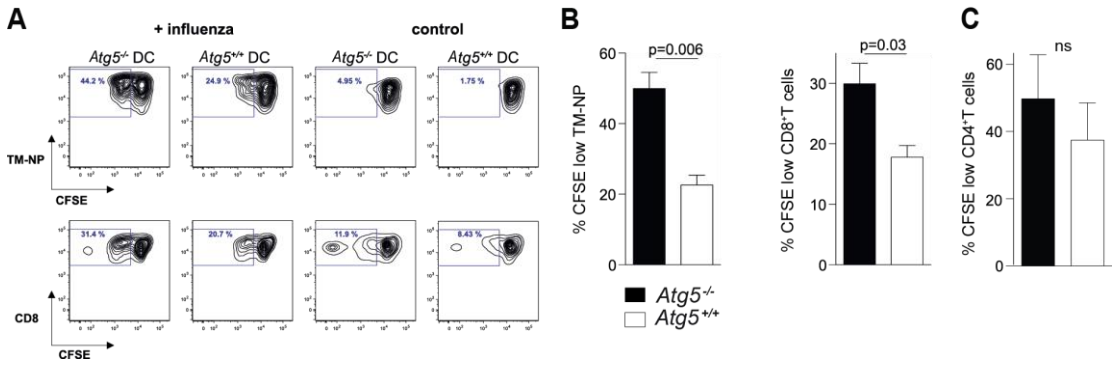

Figure 3.13 Dendritic cells deficient in the molecular autophagy machinery have greater antigen presentation capacity to CD8$^+$ T cells *in vitro*.

(A) Influenza A virus infected or control *Atg5*$^{-/-}$ and *Atg5*$^{+/+}$ splenic DCs were co-cultured with carboxyfluorescein succinimidyl ester (CFSE) labelled influenza virus-specific polyclonal memory T cells isolated from infected wild type animals. T cell proliferation was determined after 3 days of co-culture by flow cytometry. Percent of CFSE low cells of influenza NP1$_{366-374}$/H2-D^b tetramer positive (TM-NP, upper row) or total IAV specific CD8$^+$ T cells (lower row) are indicated. One representative experiment out of 3 is shown. **(B)** Graphical analysis of T cell proliferation from 3 independent experiments. P values were determined by unpaired non-parametric two tailed t tests. **(C)** *Atg5*$^{-/-}$ and *Atg5*$^{+/+}$ DCs were co-cultured with CFSE labelled influenza specific polyclonal memory T cells isolated from wild type influenza virus infected mice. T cell proliferation was determined after 3 days of co-culture by flow cytometric analysis of the percentage of CFSE low CD4$^+$ cells. Graph summarizing 3 independent experiments is shown. Statistical evaluation was performed with unpaired non-parametric two tailed t tests.

Moreover, NP1$_{366-374}$ peptide epitope pulsed *Atg5*$^{-/-}$ DCs also expanded polyclonal IAV specific memory T cells more efficiently than *Atg5*$^{+/+}$ DCs (**Figure 3.14**). Blocking CD80 during this *in vitro* restimulation did not significantly affect T cell proliferation (**Figure 3.14**). Therefore, we concluded that autophagy deficiency causes enhanced antigen presentation of MHC-I restricted IAV derived epitopes by DCs.

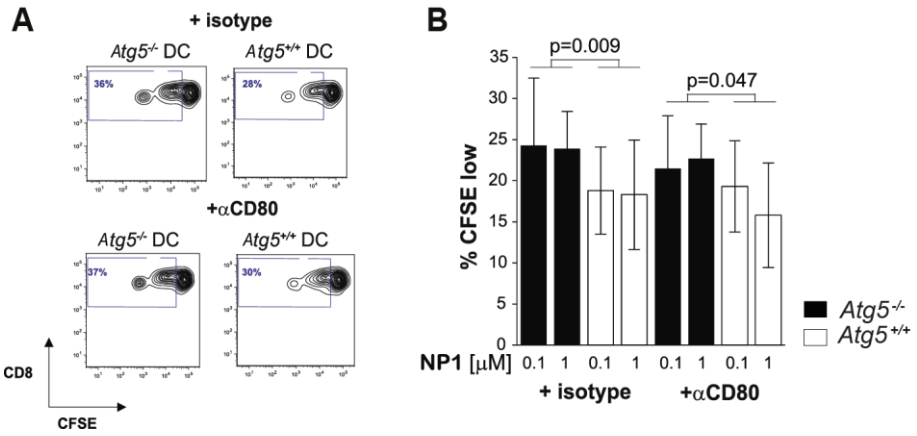

Figure 3.14 Autophagy deficiency causes enhanced antigen presentation of MHC class I restricted IAV derived epitopes by dendritic cells.

(A) $NP1_{366-374}$ pulsed *Atg5*$^{-/-}$ or *Atg5*$^{+/+}$ splenic DCs were co-cultured with CFSE labelled influenza virus-specific polyclonal memory T cells isolated from infected wild type animals. T cell proliferation was determined after 3 days of co-culture with CD80 blocking antibody (+αCD80) or isotype control (+isotype) by flow cytometry. Percent of CFSE low cells of total CD8$^+$ T cells are indicated. One representative experiment out of 3 is shown. **(B)** Summary of CD8$^+$ T cell proliferation assay with 0.1 and 1 μM $NP1_{366-374}$ peptide pulsed DCs as outlined in C values were determined by paired two tailed t tests.

3.1.6 Elevated CD8$^+$ T cell responses in DCs lacking LC3 lipidation protects from influenza A viral infection

In order to validate our results *in vivo*, we infected *Atg5*$^{-/-}$ DC mice and their wild-type littermates (*Atg5*$^{+/+}$ DC mice) with high dose (10 HAU) of IAV. The resulting CD8$^+$ T cell responses specific for influenza antigens ($NP1_{366-374}$, $NP_{2311-325}$ and $HA_{211-225}$) were markedly enhanced in mice lacking the autophagy machinery in DCs (**Figure 3.15**). Indeed, the magnitude of the specific CD8$^+$ T cell response at day 11 post-infection was two to four times greater in *Atg5*$^{-/-}$ DC than in *Atg5*$^{+/+}$ DC mice (**Figure 3.15**). In parallel, the specificity of the anti-viral CD8$^+$ T cell responses was broader in *Atg5*$^{-/-}$ DC animals since at least two additional subdominant CD8$^+$ T cell epitopes ($HA_{211-225}$ and $NP2_{311-325}$) were recognized at frequencies reaching 10% of CD8$^+$ T cells apart from the dominant $NP1_{366-374}$ epitope in the C57BL/6 mouse background (**Figure 3.15**). Accordingly, recognition of subdominant IAV epitopes reached levels of wild type dominant epitope recognition in *Atg5*$^{-/-}$ DC mice (**Figure 3.15**).

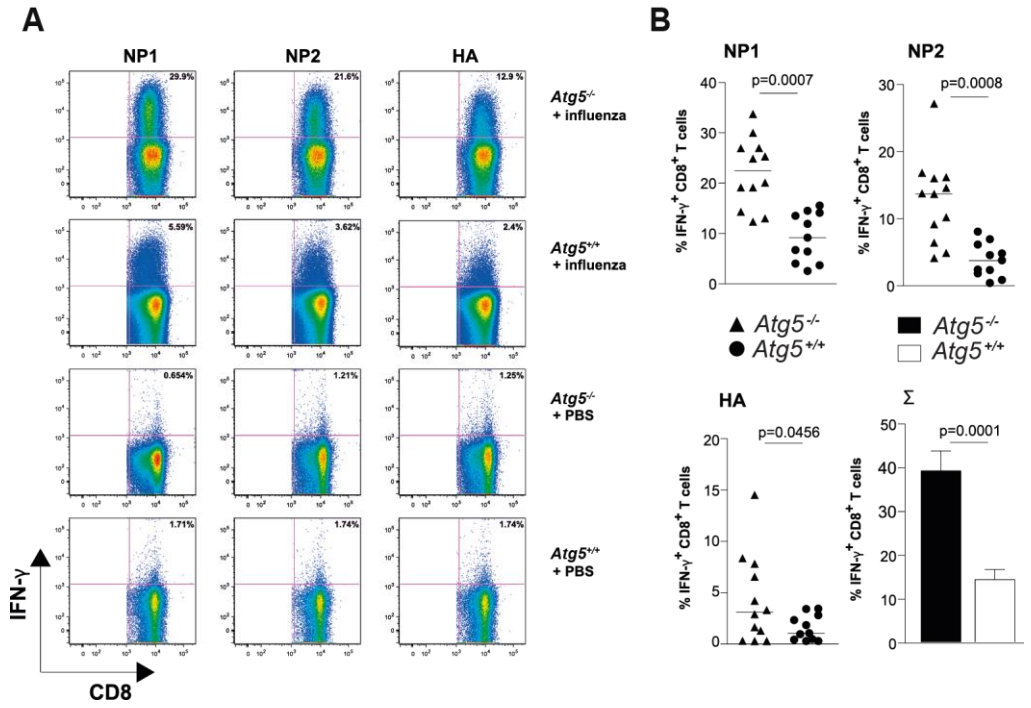

Figure 3.15 Broader specificity and enhanced magnitude of influenza specific CD8⁺ T cell responses in mice lacking *Atg5* in their dendritic cells.

(A) and **(B)** Levels of influenza virus specific CD8⁺ T cells in the lungs of wild-type mice (*Atg5*$^{+/+}$ DC) and mice with *Atg5* deficient DCs (*Atg5*$^{-/-}$ DC) were assessed 11 days after intranasal infection with 10 HA units of influenza virus strain A/PR8. Intracellular interferon-γ (IFN-γ) staining of CD8⁺ T cells after *in vitro* peptide re-stimulation with 3 different viral epitopes ($NP1_{366-374}$, $NP_{2311-325}$ and $HA_{211-225}$) was determined by flow cytometry. Background secretion was subtracted for every peptide, and determined for every mouse by using an irrelevant peptide control (Ny-ESO-$1_{157-170}$). **(A)** Representative FACS plots of PBS mock-infected or influenza infected mice. **(B)** Quantification of the specific anti-viral CD8⁺ T cell responses to the 3 different viral epitopes ($NP1_{366-374}$, $NP_{2311-325}$ and $HA_{211-225}$) or their sum (Σ). Data are from three independent experiments, each with three to four mice per group. P values are from non-parametric unpaired two tailed t tests.

Furthermore, we found that elevated CD8⁺ T cell responses correlated with protection from IAV induced disease. The infectious lung viral titres at day 8 were significantly reduced in *Atg5*$^{-/-}$ DC mice (**Figure 3.16A**) indicating that the increased CD8⁺ T cell responses in the absence of the autophagy core machinery protected from morbidity during influenza A virus infection.

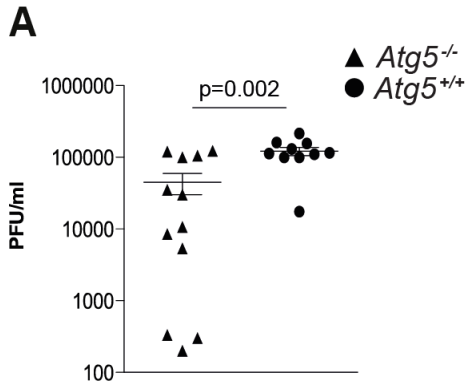

Figure 3.16 Increased CD8⁺ T cell responses in the absence of the autophagy core machinery protected from morbidity during influenza A virus infection

(A) Influenza lung viral titres were determined at day 8 post influenza infection, from supernatants of total lung homogenates from *Atg5*$^{-/-}$ or *Atg5*$^{+/+}$ DC mice infected with 10 HAU of influenza A/PR8. Unpaired non-parametric two tailed t tests were used to obtain the indicated p values.

The specific anti-viral CD4^{+} T cell responses and the influenza specific antibody titres were not significantly different in *Atg5*$^{-/-}$ DC animals compared to their wild- type littermates (*Atg5*$^{+/+}$ DC) (**Figures 3.17**).

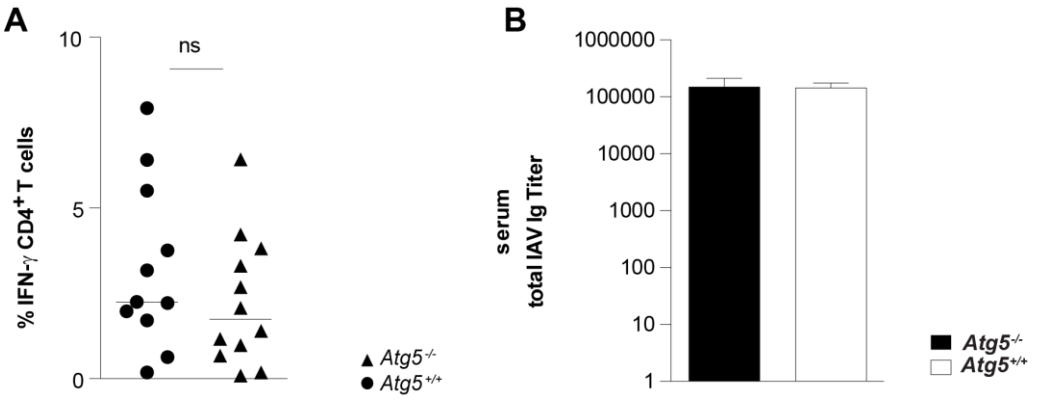

Figure 3.17 IAV-specific CD4^{+}T cells response and antibody titers are not affected in the absence of autophagy
(A) The specific antiviral CD4^{+} T cell response is not significantly different in *Atg5*$^{-/-}$ DC animals compared to *Atg5*$^{+/+}$ DC animals. Influenza virus specific CD4^{+} T cells in the lungs of infected animals were assessed 11 days after intranasal infection with 10 HA units of influenza virus strain A/PR8. Intracellular interferon gamma (IFN-γ) staining of CD4^{+} T cells after *in vitro* peptide re-stimulation with the 2 different viral epitopes NP2$_{311-325}$ (H2-Ab restricted) and HA$_{211-225}$ (H2-Ab restricted) was determined by flow cytometry. Data are from three independent experiments with three to four mice per group. **(B)** Influenza A virus PR8 specific antibody titres were determined by serial dilution of serum collected at d11 post infection with 10 HA units. Data are from three independent experiments with three to four mice per group.

In good agreement, MHC-I surface expression remained elevated on *Atg5* deficient DCs and macrophages during IAV infection (**Figure 3.18**), while with the exception of CD80 co-stimulatory molecules were unchanged (**Figure 3.18**). Thus, while the protective CD8^{+} T cell response is selectively enhanced in infected mice with *Atg5* deficient DCs, CD4^{+} T cell and antibody responses are unaffected.

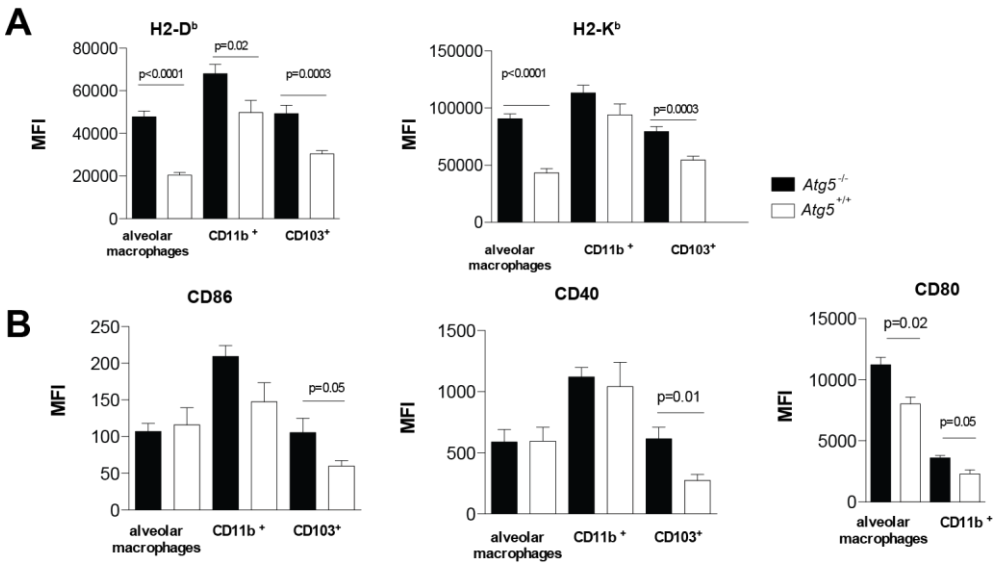

Figure 3.18 During IAV infection MHC class I levels remain elevated in absence of *Atg5*
(A) MHC -I surface levels on the indicated *Atg5*$^{+/+}$ and *Atg5*$^{-/-}$ lung DC and macrophage populations at day 4 of IAV infection. Data are from 3 independent experiments with 3 to 4 mice per group. P values are derived from unpaired non-parametric two tailed t tests. **(B)** Surface levels of the indicated co-stimulatory molecules on *Atg5*$^{+/+}$ and *Atg5*$^{-/-}$ lung DC and macrophage populations at day 4 of IAV infection. P values are derived from unpaired non-parametric two tailed t tests.

3.1.7 Cytokine production and early viral titres in Influenza A infected mice with DCs that lack components of the autophagy machinery

In the initial stage of influenza infection, innate immunity and cytokine secretion play an important role in controlling the replication rate of the virus and the following inflammation and adaptive immune response. In order to exclude that changes in early innate immune control would allow influenza A virus to replicate to higher viral titres resulting in elevated IAV specific CD8$^+$ T cell responses in *Atg5*$^{-/-}$ DC mice, we analysed cytokine production and IAV titres on day 3 after infection. Cytokine secretion in response to infection was similar for IL-6 and IFN-γ in *Atg5*$^{-/-}$ DC mice (**Figures 3.19A-B**). IL-1β, however, was increased (**Figure 3.19C**), but these elevated IL-1β levels were not able to control IAV infection early on, as demonstrated by similar viral titres between wild-type and knock-out mice on day 3 after infection (**Figure 3.19D**). Therefore, changes in innate immune control are unlikely to account for the elevated CD8$^+$ T cell responses and improved immune control in *Atg5*$^{-/-}$ DC mice.

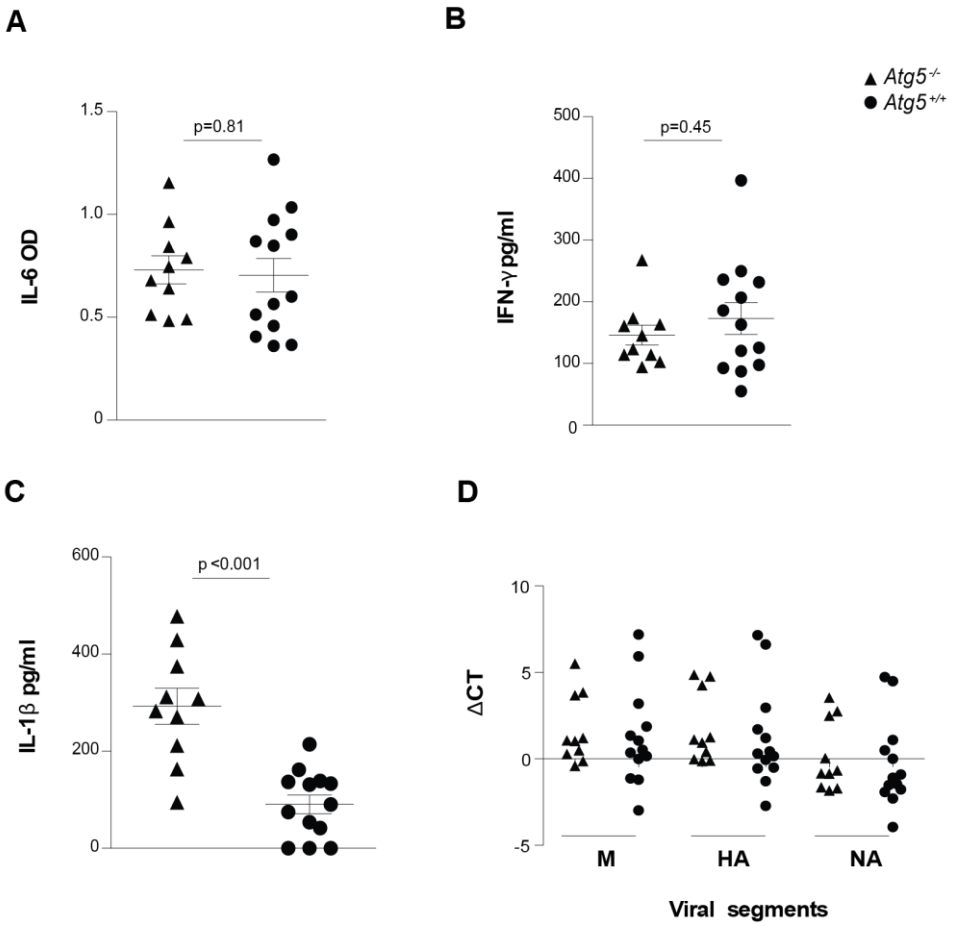

Figure 3.19 Innate immune protection to influenza A virus is not different in *Atg5*$^{-/-}$ DC mice at day 3 post infection. **(A)** *Atg5*$^{-/-}$ and *Atg5*$^{+/+}$ DC mice were infected with 10 HA units for 3 days. **(A)** and **(B)** IL-6, IFN-γ and IL-1β levels **(C)** were measured by ELISA assays in lung homogenates. **(D)** Viral RNA was quantified in lung homogenates at day 3 post infection: Graph representing delta CT values of quantitative RT-PCR for 3 viral segments (M, HA and NA) are shown. Results are from 3 independent experiments with at least 3 mice per group. In each experiment PBS treated mice were used as negative controls.

3.1.8 Elevated CD8^{+} T cell responses to two LCMV epitopes during infection of mice with DCs deficient in the autophagy machinery

In order to address the role of elevated MHC -I expression on *Atg5*$^{-/-}$ DCs for better CD8^{+} T cell priming in a different infectious model, we tested acute LCMV infection. *Atg5*$^{-/-}$ DC animals and their wild-type littermates (*Atg5*$^{+/+}$ DC) were infected intravenously with the wild type LCMV Armstrong strain at a dose of 10^{4} plaque forming unit (PFU). The specific CD8^{+} T cell response to two viral epitopes was monitored at day 6 and day 11 post infection. We did not find a difference in the anti-viral CD8^{+} T cell response at day 6 between the two groups (data not shown). However at day 11, the anti-viral CD8^{+} T cell response was significantly elevated in *Atg5*$^{-/-}$ DC animals (**Figure 3.20**). The percentages of MHC-I tetramer positive cells that are

specific to two viral LCMV epitopes, the immunodominant H2-D^b-NP_{396} and the subdominant H2-K^b-GP_{34} epitope, were up to two-fold higher in *Atg5*$^{-/-}$ DC animals (**Figure 3.20**). These data suggest that stabilized MHC -I levels on autophagy machinery deficient DCs contribute to elevated priming of anti-viral $CD8^+$ T cell responses *in vivo*.

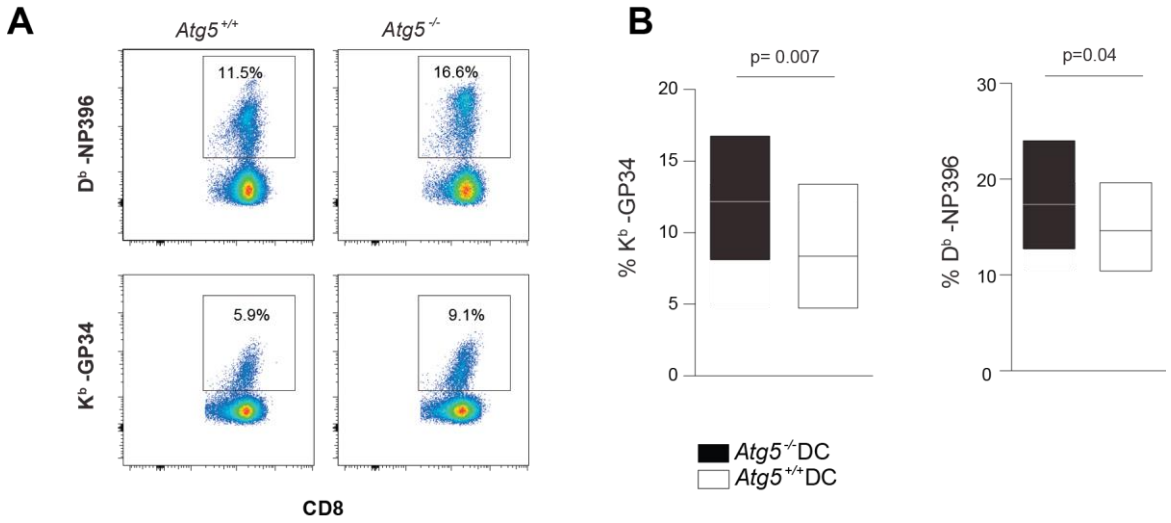

Figure 3.20 Enhanced LCMV specific $CD8^+$T cell responses in mice lacking the autophagy machinery in their DCs.
Atg5$^{-/-}$ DC animals and their wild-type littermates (*Atg5*$^{+/+}$ DC) were infected intravenously with the wild type LCMV Armstrong strain at a dose of 10^4 PFU. The specific $CD8^+$ T cell response to two viral epitopes was monitored in the blood, at day 11 post infection, using specific MHC-I tetramers. Data are from three independent experiments, each with three to four mice per group. **(A)** Percentage of MHC-I tetramer positive cells of $CD8^+$ T cells specific for the H2-D^b restricted $NP_{396\text{-}404}$ (D^b-NP_{396}, upper row) or the H2-K^b restricted $GP_{34\text{-}43}$ (K^b-GP_{34}, lower row) epitope in the blood of *Atg5*$^{+/+}$ or *Atg5*$^{-/-}$ DC mice. **(B)** Combined data as in **(A)** for all three experiments. Paired non-parametric two tailed t tests were performed on the mean values from each experiment to obtain the indicated p values.

Taking together these findings clearly demonstrate that the molecular machinery of autophagy not only serves for transporting cytoplasmic constituents for lysosomal degradation, but that it also assists in the process of MHC-I internalization and in their absence more stimulatory MHC-I molecules are present on the surface of DCs to elicit elevated $CD8^+$ T cell response

Further studies will need to address how one might selectively regulate these different autophagy functions on MHC-I-restricted antigen presentation for therapeutic interventions to boost adaptive immunity.

Part II- Autophagy in MHC class I antigen processing

3.2.1 EBNA1 targeting to autophagosomes increases MHC class I antigen presentation to CD8+ T cells mainly in TAP deficient cells

The autophagy machinery restricts MHC-I presentation by attenuating MHC-I surface expression levels. However, as it is a catabolic process by nature, it is also tempting to speculate that autophagy has a role in antigen processing for MHC-I presentation, especially under conditions of classical MHC-I pathway impairment, for example during viral infection such as by herpes viruses. The involvement of autophagy in unconventional MHC-I antigen presentation were addressed by investigating the MHC-I presentation of intracellular Epstein Barr virus (EBV) antigens, such as the latency protein EBNA1 in lymphoblastoid cells (LCLs), namely HLA-B*3501 transgenic TAP-deficient (T2.B35) and TAP-sufficient (T1.B35) B cells. Both of these cell lines are latently infected with EBV but T2 cells express at their surface lower levels of MHC-I molecules in comparison to T1 since the lack of TAP results in inefficient formation of peptide-MHC-I complexes due to poor availability in the ER of high affinity peptides (**Figure 3.21A**). Moreover, in order to investigate to what extent epitope display could be enhanced by increasing EBNA1 expression and subcellular targeting, T2.B35 and their HLA-B*3501-expressing parental cells T1.B35 have been transduced with GFP-tagged lentiviral vectors expressing different constructs of the immunogenic C-terminus of the EBV latency protein EBNA1 ($EBNA1_{400-641}$), defective for the glycine-alanine repeats (GAr) that are responsible for the inhibition of EBNA1 presentation on MHC-I molecules via compromising EBNA1 mRNA translation as well as its own proteasome degradation (Yin, Manoury et al. 2003; Daskalogianni, Apcher et al. 2008). These include GAr-depleted EBNA1 (E1Δ), Invariant chain-EBNA1 (Ii-E1Δ), which would allow a more efficient delivery into the MHC-II loading compartment, and EBNA1-LC3 (E1Δ-LC3) to target autophagosomes (**Figure 3.21B**).

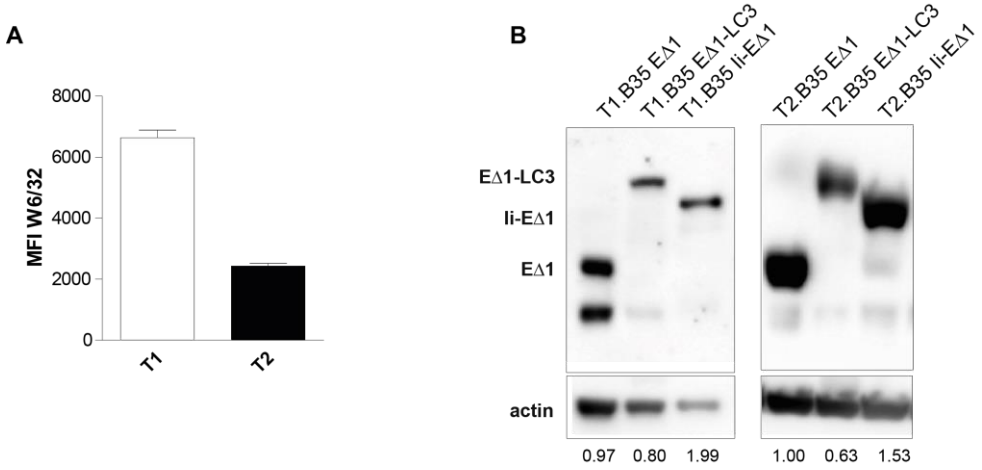

Figure 3.21 Characterization of the cellular model used for the study
(A) Surface expression of MHC-I molecules on untransfected wild type (T1) and TAP-deficient (T2) lymphoblastoid cell lines (LCLs). Cells were stained with FITC-labelled anti-MHC-I (w6/32) and analysed by FACS. Graph summarize the mean fuorescence intensity (MFI) and SEM. **(B)** LCLs were lentiviral transduced with different EBNA1 constructs (GAr-depleted EBNA1 (E1Δ), EBNA1-LC3 (E1Δ-LC3), and Invariant chain-EBNA1 (Ii-E1Δ)) and their protein content was analysed by Western blot. Numbers below bands indicate the ratio of normalised intensity of the EBNA1 construct band compared to actin.

The specific $CD8^+$ T cell recognition of an EBNA1 epitope ($EBNA1_{407-417}$) was then evaluated by IFN-γ production after overnight coculture of TAP-sufficient and –deficient HLA-B*3501 cells with an $EBNA1_{407-417}$ specific $CD8^+$T cell clone. Preliminary data surprisingly show that overall T2.B35 cells were slightly better than T1.B35 in triggering IFN-γ release (**Figure 3.21A**). More interestingly, epitope presentation increased with elevated antigen expression, especially when EBNA1 was fused with LC3 and targeted to autophagosomes in T2.B35 cells, providing the first promising evidence that in this model, for this epitope, autophagy could be involved in antigen presentation on MHC-I molecules, preferentially in the absence of TAP (**Figure 3.22A**). Interestingly, fusion with Ii also led to an increased antigen presentation by cells lacking in TAP expression, suggesting a targeting of MHC-I to the endolysosomal compartment for loading in conditions of defective MHC-I pathway (**Figure 3.22A**).

3.2.2 Effects of autophagy manipulation on MHC class I presentation of EBNA1

To evaluate the involvement of autophagy in MHC-I presentation of EBNA1 epitopes, changes in EBV antigen presentation were evaluated after pharmacological inhibition of autophagy. Untransfected and EBNA1 constructs transfected T1.B35 and T2.B35 cells were exposed to the lysosomotropic agent chloroquine for 6 h prior overnight coculture with the

EBNA1-specific CD8+T cell clones (**Figure 3.22B**). Surprisingly, the overall effect of CQ was to increase IFN-γ production in response of antigenic presentation provided by all cells treated with CQ in comparison to the untreated ones (**Figure 3.22C**), with a more pronounced effect on T2.B35 cells. Indeed, upon CQ treatment the difference between T1.B35 and T2.B35 in their ability to present EBNA1$_{407-417}$ became more pronounced (**Figure 3.22B**). Similarly, targeting of EBNA1 to autophagosomes and to MIIC in the presence of CQ results in a statistically significant increase in IFN-γ production in comparison to untransfected cells (**Figure 3.22B**).

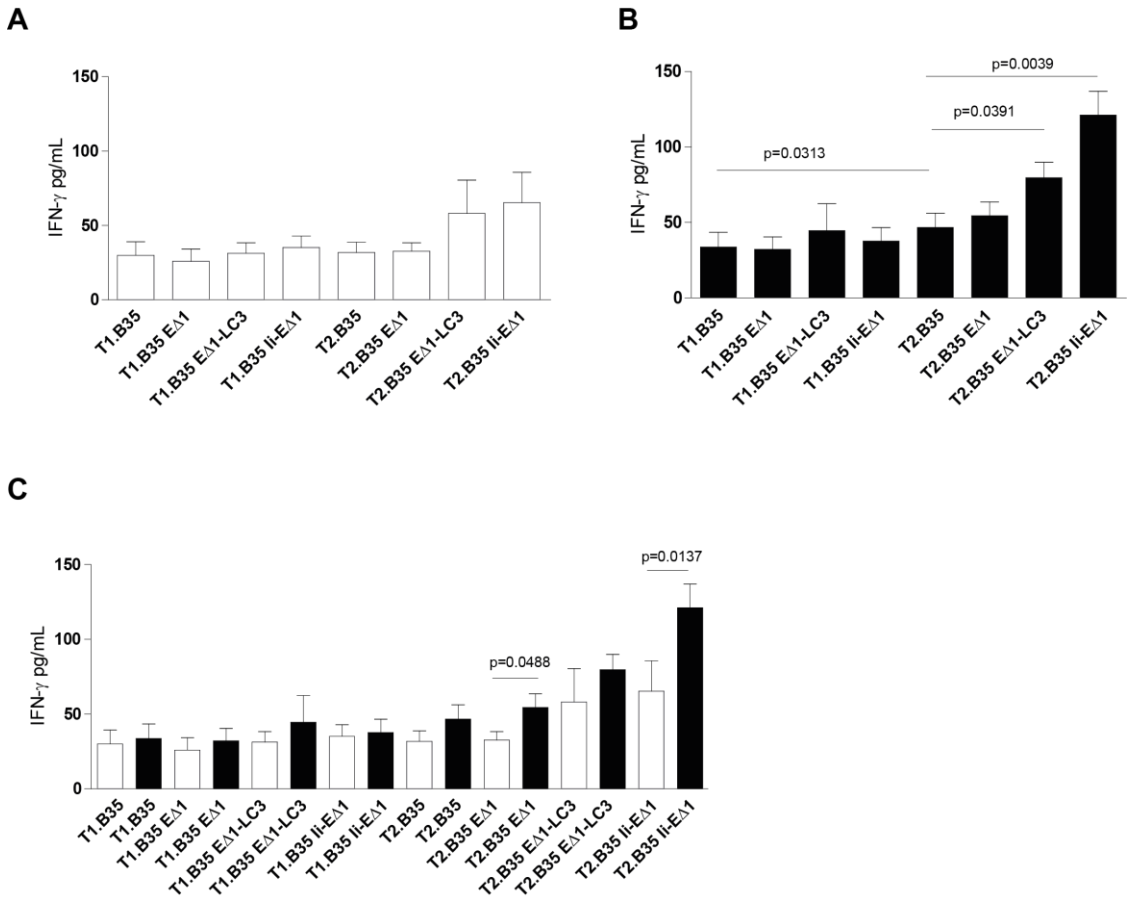

Figure 3.22 Increased EBNA1 MHC class I-restricted presentation in absence of TAP

Untransfected and EBNA1 constructs (GAr-depleted EBNA1 (E1Δ), EBNA1-LC3 (E1Δ-LC3), and Invariant chain-EBNA1 (Ii-E1Δ)) transfected HLA-B*3501 TAP-sufficient and deficient cells (T1.B35 and T2.B35, respectively) were coculture with EBNA1$_{407-417}$-specific CD8+ T cell clones (ratio LCLs:T cells 10:1) and IFN-γ production was quantified by ELISA assays. **(A)** untreated cells; **(B)** LCLs were treated with chloroquine (CQ) for 6 hours before overnight coculture with CD8+T cell clones; **(C)** Comparison of IFN-γ production by CD8+T cells clones after coculture with either untreated and CQ treated LCLs. Graphs summarise data from 5 independent experiments. Bars indicate mean +/- SEM. If not indicate data are not statistically significant.

These preliminary data suggest that CQ, by blocking the final step of autophagy, such as the acidification of the autophagosomes, might redirect the fusion of autophagosomes with

endosomal compartment rich in MHC-I molecules that are available for loading and recycling to the cell surface. Alternatively, CQ also prevents internalized MHC-I degradation and allows it to also more efficiently gain access to vesicular loading compartments. Moreover, CQ-dependent enhancement of LC3 lipidation might result in a higher contribution of autophagy to antigen presentation. Studies on the effects of autophagy manipulation via different pharmacological agents or via specific silencing are ongoing.

3.3.3 Characterization of autophagy in antigen presentation in TAP deficient cells

Subsequently, the possible role of autophagy in intracellular antigen processing was studied in more detail by immunofluorescence. Analysis of MHC-I and LC3 localization in both HLA-B*3501 wild type and TAP-negative cells by confocal microscopy revealed that MHC-I molecules reside within LC3-positive compartments preferentially in the absence of TAP, strengthening the hypothesis mentioned earlier that autophagosomes could fuse with MHC loading endosomal compartment. Accordingly, the supply of more antigens seemed to result in a further increase of LC3/MHC-I colocalization, when EBNA1 is targeted to $LC3^+$ or Ii^+ compartments (**Figure 3.23**).

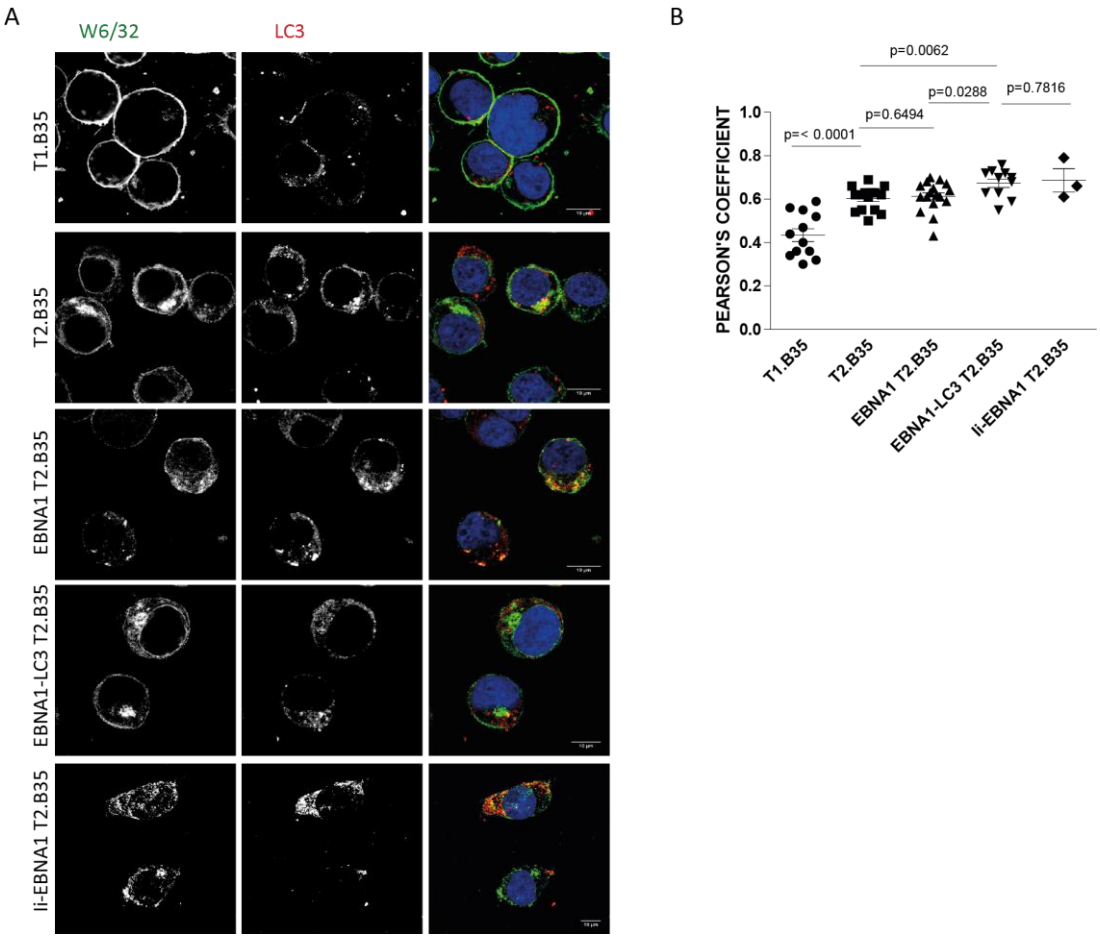

Figure 3.23 Immune fluorescence staining and colocalization analysis for MHC class I and LC3
LCLs were cytospun onto slides, fixed in 4% paraformaldehyde 20 min at RT and then assessed for the localisation of either MHC-I with LC3 **(A)** by co-staining with the pan MHC-I w6/32 and anti-LC3 antibodies followed by AlexaFluor-488-labelled goat anti-mouse and AlexaFluor-555 goat anti-rabbit antisera, respectively. **(B)** Pearson's coefficient for MHC-I and LC3 colocalization. Unpaired non-parametric two tailed t tests were performed to obtain the indicated p values.

3.3.4 Characterization of MHC-I source and MHC-I loading compartment in absence of TAP

As in absence of TAP it is unlikely that the MHC-I loading would take place within the ER, we tried to investigate in which compartment the alternative MHC-I loading could take place and which is the source of MHC-I molecules for this compartment. In order to address where the MHC-I molecules come from, we stained wild type and TAP-deficient HLA-B*3501 cells for AAK1, a kinase shown to facilitate MHC-I internalization upon LC3 lipidation in mouse DCs (See **Part I**). Accordingly, preliminary data show that in TAP-negative cells, AAK1 colocalizes to a higher extent with MHC-I molecules in comparison to T1.B35 cells (**Figure 3.24 A-B**), suggesting that the upregulation of AAK1 mediated internalization could be needed to supply

MHC-I molecules that can be loaded in the absence of TAP. Studies investigating the contribution of AAK1-mediated internalization in providing the MHC-I pool for peptide loading in the absence of TAP are ongoing.

Furthermore, in order to characterize the MHC -I reservoir that is preferentially used for autophagic antigen processing towards $CD8^+$ T cell stimulation, T2.B35 and T1.B35 cells were stained for the recycling endosome-specific marker RAB11. MHC -I molecules colocalize with RAB11 preferentially in the absence of TAP (**Figure 3.24C-D**). This suggests that in TAP-deficient cells, large MHC-I pools might be contained within endosomal recycling compartments fed by endocytosis mediated by AAK1 and the autophagy machinery. Staining for other compartment-specific markers, such as SNAREs and Rabs are ongoing.

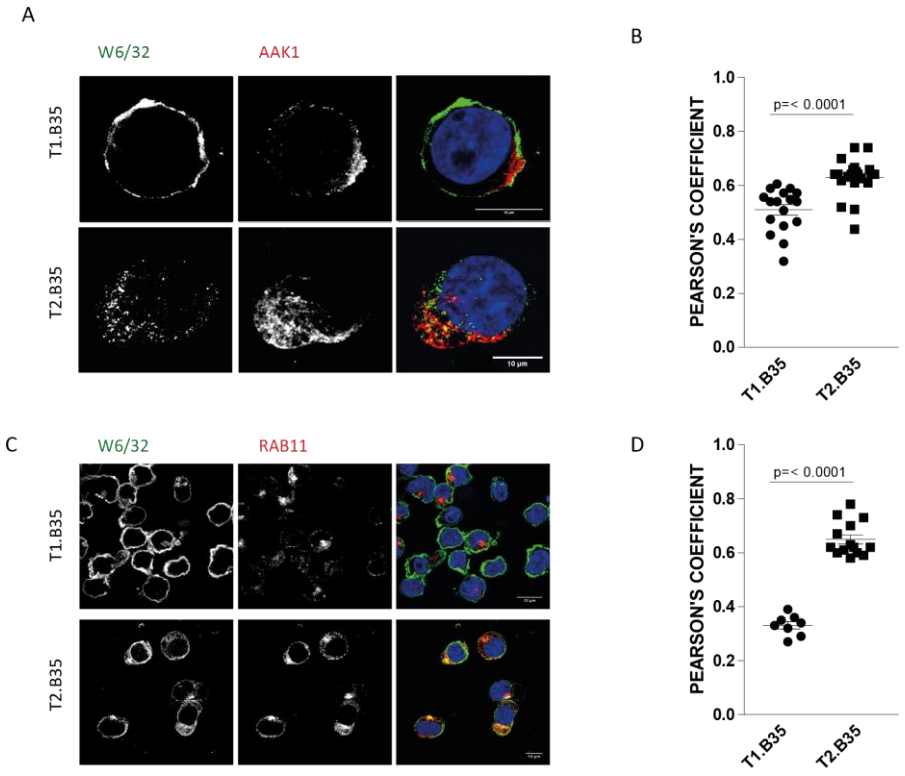

Figure 3.24 Immune fluorescence staining and colocalization analysis for MHC class I with AAK1 and RAB11
LCLs were cytospun onto slides, fixed in 4% paraformaldehyde 20 min at RT and then assessed for the localisation of MHC-I with either AAK1 **(A)** or RAB11 **(C)** by co-staining with w6/32 and anti-AAK1 or anti-RAB11 antibodies followed by AlexaFluor-488-labelled goat anti-mouse and AlexaFluor-555 goat anti-rabbit antisera, respectively. Cell nuclei were stained with 4',6-diamidino-2-phenylindole (DAPI). Image acquisition was performed using a confocal laser scanning microscope. Image deconvolution and colocalisation analysis was performed with ImageJ software. The presented data summarize one experiment. **(B)** Colocalization coefficient for AAK1 and MHC-I; **(D)** Colocalization coefficient for MHC-I and RAB11. Unpaired non-parametric two tailed t tests were performed to obtain the indicated p values.

Thus, the presented preliminary data suggest that autophagy might play a role in antigen processing when the classical pathway is defective, as in the absence of TAP. $CD8^+$T cell activation could be regulated upon inhibition of autophagic cargo degradation by lysosomes. On the other hand autophagy might to also supply the endosomal antigen-loading compartment with MHC-I molecules via its interaction with AAK1. These MHC-I molecules might be internalized from the plasma membrane to be loaded in a TAP-independent manner.

Chapter 4 - Discussion

Our studies describe a dual role of autophagy in MHC-I-restricted antigen presentation (**Figure 4.1**). On one hand, we showed that in murine CD11c-expressing cells lipidated LC3 recruits the internalization machinery to MHC-I molecules. In the absence of this recruitment, MHC-I gets stabilized on the surface of myeloid antigen presenting cells resulting in elevated $CD8^+$ T cell responses during IAV and LCMV infections. On the other hand, preliminary data on EBV-immortalized B cells strongly suggest that the autophagy pathway participates in antigen processing for MHC-I of the endogenous EBNA1 in the absence of TAP.

4.1 Autophagy-mediated internalization of classical MHC class I molecules in comparison to MHC class II and non-classical MHC class I molecules

Intracellular trafficking routes of MHC-I molecules have not been clearly defined yet, because they vary according to cell type, to the specific MHC allele investigated, to the conformation and the type of the MHC-I molecule. While in non-professional APCs MHC-I internalization seems to follow clathrin-independent endocytosis mediated by Arf6 (Naslavsky, Weigert et al. 2004), in mouse DCs it was shown that the MHC-I cytoplasmic tail contains a cryptic tyrosine-based motif for clathrin-mediate endocytosis responsible for internalization and targeting of MHC-I to endosomal compartments in the context of cross-presentation of exogenous antigens and anti-viral cytotoxic T cell priming (Lizee, Basha et al. 2003; Basha, Lizee et al. 2008). Upon Arf6 internalization, cargo-containing vesicles fuse with early endosome compartment and their subsequent trafficking requires Rab22a (Cebrian, Croce et al. 2016). Interestingly, this pathway intersects with the clathrin-mediated endocytosis pathway as Rab11, the classical marker associated with the tubular structures of endosomal recycling compartments involved in clathrin-dependent cargo recycling, such as transferrin receptor, is involved in the Arf6-dependent pathway (Weigert, Yeung et al. 2004). It is important to note that the Arf6 pathway together with the associated proteins have not been investigated yet in professional antigen presenting cells such as DCs. Moreover, a fairly recent study described that in mouse DCs a MHC-I pool exists that resides in Rab11-positive, but Arf6-negative endolysosomal compartment (Nair-Gupta, Baccarini et al. 2014), strengthening the concept that MHC-I molecules follow different intracellular

pathways based on the cell type. On the other side, the mentioned study is in line with the reported role on the recognition of the tyrosine motif as important element in DCs to target internalized MHC-I molecules to cross-presentation compartments. The tyrosine motif is implied in clathrin-mediated endocytosis as it is specifically recognized by adaptor proteins, such as AP-2 that upon phosphorylation by adaptor-associated kinase (AAK1), increases its affinity for the tyrosine motif within the target molecule (Honing, Ricotta et al. 2005), resulting in the invagination of the plasma membrane and formation of clathrin-coated vesicles. However, there is a caveat. In spite of the data showing the importance of the tyrosine motif in MHC-I trafficking, the involvement of clathrin in this process is just an assumption as no study has provided a formal demonstration so far. However, the involvement of AAK1, a kinase involved in clathrin-mediated endocytosis, in MHC-I internalization reported in the present thesis further supports a role of clathrin-mediated endocytosis for MHC-I. Similar considerations concern the CD1 family of MHC-I-like protein (CD1a, CD1b, CD1c, CD1d and CD1e), which present lipid antigens to T cells. CD1a molecules lack the tyrosine motif in their cytoplasmic tail and in HeLa cells have been shown to follow clathrin-independent internalization and Arf6- and Rab22a-dependent trafficking (Barral, Cavallari et al. 2008; Cebrian, Croce et al. 2016). On the other hand, CD1b, CD1c and CD1d can bind AP-2 via their tyrosine sorting motif and CD1b and CD1c have been shown to localize in clathrin-coated vesicles (Sugita, Jackman et al. 1996; Briken, Jackman et al. 2002; Lawton, Prigozy et al. 2005). Moreover, like for MHC-I molecules, the sorting motif has been shown to be indispensable for the trafficking into endolysosomal compartments (Sugita, Jackman et al. 1996). MHC-II molecules trafficking and internalization also follows multiple pathways. In the case of MHC-II a distinction has to be made according to endocytosis in association with invariant chain (Ii), which stabilized MHC-II in the absence of peptide, or as the peptide-loaded mature MHC-II form. While the former enters the endocytic pathway by clathrin-mediated endocytosis dependent on dileucine-based sorting signals in the cytosolic domain of Ii (Lotteau, Teyton et al. 1990), the internalization of peptide-MHC-II complexes seems to be dependent on Arf6 (Walseng, Bakke et al. 2008).

Here, my studies have provided evidence that in murine CD11c-expressing cells, internalization of classical MHC-I molecules is mediated by the recruitment of the clathrin-mediated endocytosis machinery, specifically the adaptor protein kinase AAK1, by LC3 lipidation. Interestingly, AAK1 carries two putative LIR motifs that might explain the association with LC3. Of note, the adaptor protein 2 (AP2), substrate of AAK1, was not found enriched in MHC-I immunoprecipates of wild type cells suggesting that, in our system, AAK1 likely supports the previously described AP2-independent, but clathrin-dependent endocytosis pathways (Henderson and Conner 2007; Gupta-Rossi, Ortica et al. 2011). The model depicted in **Figure 4.1D** is inferred from the data presented in my PhD thesis and from published literature. The mechanism proposed considers that AAK1 associates with cytosolic LC3. When LC3 gets lipidated at the plasma membrane (Fujita, Itoh et al. 2008), AAK1 comes in proximity of MHC-I molecules resulting in their internalization by an AP-2-independent process and presumably in LC3-coated vesicles. In absence of *Atg5*, MHC-I molecules get stabilized at the cell surface, resulting in an enhanced $CD8^{+}$T cell response during IAV and acute LCMV infections, demonstrating a functional role of the autophagy mediated MHC-I endocytosis. Additionally, preliminary data suggest that AAK1 plays a role in MHC-I internalization in EBV-infected B cells mainly during impairment of the classical MHC-I pathway. Similarly, a recent study found that internalization of the MHC-I-like molecule CD1d, which, as mentioned above, similar to classical MHC-I contains a tyrosine-based motif in its cytoplasmic tail, follows a clathrin-dependent endocytosis mediated by AP2 that is regulated by autophagy proteins. In absence of *Atg5*, CD11c-expressing cells, display higher levels of CD1d at their surface, linked to a prolonged glycolipid presentation on CD1d, which in turn enhanced activation of a subset of T cells known as invariant natural killer T (NKT) cells and improved the clearance of *Sphingomonas paucimobilis* infection (Keller, Loi et al. 2017). In line with these studies, the Alzheimer precursor protein has been shown to be internalized by a LC3-dependent mechanism based on the presence of a LIR motif within AP-2 sequence (Tian, Chang et al. 2013). Moreover, clathrin itself has been shown to contain a LIR motif and to contribute to autophagosome formation (Ravikumar, Moreau et al. 2010; Mari, Tooze et al. 2011). Interestingly, a possible role of autophagy in membrane

receptor trafficking, could have been envisioned already more than 25 years ago when Reid and Watts showed that primaquine, now being shown to also inhibit autophagy (Goodall, Wang et al. 2014), and previously known to inhibit transferrin receptor recycling, transiently blocks the recycling of MHC-I within cells (Reid and Watts 1990). Thus, the autophagy machinery seems to affect different clathrin-dependent internalization and degradation steps of surface receptors, including MHC-I endocytosis. However, it cannot be excluded that, in our model, in addition to MHC-I stabilization, trafficking of other molecules might be regulated by autophagy, and thereby contribute to enhanced $CD8^+$T cell responses after viral infections in the absence of *Atg*s. Indeed, the elevated CD80 surface expression on some subsets of DCs and the increased IL-1β production early during influenza A virus infection could contribute. Along this line, it has been reported using other models that absence of autophagy proteins resulted in a hyper-reactivity of $CD8^+$ T cell responses to allogeneic APCs (Hubbard-Lucey, Shono et al. 2014) and to colorectal tumour cells (Levy, Cacheux et al. 2015).

From the data shown in this thesis, it is also possible to speculate that as LC3 gets lipidated, AAK1 is recruited to the MHC-I at the cell surface not only for internalization but also for possible degradation by an ubiquitin, clathrin- and dynamin-dependent internalization pathway. Indeed, besides endosomal targeting mediated by the tyrosine-based motif, the cytoplasmic domain of MHC-I molecules contains two or three conserved lysine residues (Duncan, Piper et al. 2006). Lysines are targets for ubiquitination that can also induce clathrin-dependent endocytosis. The ubiquitylation of the cytoplasmic domains on MHC-I targets them to the late endosome pathway for degradation. Studies on immune evasion by herpes simplex viruses have provided a potential mechanism for this degradation, leading to the identification of membrane-associated RING-CH (MARCH) E3-ubiquitin ligases, human homologs of RING-CH viral proteins K3 and K5 of KSHV (Bartee, Mansouri et al. 2004). Indeed, MARCH IV and IX are related in sequence and when overexpressed, each one causes ubiquitylation and downregulation of MHC-I, CD4 and ICAM-1 (Nathan and Lehner 2009). Recently, it has been shown that MARCH IX overexpression prevents surface accumulation of MHC-I in monocyte-derived DCs, as well as the MHC-I-like molecule CD1a,

through the ubiquitination of lysine residues present in the cytoplasmic tails of these transmembrane proteins (De Angelis Rigotti, De Gassart et al. 2017). Similarly to MHC-I, in immature DCs, a role for ubiquitylation in mitigating the surface expression of peptide-MHC-II complex has been described (Cho and Roche 2013). Specifically, peptide-MHC-II complexes are ubiquitylated by the E3 ubiquitin ligase MARCH I in B cells and DCs, enhancing their endocytosis (Matsuki, Ohmura-Hoshino et al. 2007).

Thus, autophagy proteins seem to participate in clathrin-dependent endocytosis pathways for the internalization and, possibly, degradation of both classical and non-classical MHC-I molecules.

4.2 Autophagy in antigen processing for MHC class I versus MHC class II

Autophagy mediates antigen processing for MHC-II presentation via autophagy and LAP. Indeed, both autophagosomes and LAPosomes (LC3-coated single membrane vesicles formed upon LAP) supply either endogenous or exogenous antigens, respectively, to endosomal antigen-loading compartment for MHC-II presentation. Similarly, however still controversial, classical MHC-I restricted antigen presentation and cross-presentation seems to be regulated by autophagy (**Figure 4.1**). With respect to MHC-I presentation of endogenous antigen, it has been shown that antigens targeting to autophagosomes by fusion constructs with LC3 did not result in an increased MHC -I presentation (Schmid, Pypaert et al. 2007) and autophagy seems to even restrict MHC-I antigen presentation of DRiPs (Wenger, Terawaki et al. 2012). However, under conditions of inhibition of the classical MHC-I antigen-processing pathway such as during herpesvirus infection, alternative MHC-I pathways, such as autophagy, exist and circumvent viral immune escape mechanism. Indeed, late in herpes simplex virus 1 and human cytomegalovirus infection, it was reported that autophagy can deliver endogenous antigens for MHC-I presentation (English, Chemali et al. 2009; Tey and Khanna 2012). Accordingly in my studies in TAP-deficient EBV transformed B cells, fusion of LC3 to EBNA1 defective for proteasome inhibiting glycine-alanine repeats, results in an increased MHC-I presentation confirming the suggested role of autophagy during herpes virus infection. Interestingly, in the absence of TAP, fusion constructs with Ii seem also increase endogenous EBV antigen presentation on MHC-I, likely targeting antigen to the

endosomal compartment where the MHC-I loading takes place. It is then tempting to speculate that similarly to the autophagy-dependent MHC-II loading pathway, autophagosomes can fuse with endosomal-loading compartments, thereby providing endogenous antigens for MHC-I presentation. Additionally, blocking the acidification of autophagolysosomes by chloroquine treatment resulted in an increase of IFN-γ release by EBNA1-specific $CD8^+$T cell clones suggesting that the inhibition of the autophagic flux might redirect the resulting accumulated autophagosomes to fuse with endosomal compartments eventually rich in MHC-I molecules that are available to be loaded and recycled back to the cell surface. However, it might be also possible that chloroquine enhances an LAP-like pathway and increases LC3 lipidation on endolysosomal compartments, possibly by preventing their degradation (Florey, Gammoh et al. 2015) could result in a higher contribution of the autophagy machinery to supply internalized MHC-I to endosomal-loading compartments. Moreover, it was shown that in TAP-deficient cells, exogenous vaccinia virus antigen follows a TAP-independent MHC-I antigen-presentation pathway that requires autophagy for $CD8^+$T cell activation (Johnstone, Ramos et al. 2012). Nevertheless, the contribution of autophagy to cross-presentation is still controversial. While some studies found that *Atg* deficiency in antigen presenting cells did not affect exogenous antigen cross- presentation to $CD8^+$ T cells (Lee, Mattei et al. 2010), others have shown that the autophagy machinery enhances (Fiegl, Kagebein et al. 2013; Mintern, Macri et al. 2015) or inhibits (Baghdadi, Yoneda et al. 2013; Hubbard-Lucey, Shono et al. 2014) cross-presentation. Moreover, it has been suggested that the autophagy machinery supplies antigens for cross-presentation by helping the packaging of antigens to be transferred from cell to cell (Li, Wang et al. 2008; Uhl, Kepp et al. 2009).

Thus, autophagy proteins participate in MHC-II and balance MHC-I antigen presentation. Indeed, $CD8^+$T cell response could be restricted in normal physiological conditions while during impairment of the classical MHC-I pathway, the autophagy machinery could participate in antigen processing for presentation to $CD8^+$ T cells.

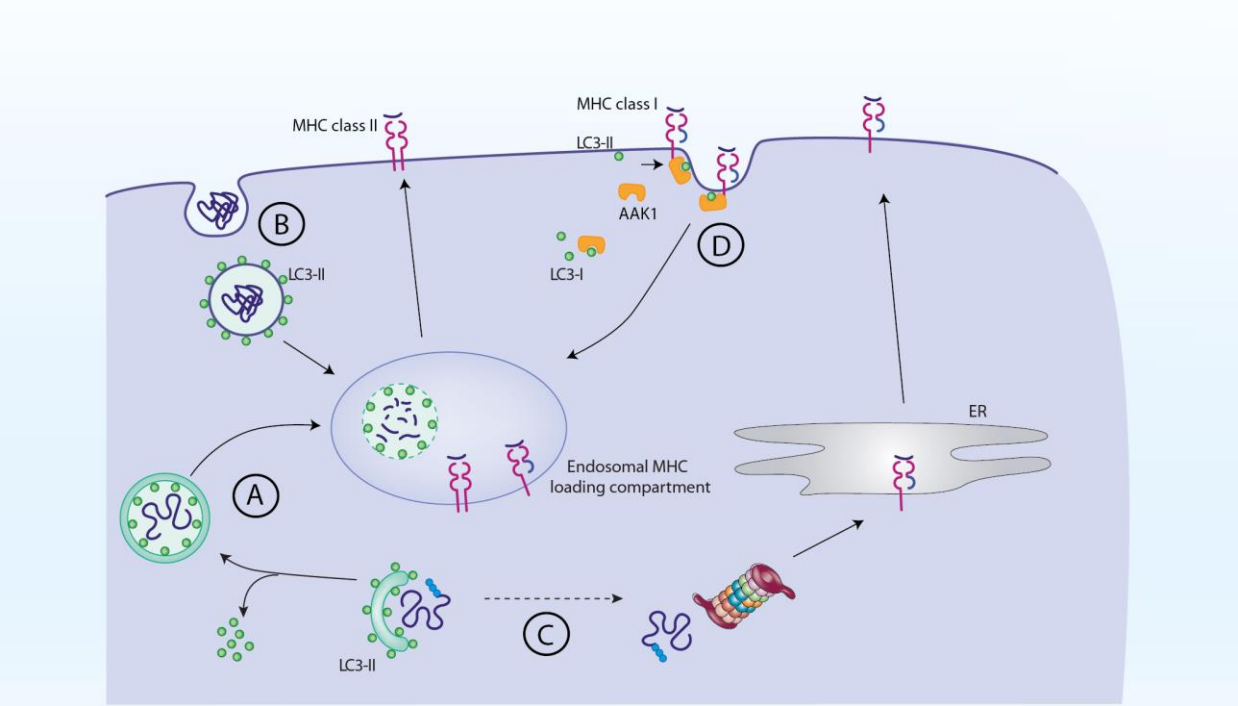

Figure 4.1 Autophagy in MHC-I and MHC-II presentation.

(A) Macroutophagy involves the engulfment of cytoplasmic material and the formation of autophagosomes, which then can fuse with MHC-II-containing compartments. Antigenic peptides are then loaded onto MHC -II molecules, which can be delivered to the plasma membrane for $CD4^+$ T cell stimulation. Some evidence suggests that autophagy could also supply antigens to a similar compartment for vacuolar MHC-I loading **(B)** During LC3-associated phagocytosis (LAP) phagosomes are decorated with LC3. After LC3 cleavage from their membrane, phagosomes fuse with MHC -II loading compartments. Their cargo is degraded and fragments are loaded onto MHC-II molecules. LAP facilitates lysosome-phagosome fusion or prolonged antigen processing for presentation by MHC-II in a species–specific manner. Similarly, LAP could also be involved in MHC-I cross-presentation **(C)** Macroautophagy degrades intracellular proteins, which otherwise might serve as substrates for proteasomes. The resulting proteasome products give rise to MHC -I ligands after import into the ER by the canonical MHC-I antigen processing pathway. **(D)** In addition, autophagy attenuates MHC-I-restricted presentation by recruiting the internalization machinery to the MHC-I molecules at the cell surface. Here, AAK1 associates with, presumably membrane-bound, LC3-II and triggers MHC-I internalization resulting in a diminished stimulation of $CD8^+$ T cells. Moreover, MHC-I that is internalized by such LAP-like processes could serve as a source for vacuolar MHC-I loading.

4.3 Peptide loading compartment in absence of TAP in comparison to cross-presentation

As mentioned, alternative pathways for MHC-I presentation exist and they are particularly important when the classical pathway is impaired for example during viral infections. These pathways are under intense investigation and some questions still need to be addressed. Since during cross-presentation, loading and MHC-I source do not follow the classical pathway, it can be hypothesized that common compartments/processes exist that support both alternative pathways of endogenous MHC-I antigen loading and cross-presentation. The characterization of such MHC-I

loading compartments and the supply to them as well as characteristics of MHC-I molecules in them are still important open questions.

Evidences from cross-presentation studies have demonstrated that 20% of the protein in early phagosomes in DCs (Campbell-Valois, Trost et al. 2012) depends on functional TAP and PLC recruitment from the ERGIC via the SNARE Sec22b (Ackerman, Kyritsis et al. 2003; Guermonprez, Saveanu et al. 2003; Houde, Bertholet et al. 2003; Cebrian, Visentin et al. 2011). With the same mechanism, it is likely that also MHC-I can be recruited from the ERGIC to the phagosome where they can be loaded. Alternatively, newly synthetized MHC-I could reach the phagosome after exiting the ER in association with Ii (Basha, Omilusik et al. 2012). Nevertheless, strong evidence supporting the use of ER-derived MHC-I as a source for the endosomal-loading compartment is lacking and the most accepted hypothesis suggests that the primary source is the recycled MHC-I from the cell surface. Indeed, in mouse DCs clathrin-mediated endocytosis has been shown to supply MHC-I molecules for cross-presentation (Reid and Watts 1990; Lizee, Basha et al. 2003; Basha, Omilusik et al. 2012). We showed that in mouse CD11c-expressing cells, the impairment of autophagy-dependent internalization of MHC-I via an unconventional use of the autophagy machinery in AAK1-dependent endocytosis depletes the intracellular vesicular pool of MHC-I. Interestingly, LC3-PE–coated vesicles have been reported to possibly fuse with vesicular MHC-I loading compartments for cross-presentation of antigens from respiratory syncytial virus, HIV, Chlamydia bacterial species and Aspergillus mold species (Blanchet, Moris et al. 2010; De Luca, Iannitti et al. 2012; Johnstone, Ramos et al. 2012; Fiegl, Kagebein et al. 2013). Additionally, our preliminary data indicate that MHC-I molecules traffic into RAB11^{+} vesicles, thereby suggesting that *Atg*-dependent internalization pathways shuttle MHC-I from the cell surface to the recently identified vesicular MHC-I storage compartment that is marked by Rab11a, VAMP3 and VAMP8 (Nair-Gupta, Baccarini et al. 2014), which has been demonstrated to supply MHC-I molecules during cross-presentation.

Thus, in absence of TAP, the autophagy machinery might play a dual role in vesicular loading of MHC-I by delivering antigen and supplying MHC-I molecules to the endosomal-loading compartment.

Taking together, data reported in the present PhD thesis provide evidence that autophagy is not simply a catabolic process but it also influences antigen processing, vesicular MHC-I loading and trafficking, that results in the regulation of T cell immunity (**Figure 4.1**). Further studies will need to be conducted in order to understand how one might selectively regulate these different A*tgs* functions during MHC-restricted antigen presentation for therapeutic interventions to boost adaptive immunity in response to several virus-associated antigens, especially when the classical MHC-I antigen presentation route is compromised.

Chapter 5 - Materials and Methods

5.1 Peptides, Chemical, Cytokines and Antibodies

Peptides $NP_{366-374}$ (NP1), $HA_{211-225}$, $NP_{311-325}$ (NP2), and NY-ESO-$1_{157-170}$ were synthesized by GL Biochem (Shanghai) at a purity >90 %. $EBNA1_{407-417}$ peptide (HPV peptide) was synthesized by peptides&elephants. CarboxyFluorescein Succinimidyl Ester (CFSE) was used at 0.5 mM and was from Molecular Probes. Chloroquine was used at concentration of 25 μM and 50 μM, at the indicated time points and purchased from Sigma. Mouse recombinant GM-CSF (BioLegend) and IL-2 (R&D) were used at 20 ng/ml and 40 IU/ml respectively.

Antibodies used are listed in **Table 5.1a and b**.

Antibody	Clone	Conjugation	Company	Assay
Anti-mouse MHC-II	M5/114.15.2	APC	Biolegend	FC
Anti-mouse CD11c	N418	PE-Cy7	Biolegend	FC
Anti-mouse CD4	GK1.5	PB	Biolegend	FC
Anti-mouse CD8	53-6.7	APC	Biolegend	FC
Anti-mouse CD11b	M1/70	APC-Cy7	Biolegend	FC
Anti-F4/80	BM8	Alexa 700	Biolegend	FC
Anti-mouse Ly6C	HK1.4	PerCP/Cy5.5	Biolegend	FC
Anti-mouse CD103	2E7	APC	Biolegend	FC
Anti-mouse-H2-D^b	KH95	Biotin	Biolegend	FC
Anti-I-A/I- E	M5/114.15.2	PB	Biolegend	FC
Anti-IFN-γ	XMG1.2	PE	BD Pharmingen	FC
Purified rat anti–mouse CD16/32 (mouse BD Fc block)	-	-	BD Pharmingen	FC
H2-K^b-GP_{34-43}	-	PE	Tcmetrix	FC
H2-D^b-$NP1_{396-404}$	-	PE	Tcmetrix	FC
H2-D^b-$NP1_{366-374}$	-	PE	Immudex	FC
CD80 blocking Ab	16-10A1	-	Biolegend	FC
Mouse anti-human w6/32	-	FITC	Biolegend	FC/IF
Anti-mouse H2-K^b	AF6-88.5	Biotin	Biolegend	FC/IF
Anti-mouse-H2	M1/42	PE	Biolegend	FC/IF
Anti-mouse CD28	-	-	BD Pharmingen	ICS
Anti-mouse CD3	-	-	BD Pharmingen	ICS
Rabbit anti-Rab11	-	-	Invitrogen	IF
SIGLEC-F	E50-2440	Alexa 647	BD Bioscience	IF
Rabbit anti-mouse H2-K^b	Exon-8	-	A gift from Dr. Jack Bennink, Bethesda, MD	IP/WB
Rabbit anti-LC3	PM036		MBL	IP/WB/IF
Mouse anti ATG5	7C6	-	Nanotools, Teningen, Germany	WB
Anti-β-actin	AC-15	HRP	Abcam	WB
Rabbit anti-RALBP1	-	-	EMELCA	WB
Rabbit anti-AAK1			Abcam	WB/IF
Rat anti-EBNA1	IH4	-	Kindly provided by Dr. Friedrich Graesser (Uniklinikum Saarland)	WB

Table 5.1a List of primary antibodies
FC, Flow Cytometry; IF, ImmunoFluorescence; ICS, IntraCellular Staining; IP, ImmunoPrecipitation; WB, western Blot.

Antibody	Clone	Conjugation	Company	Assay
Streptavidin	-	PE	Biolegend	FC
Goat anti mouse	-	Alexa555	Invitrogen	IF
Donkey anti rabbit Ig	-	Alexa 647	Invitrogen	IF
Goat anti rabbit Ig	-	Alexa 555	Invitrogen	IF
Goat anti mouse Ig	-	Alexa 647	Invitrogen	IF
Normal rabbit anti serum, Jackson	-	-	Jackson	IP
Goat anti rat	-	HRP	Jackson Lab, Maine USA	WB
Goat anti rabbit	-	HRP	Jackson Lab, Maine USA	WB
Goat anti mouse	-	HRP	Biorad Lab, Hercules, CA, USA	WB
AffiniPure Goat Anti-Rabbit IgG (H+L)		HRP	Jackson	WB

Table 5.1b List of secondary antibodies

FC, Flow Cytometry; IF, ImmunoFluorescence; ICS, IntraCellular Staining; IP, ImmunoPrecipitation; WB, western Blot.

5.2 Cell Lines and Cell Culture

All suspension lymphoblastoid cell lines (LCLs) (721.45 T1 cells and CEMx174 T2 cells) were routinely cultivated in RPMI 1640 medium (Gibco) supplemented with 10% heat inactivated fetal calf serum (FCS) (R10) and 50 U/ml Penicillin/Streptomycin (Gibco). Cells expressing HLA-B*3501, T2.B35 (generous gift from Prof. Rajiv Khanna, QIMR Berghofer Medical Research Institute, Brisbane, Australia) and T1.B35 cells, generated for this project by lentiviral infection, were additionally grown in selection R10 containing Geneticin, G418 (Thermo Fisher) (500 µg/ml).

Adherent wild-type MEFs, used at maximum 25 passages, and human embryonic kidney (HEK) 293T cells, which constitutively express the simian virus 40 (SV40) large T antigen, were cultured in Dulbecco's Modified Eagle Medium High Glucose medium (Gibco) with 10% FCS.

Primary cells, bone marrow-derived DCs (BM-DCs) were cultured in RPMI-1640 supplemented with 50 U/ml penicillin/streptomycin, 20 ng/ml GM-CSF and 20% heat inactivated FCS.

All cells were kept at 37°C and 5% CO_2, in a humidified incubator and routinely checked for Mycoplasma following MycoScope™ PCR Mycoplasma Detection Kit (Genlantis).

5.2.1 Expression constructs

HLA-B*3501 has been cloned in frame with a sequence coding for green fluorescent protein (GFP; pEGFP-N1; CLONTECH Laboratories,Inc.) in the laboratory of Prof. Rajiv Khanna, QIMR Berghofer Medical Research Institute, Brisbane, Australia and kindly shared with us. This vector expresses HLA-B*3501 and GFP as fusion protein and contains resistance for Geneticin.

Three different modified EBNA1 (E1) construct were used. E1Δ, in which the GAr domain was deleted (Tellam, Sherritt et al. 2001); E1Δ-LC3 and Ii-E1Δ, in which the cDNA sequence of human LC3 or invariant chain (Ii) (Schmid, Pypaert et al. 2007; Leung, Haigh et al. 2010) were cloned upstream and in frame of the E1Δ gene. All constructs were cloned in pHR-SIN-CSGWDNotI (pCSGW) backbone with IRES-GFP-tag.

5.2.2 Lentiviral production

To produce lentivirus carrying the HLA-B*3501, GFP-E1Δ, GFP-E1Δ-LC3, and Ii-E1Δ constructs, HEK 293T cells were used. Cells were transfected with the plasmid of interest and two lentiviral packaging plasmids (pCMVΔR8.91 and pMDG) using a $CaCl_2$ and 2X Hepes mix. Cells were incubated at 37°C for about 20 hours and then the medium was changed. About 30-32 hours after, the viral supernatant was collected, centrifuged at 3000 rpm for 8 min at 8°C and then filtered through a 0.22 µm filter. The harvested virus was aliquoted and store at -80°C.

5.2.3 Lentiviral Transduction

LCLs were resuspended at a concentration of $5x10^6$ cells/ml in the lentivirus supernatant and spin infected at 800 g for 1 hour. After centrifugation, cells were plated in 12 well plate over night at $2.5x10^6$ cells/ml. Next day, cells were centrifuged and suspended in fresh R10. Five days after infection, the antibiotic G418 was added to select HLA-B*3501-positive cells. For E1Δ constructs, cells were FACS sorted for GFP on a FACS Aria Cell Sorter II (BD Biosciences).

5.2.4 AAK1 silencing

Stealth siRNA Primer Set Aak1 Mouse (Life Technology), referred to as C10 (UCUACCCAGUGUUUCCCAACCUAAA), C12 (CAGAAGGCUCCACAUGGAAUCCUUU), and D02 (CAGAGAAUGAAGUGCUGCGCAGAUAUU) were used to silence AAK1 expression in MEFs and *Atg5*$^{-/-}$ and *Atg5*$^{+/+}$ BM-DCs. Stealth siRNA at a concentration of 20 nM were introduced into $2x10^5$ MEFS by oligofectamine (Life Technology) transfection in 6-well plate, following manufacturer's instructions. After overnight incubation in serum-free medium, FCS was added at final concentration of 10%. Total incubation time for transfection was 96 hours in R10. BM-DCs were

silenced by electroporation using Neon transfection system (Thermo Fisher) with 200 pmol of siRNA for 2-3x10^6 cells. Cells were kept for 48 hours in GM-CSF supplemented R10. After AAK1-targeting siRNA transfection, cells were harvested and analysed by western blot to assess AAK1 expression levels and by FACS to evaluate changes on MHC-I levels at the surface.

5.2.5 Generation of CD8+T cell clones

EBNA1$_{407-417}$-specific CD8+ T cell clones were generated from EBV-specific T cells sorted from the blood of a healthy HLA-B*3501 positive EBV carrier as previously described by Antisiferova and colleagues (Antsiferova, Muller et al. 2014).

5.3 Animals and cell isolation

Eights to 12 weeks old C57BL/6 mice (female and male) were purchased from Janvier Labs. *Atg5$^{fl/fl}$* mice backcrossed for more than 9 generations on the C57BL/6 background (Hara, Nakamura et al. 2006), were a kind gift of Dr. Mizushima (University of Tokyo, Japan). *Atg7$^{fl/fl}$* mice (Komatsu, Waguri et al. 2005) were kindly provided by Dr. Komatsu (Tokyo Metropolitan Institute of Medical Science, Japan). CD11c-Cre transgenic mice were from Jackson Laboratories. In these mice, the expression of a pIRES2-EGFP-based plasmid in CD11c positive cells is under control of the CD11c (Itgax) promoter and enhancer. Breeding CD11c-cre transgenic mice with any mouse containing a loxP-flanked sequence of interest, results in the constitutive Cre-mediated recombination of the flanked sequence in the offspring in tissues where the Itgax promoter is active. Accordingly, *Atg5$^{fl/fl}$* or *Atg7$^{fl/fl}$* mice were crossed to CD11c-Cre transgenic mice to obtain *CD11c-cre* x *Atg5$^{fl/fl}$* or *Atg7$^{fl/fl}$* (*Atg5$^{-/-}$* or -*Atg7$^{-/-}$* DCs, respectively) and Cre negative x *Atg5$^{fl/fl}$* or *Atg7$^{fl/fl}$* (*Atg5$^{+/+}$* or *Atg7$^{+/+}$* DCs, respectively) on a C57BL/6 background.

All animals were bred and housed in the University of Zurich animal facility according to institutional guidelines and Swiss animal laws. All animal protocols were approved by and conducted in accordance with the cantonal veterinary office of the canton of Zurich, Switzerland (protocol nos. 117/2008, 134/2011, Medecine FRM 1005 and ZH210/2014).

5.3.1 Mouse organ collection

Mice were euthanized by CO_2 inhalation. Depending on the organ of interest, different leukocyte isolation protocols were applied.

5.3.2 Isolation of splenocytes

Fresh spleens were collected from *Atg5*$^{-/-}$ DC mice and their littermates, either infected or not with influenza virus and enzymatically digested with 200 µg/ml Collagenase D, 50 µg/ml DNase I, 25 mM Hepes in R10 and incubate for 30 min at 37°C on shaker. To stop the reaction, 10 mM EDTA was added. Digested spleens were then smashed through the 70 µm strainer using piston of 2.5/5 ml syringe, and washed with cold PBS. After centrifugation, erythrocytes were lysed by incubating samples with 1 ml ACK for Erythrocyte lysis (0.15 M NH_4Cl, 1 mM $KHCO_3$, and 0.1 mM EDTA, pH 7.2) for 3 min at room temperature. After wash, cells were resuspended in PBS and counted. For a detailed description see Loi et al. 2017 (Loi, et al. *submitted*).

5.3.3 Isolation of CD45-positive cells from the lung

After perfusion with 10 ml PBS, lungs from either influenza A infected or not infected *Atg5* and *Atg7* sufficient and deficient mice were collected, cut into small pieces and digested with 400 µg/ml Collagenase A, 50 µg/ml DNase I, 25 mM Hepes in R10 and incubate for 45 min at 37°C on shaker. Ten mM EDTA was added the last 5 min to stop the reaction. The tissue was then forced through a 40 µm strainer using piston of 2,5/5 ml syringe. Cells were washed with cold PBS and the CD45 positive fraction was isolated by Percoll. Cells were resuspend in PBS and counted. For a detailed description see Loi et al. 2017 (Loi, et al. *submitted*).

5.3.4 Isolation of CD11c-positive cells

Splenic and lung CD11c$^+$ cells were isolated by positive magnetic cell separation (MACS) (Miltenyi Biotec) by resuspending the cells at a concentration of 2.5 x 10^8 cells/ml with cold MACS buffer (0.5% BSA, 2mM EDTA in PBS) and incubating with 100 µL CD11c beads (Miltenyi Biotec) per 10^8 cells at 4°C for 20 min. After wash in cold MACS Buffer, cells were resuspended 2 x 10^8 cells/ml in cold MACS buffer and magnetic separation in the autoMACS separator (Miltenyi Biotec)

was performed by positive selection. MACS sorted CD11c$^+$ cells, with a purity of 72-80% were then cultured in R10 supplemented with 20 ng/ml GM-CSF. Where indicated, CD11c$^+$ MHC class II^{high} cells were sorted on a FACS Aria Cell Sorter II (BD Biosciences). For a detailed description see Loi et al. 2017 (Loi, et al. *submitted*).

5.3.5 Bone marrow derived DCs

Bone marrow-derived DCs (BM-DCs) were obtained from femur and tibia of *Atg5* and *Atg7* sufficient and deficient mice, flushed out with cold PBS, strained through a 70 µm cell strainer, centrifuged and then erythrocytes were lysed by ACK lysis for 5 min at room temperature. After PBS wash, cells were resuspended in pre-warmed BM-DC medium and plated out at 3-5 x 10^6/ml in 100 x 15 mm non-tissue coated petri dish in BM-DC medium and incubated at 37°C. The medium was changed every second day by collecting the cells in suspension, centrifugation at 500 g for 10 min at 4°C and resuspending in new BM-DC medium. Cells were plated back in the original plate. After 8/10 days of incubation BM-DCs were used. BM-DCs purity was checked by FACS analysis and if necessary (<80% CD11c$^+$ MHC class II^{high} cells) cells were enriched by MACS positive CD11c selection. For a detailed description see Loi et al. 2017 (Loi, et al. *submitted*).

5.3.6 Flow cytometry

Cells were acquired on a FACS Fortessa flow cytometer using FACS Diva Version 6.1.3 software (BD Biosciences) or a FACS Canto II (BD Biosciences) and all flow cytometry analyses were performed with FlowJo Version 9.3.1 software (Treestar).

5.4 Biochemical Assays

5.4.1 Lysate Preparation and Co-Immunoprecipitation

Lysate preparation and co-immunoprecipitation (co-IP) was performed as described in Loi et al. 2017 (Loi, et al. *submitted*). Briefly, cell protein extracts were obtained after PBS wash and either stored at -80°C or immediately resuspended in ice-cold lysis buffer (50 mM Tris pH 8.0, 140 mM NaCl, 1.5 mM $MgCl_2$, 1% NP40) or in co-IP Lysis Buffer (50 mM Tris-HCl pH 7.5, 150 mM NaCl, 1% NP-40) for Western blot and co-IP, respectively, freshly supplemented with complete Proteinase

Inhibitor cocktail (Roche) and incubated for 30 min on ice (1 x 10^6 cells/ 50 µl). Cells and debris were centrifuged and protein amount was quantified using Pierce BCA Protein Assay Kit (Pierce) accordingly to the manufacturer's recommendation.

For IP, cell lysate were precleared with 50 µl of protein A beads (Pierce) and then equal amount of protein was incubated with 5µl of rabbit-anti *Atg*8/LC3 or 5µl of anti-H2-K^b (Exon8) (See **Table 5.1a**) overnight on constant rotation. The next day, cell lysate was incubated with protein A beads, and after 1 hour extensively wash with PBS.

Total protein extracts and IP fraction were boiled for 5 min in the presence of Sodium Dodecyl Sulphate (SDS)- PolyAcrylamide Gel Electrophoresis (PAGE) loading buffer (60 mM Tris-Cl, pH 6.8, 2% SDS, 10% Glycerol, 0.01% Bromophenol Blue) with 1% β-mercaptoethanol. Western blot lysates were loaded onto a SDS-PAGE gel, while IP lysates were analysed by Western blot and/or mass spectrometry.

5.4.2 Western blotting (WB)

Western blotting was performed as described in Loi et al. 2017 (Loi, et al. *submitted*). Briefly, protein extracts were resolved in 7% or 12.5% SDS-PAGE gels 1.5mm thick. Primary antibodies (rabbit anti- LC3 1:1.000, rabbit anti-AAK1 1:1000, rabbit anti-RALBP1 1:1000, rat anti-EBNA1 (See **Table 5.1a**) in 5% milk PBS containing 0.1% Tween 20 (Sigma) (PBS-T)) were incubated overnight at 4°C. After extensively washes with PBST, cells were incubated with appropriate HRP-coupled secondary antibody (goat anti-rabbit Ig 1:50.000, goat anti-rat Ig 1:10.000 in PBS-T) for 1 hour at room temperature. Anti actin-conjugated HRP antibody (1:100.000) was incubated on membrane for 30 min at room temperature as loading control. Protein bands were detected by application of ECL western blot substrate (Witec) and visualized with Fusion FX Detector (Vilber-Lourmat). Quantification of protein levels by densitometry was performed using the Image J software.

5.4.3 Mass Spectrometry (MS)

Samples obtained from co-IP were reduced with 1 mM Dithiothreitol (Sigma-Aldrich) and alkylated using 5.5 mM iodoacetamide (Sigma-Aldrich). Proteins were separated by SDS-PAGE and

digested in gel using trypsin (Promega) at 37°C overnight and the resulting peptide mixtures were processed on STAGE tips. Mass spectrometric measurements were performed on a LTQ Orbitrap XL mass spectrometer (Thermo Fisher Scientific) coupled to an Agilent 1200 nanoflow-high-performance liquid chromatography (HPLC) (Agilent Technologies GmbH). The mass spectrometer was operated in the data-dependent mode and switched automatically between MS (max. of 1 x10^6 ions) and MS/MS. Each MS scan was followed by a maximum of five MS/MS scans in the linear ion trap using normalized collision energy of 35% and a target value of 5,000. Parent ions with a charge state from z = 1 and unassigned charge states were excluded for fragmentation. The mass range for MS was m/z = 370 to 2,000. The resolution was set to 60,000. Mass-spectrometric parameters were as follows: spray voltage 2.3 kV; no sheath and auxiliary gas flow; ion-transfer tube temperature 125°C. The MS raw data files were uploaded into the MaxQuant software (PMID (PMID): 19029910) version 1.3.0.5, which performs peak detection, quantification, and generates peak lists of mass error corrected peptides using the following parameters: carbamidomethylcysteine was set as fixed modification, methionine oxidation and protein amino-terminal acetylation were set as variable modifications. Three miss cleavages were allowed, enzyme specificity was trypsin/P, and the MS/MS tolerance was set to 0.5 Da. Peak lists were searched by Andromeda for peptide identification using a Uniprot mouse database containing common contaminants such as keratins and enzymes used for in-gel digestion. Peptide lists were further used by MaxQuant to identify and relatively quantify proteins using the following parameters: peptide, and protein false discovery rates were set to 0.01, maximum peptide posterior error probability (PEP) was set to 1, minimum peptide length was set to 7, the PEP was based on Andromeda score, minimum number peptides for identification and quantitation of proteins was set to one and must be unique, and identified proteins have been re-quantified.

5.5 MHC class I assays

5.5.1 Internalization assay

CD11c$^+$ MACS sorted DCs were stained in FACS buffer (PBS supplemented with 2% FCS and 0.01% Na azide) with either anti-H2-D^b or anti-H2-K^b biotinylated antibodies, or their respective

isotypes, 1:50 for 30 min at 4°C. Cells were washed 2 times in PBS, resuspended in R10, and kept at 4°C or incubated at 37°C, for 10, 30, 60 and 90 min. After the incubation time, cells were washed and surface staining was performed at 4°C with 1:400 PE-coupled streptavidin, 1:400 PE-Cy7-anti-CD11c, 1:400 PB-anti-MHC-II, and 1:500 Aqua in FACS buffer. The rate of internalization of MHC-I molecules was evaluated by the decrease of MFI intensity compared to the MFI of control DCs incubated at 4°C and set as a reference at 100%. For a detailed description see Loi et al. 2017 (Loi, et al. *submitted*).

5.5.2 Acid stripping assay

CD11c$^+$ MACS sorted DCs were incubated for 2 min with ice cold acid stripping buffer (131 mM sodium citrate, 66 mM sodium phosphate and 1% BSA, pH 3) then washed 2 times in R10, and kept at 4°C or incubated in R10 at 37°C for the indicated time points. After the incubation time, cells were washed and surface staining was performed at 4°C with anti-H2-D^b or anti-H2-K^b, anti-CD11c, anti-MHC-II, and Aqua. Isotype staining was used as control. The rate of restoration of MHC-I molecules at the surface was evaluated by the increase of MFI intensity compared to the MFI of control DCs incubated at 4°C and set as a reference at 0%.

5.6 Imaging Techniques

5.6.1 Immunofluorescence of CD11c$^+$ cells

CD11-c positive cells were cultured overnight on Poly-L-Lysine coated glass slides (Menzel-Gläser; 1.5mm) at 37°C in R10. The next day, cells were centrifuged 1500 rpm 3 min, washed in PBS and labelled with Fc blocker 2.4G2 Fcc III/II (BD PharMingen) at 4°C, followed by labelling for H2-K^b or H2 (see **Table 5.1a**) for 30 min at 4°C in PBS. Next, they were incubated at 37°C for 1 h, washed with PBS and fixed in 4% paraformaldehyde 20 min at room temperature. After fixation, cells were washed with PBS, permeabilized with 0.1% Triton X100 for 5 min room temperature, wash with PBS and saturated with 1% BSA for 1 hour. Binding of the primary antibody was detected with Alexa Fluor 555 goat anti-mouse or anti-rat IgG H&L (Invitrogen) and cell nuclei were stained with 4',6-diamidino-2-phenylindole (DAPI). Fluorescence was analysed with a 63×, 1.4 NA oil immersion lens with a confocal laser-scanning microscope (SP8; Leica). Analyses have

been performed using ImageJ software. For a detailed description see Loi et al. 2017 (Loi, et al. *submitted*).

5.6.2 Immunofluorescence of LCLs

LCLs cells were seeded on Poly-D-Lysine coated round glass coverslips in a 24 well plate and fixed in 4% PFA 20 min after centrifugation (800 g, 5 min). All steps were performed at room temperature and all washes done with PBS supplemented with 1% BSA (Sigma). Cells were permeabilized with 0.5% Saponin 1%BSA in PBS for 5 min, washed 3 times 10 min followed by staining with primary antibodies mouse anti-human w6/32, rabbit anti-LC3, rabbit anti-RAB11, guinea pig anti-p62 (See **Table 5.1a**) for 1 hour. Suitable secondary antibodies conjugated with either Alexa Fluor 488 or Alexa Fluor 555 were incubated for 30 min. Slides were counterstained with DAPI (Invitrogen) and mounted with Fluorescence mounting medium (Dako). Cells were visualized through a 63×, 1.4 NA oil immersion lens with a confocal laser-scanning microscope (SP8; Leica). Colocalization analyses have been performed using the Coloc2 Plugin of ImageJ software. A Pearson coefficient >0.5 indicates a statistically relevant colocalization of the signals.

5.7 Enzyme-linked immunosorbent assay (ELISA)

5.7.1 IFN-γ production of EBNA1-specific CD8⁺ T cell clone

The $EBNA1_{407-417}$-specific $CD8^+$ T cell clones were incubated overnight with HLA-B*3501 T1 and T2 cells in an effector to target ratio of 1:10. IFN-γ released was quantified by ELISA. As positive controls were pulsed with 1µM peptide $EBNA1_{407-417}$ prior coculture.

5.7.2 Lung homogenate preparation

For detection of cytokines in the lungs, lungs were weighted and resuspended in PBS (400 mg in 1.5 ml), then disrupted mechanically, using a Polytron. Homogenates were then centrifuged at 13,000 RPM for 30 min, and supernatants were tested for cytokine detection.

5.7.3 IL-6, IL-1β, IFN-γ ELISAs

Murine lung homogenates and human cell supernatants were added undiluted onto previously coated 96-well ELISA plates (Nunc-Immuno MaxiSorp; Thermo Fisher Scientific). Cytokines were

then detected with the biotinylated specific antibodies (IL-6 eBioscience kit 88-7013-88; IL-1β BioLegend kit 431303; mouse IFN-γ eBioscience kit 88-7314-86; human IFN-γ Mabtech 3420-1H-20) and streptavidin-HRP (Mabtech), using the peroxidase substrate tetramethylbenzidine (TMB, Sigma). Recombinant cytokines were used as standard. Plates were read using Microplate Reader Infinite M1000 Pro (Tecan) at 450 nm and 570 nm as reference value.

5.7.4 Serum isolation

Blood for serum cytokine analysis was collected via cardiac puncture after euthanasia with CO_2 inhalation. After collection in Microtainer SST tubes (BD), the whole blood has been allowed to clot by leaving it at room temperature. After 15-30 min the clot was removed by centrifuging at 2000 g for 10 min at 4°C. Serum was aliquoted and stored at -80°C.

5.7.5 Influenza specific IgG detection

ELISA plates were coated with 100 µl/well PR8 Virus 1:1000 in PBS, and incubated o/n at 4°C.the day after the virus were inactivated with 2x auto-linking modus (=240mjoules). After blocking with 200 µl/well blocking solution (1% BSA in PBS pH 7.4) for 2 hours at room temperature, 50 µl/well of serum of infected mice previously titrated 1/800 to 1/102400 in 0.1% BSA/PBS were incubated for 2hours at room temperature. Serum from PBS treated mice were used as control. Washes with PBS 0.05% Tween were followed by incubation with 50 µl/well goat anti-mouse HRP antibody 1:500 in PBS/0.1% BSA and incubate for 1.5 hours at room temperature. TMB was used as peroxisade substrate and plates were read using Microplate Reader Infinite M1000 Pro (Tecan) at 450 nm and 57 0nm as reference value.

5.8 Molecular Assays

5.8.1 DNA extraction from biopsies

Tail or ear biopsies (0.3-0.6 cm) were obtained from mice were either stored at −20 °C or immediately immersed in 100 µl of tail lysis buffer (100 mM Tris, pH 8.0, 100 mM NaCl, 10 mM, pH 8.0, 0.2% SDS) freshly supplemented with 1:50 of proteinase K (Roche). Tissue biopsies were digested between 4-12 hours at 56 °C at 550 rpm, centrifuged to remove the tissue debris and

transferred to a collection tube containing 200 µl isopropanol. After centrifugation, supernatants were discarded and 200 µl of 70%-Ethanol was added. Tubes were centrifuged, supernatants discarded and let them dry. DNA was resuspended in 100 µl of ddH_2O and stored at-20°C.

5.8.2 Genotyping

For *Atg5*$^{fl/fl}$ allele and *Atg7*$^{fl/fl}$ allele genotyping, respectively, the Taq DNA Polymerase (Roche, stock 5 U/µl) and the TaKaRa LA Taq® DNA Polymerase (Clontech) were used. *Cre* allele was genotyped with the FIREPol® 5× Mix 7.5 mM Ready to Load system (SOLIS BIODYNE).

A PCR master mix was prepared in water accordingly to the different protocol. Water and a negative mouse sample were used as negative control, a positive mouse sample served as positive control. For primers used see **Table 5.2**; Master mix for PCR **Table 5.3**. The PCR was run according to **Table 5.4**. DNA bands were resolved in 1% agarose gel in tris-borate-EDTA buffer supplemented with GelRed to stain the DNA. Samples were analyzed with the AlphaImagerTM 2200.

5.8.3 qRT-PCR

Atg5$^{+/+}$ and *Atg5*$^{-/-}$ lung DCs were FACS sorted for CD11c, MHC-II, SIGLEC-F, CD103 and CD11b while splenic DCs for CD11c, MHC-II, CD8 and CD11b. mRNA was extracted with Quick-RNA MicroPrep kit (Zymo Research) following the manufacturer instructions. Briefly, after adding 300 µl of RNA lysis buffer, samples were stored at -80°C as recommended by the manufacturer's instructions. The day after, 1 volume of ethanol was added and after mixing samples were transfered into a Zymo-Spin IC Column and briefly centrifuge. DNase treatment was performed in-column followed by RNA Prep Buffer and washing steps. RNA was eluted with DNase/RNase- free H_2O and either used immediately or store at -80°C.

Primer name	Primer Target Primer sequence (5'- 3')
Genotyping	
CS003 *Atg5*$^{fl/fl}$	GAATATGAAGGCACACCCCTGAAATG
CS004 *Atg5*$^{fl/fl}$	GTACTGCATAATGGTTTAACTCTTGC
CS005 *Atg5*$^{fl/fl}$	ACAACGTCGAGCACAGCTGCGCAAGG
CS006 *Atg5*$^{fl/fl}$	CAGGGAATGGTGTCTCCCAC
CS014 *Atg7*$^{fl/fl}$	TGGCTGCTACTTCTGCAATGATGT
CS015 *Atg7*$^{fl/fl}$	CAGGACAGAGACCCATCAGCTCCAC
CS007 CD11c-Cre-GFP	GCGGTCTGGCAGTAAAAACTATC
CS008 CD11c-Cre-GFP	GTGAAACAGCATTGCTGTCACTT
CS009 CD11c-Cre-GFP ($^{+}$ve ctr)	CTAGGCCACAGAATTGAAAGATCT
CS010 CD11c-Cre-GFP ($^{+}$ve ctr)	GTAGGTGGAAATTCTAGCATCATCC
Virology	
GAPDH-Forward	CCTGGAGAAACCTGCCAAGTA
GAPDH-Reverse	AGAGTGGGAGTTGCTGTTGAA
PR8 NA-Forward	TTGGTCAGCAAGTGCATGTC
PR8 NA-Reverse	ACAGCCACTGCTCCATTATC
PR8 M-Forward	CAAGCAGCAGAGGCCATGGA
PR8 M-Reverse	GACCAGCACTGGAGCTAGGA
PR8 HA-Forward	CTGCTCGAAGACAGCCACAA
PR8 HA-Reverse	GAGCCATCCGGCGATGTTAC

Table 5.2 List of primers

For the RNA→cDNA reverse transcription, 1 µl Random Hexamer Primers (Promega) was added to 9.5 µl of RNA (max 5 µg), and placed for 5 min into a heat-block at 70°C. After centrifugation, 9.5 µl of the reaction mix (Promega) was added and the amplifying program was set as in **Table 5.5.**

cDNA was stored at -20°C or used immediately for qRT-PCR used to quantify H2-Kb mRNA levels. qPCR reaction was set as in **Table 5.6** in 384 well plate. For each sample duplicates of triplicates were performed. 1 µl of DNase/RNase free H_2O was used as negative control. Additionally, GAPDH mRNA quantification was used as reference gene. qRT-PCR was run as in **Table 5.6**.

Cq values were determined using the regression method. Briefly, average Ct (threshold cycle) value was calculated for all samples and GAPDH average Ct values were subtracted from the average Ct values of the H2-K^{b} obtaining the ΔCt. Normalized gene of interest expression levels were calculated as $2^{\Delta Ct}$.

Reagent	*Atg5* Master Mix		*Atg7* Master Mix		*Cre* Master Mix	
	Volume	*Concentration*	*Volume*	*Concentration*	*Volume*	*Concentration*
DNA	5 µl		5 µl		2 µl	
PCR buffer	5 µl	10x buffer	2 µl	10x Takara buff	4 µl	5x FIREPol
dNTPs	1 µl	10 mM	3.2 µl	2.5 mM	0 µl	
primers	1 µl	10 µM	0.2 µl	20 µM	0.5 µl	10 µM
Taq Polymerase	0.4 µl		0.2 µl		0 µl	
H_2O	34.6 µl		12.2 µl		12 µl	
Final Volume	**50 µl**		**20 µl**		**20 µl**	

Table 5.3 Recipes Master Mix for genotyping

Atg5			*Atg7*			*Cre*		
Temperature	*Time*		*Temperature*	*Time*		*Temperature*	*Time*	
95°C	3 min		94°C	5 min		94°C	4 min	
95°C	30 sec		94°C	30 sec		94°C	30 sec	
60°C	30 sec	X 35	65°C	30 sec	X 30	63°C	45 sec	X 35
72°C	1 min		68°C	90 sec		72°C	1 min	
72°C	10 min		72°C	10 min		72°C	10 min	
4°C	∞		4°C	∞		4°C	∞	

Table 5.4 PCR programs for genotyping

Reagent	Master Mix	
	Volume	*Concentration*
PCR buffer	4 µl	5x buffer
MgCl2	1 µl	3.8 mM
dNTPs	1 µl	10 mM
RNase Inhibitor	0.5 µl	10 µM
Retrotranscriptase	1 µl	
DNase/RNase free H_2O	2 µl	
Final Volume	**9.5 µl**	

PCR Retrotranscription	
Temperature	*Time*
25°C	5 min
42°C	60 min
70°C	15 min
4°C	∞

Table 5.5 Master mix (left) and PCR programs (right) for retrotranscription

Reagent	Master Mix	
	Volume	*Concentration*
cDNA	1µl	
SYBR Green SuperMix	5 µl	
Primers	0.4 µl	10 µM
DNase/RNase free H_2O	3.6 µl	
Final Volume	**10 µl**	

qRT-PCR		
Temperature	*Time*	
50°C	2 min	
95°C	2 min	
95°C	15 sec	X 30
60°C	1 min	
4°C	∞	

Table 5.6 Master mix (left) and PCR programs (right) for qRT-PCR program

5.9 Virology

5.9.1 Influenza virus infection *in vitro* and *in vivo*

CD11c$^+$ MACS sorted splenic DCs were infected at a MOI of 200 for 45 min in RPMI without serum. Influenza A/PR8 virus (H1N1) virus was used for all experiments and purchased from Charles River. Mice were anesthetized using isoflurane and infected intranasally by the application of 25 µl of virus suspension (doses of virus were chosen between 0.1 to 10 HA units depending on the experiment). Weight loss was used to follow the development of the infection.

5.9.2 LCMV infection *in vivo*

Animals were infected intravenously with the wild type LCMV Armstrong strain at a dose of 10^4 PFU.

5.9.3 Quantification of viral RNA

Lungs were weighted and resuspended in PBS (400 mg in 1.5 ml). Briefly, lungs were disrupted mechanically using a Polytron and viral RNA was isolated according to the manufacturer's instructions (Qiagen viral RNA isolation kit). Reverse transcription was performed using the GoScript reverse transcription system (Promega). The RT product was diluted and used as a template for quantitative PCR (qPCR) on a Bio-Rad MyIQ detection system using the Platinum SYBR Green qPCR SuperMIx-UDG (Invitrogen). The specific forward (F) and reverse (R) primer pairs (all Eurofins MWG, Ebersberg, Germany) were used. Relative concentrations of viral RNA in the cells was determined by analysis of cycle threshold values (Ct), normalizing the mean Ct for PR8-M, PR8-HA and PR8-NA to the expression of the product of the housekeeping gene GAPDH obtaining the ΔCt. ΔCt of PBS treated mice was subtracted for the ΔCt obtained from influenza infected mice and the normalized gene of interest expression levels were calculated as $2^{\Delta\Delta Ct}$.

5.9.4 Influenza infectious titre plaque assay

Virus titration was performed by plaque assay. MDCK cells were seeded in 12-well tissue culture plates in high-glucose Dulbecco's modified Eagle's medium (DMEM) with 10% heat-

inactivated FCS and 1% penicillin–streptomycin. Serial 10-fold dilution of the samples (0.1 ml) were prepared in infection buffer (0.3% BSA, 1% penicillin–streptomycin, 0.02 mM $Ca_2^+$and 0.01Mg_2^+in PBS) and added onto the MDCK cell monolayer for 1 h at 37°C with intermittent shaking. Each dilution was plated in triplicates. After incubation, the inoculum was taken off and 1ml of agar overlay (2x MEM, 0.02% DEAE-Dextran, 0.15% Sodiumcarbonate and 0.04% Oxoid agar) supplemented with 0.5 µg/ml of tosyl phenylalanyl chloromethyl ketone (TPCK)-trypsin was added to each inoculated well. Solidified agar plates were incubated at 37°C for 1.5 days. Plates were then fixed with 4% paraformaldehyde for 20 min and, after removal of the agar layer, crystal violet solution (40ml of 1% crystal violet, 80ml methanol in H_2O) was added for 10 min. Plates were rinsed with tap water and plaques were counted to determine the viral titer as plaque-forming units (PFU) per ml.

5.9.5 Influenza virus specific T cell proliferation

Influenza specific polyclonal T cells were expanded from splenocytes or lung of C57BL/6 mice at day 12/14 post-influenza infection, as previously described (Longhi, Trumpfheller et al. 2009). Briefly, C57BL/6 mice were intranasally infected with 10 HAU of PR8 virus. After 12/14 days were sacrificed and organs collected and processed as described in Isolation of mouse cells section. One third of the cells $5x10^6$ cells/ml was then infected with PR8 *in vitro* at a MOI of 10 in plain RPMI at 37°C. After 1 hour, cells were washed, resuspend at $2.5x10^6$/ml and irradiate at 30 Grays. Irradiate and not irradiate cells were plate in 24-well plate at $2.5x10^6$/ml and cultured for 6/7 days in RPMI supplemented with 10% FCS, and 40 units/ml of IL-2.

For DC/T cell co-cultures, *Atg5*$^{+/+}$ and *Atg5*$^{-/-}$ $CD11c^+$ splenic or lung DCs were influenza infected *in vitro* at a MOI of 200 and seeded overnight in R5 supplemented with GM-CSF or pulsed with 0.1 or 1 µM $NP1_{366-374}$ peptide for 1 hour. $CD11c^+$ DCs were then co-cultured in 96 flat bottom plates, at a 1/1 ratio with CFSE labelled IAV specific T cells obtained from spleen or lungs of C57BL/6 infected animals as described above for 3/4 days. Proliferation of $CD8^+$T cells was evaluated by FACS staining. Co-culture with non-infected DCs was used as a control. In some experiments, CD80 specific blocking antibodies were added (10 µg/ml) during the DC co-culture with T cells.

5.9.6 Intracellular IFN-γ staining

Lung single cell suspensions obtained after Percoll gradient centrifugation were incubated in RPMI at 37°C for 5 hours in the presence of anti-CD28 (2 µg/ml) and influenza specific peptides (10 µg/ml). Brefeldin A (10 µg/ml) (Sigma) was added after the first hour. As positive control anti-CD3ε/anti-CD28 or phorbol myristate acetate (PMA)/Ionomycin (Sigma) was added. Extracellular staining was performed with the following mix: 1:500 PB anti-mouse CD4, 1:125 APC anti-mouse CD8, 1:50 APC-Cy7 anti-mouse CD45, 1:500 Aqua Live/Dead for 20 min on ice. Then cells were fixed and permeabilized using BD Cytofix Cytoperm Fixation/Permeabilization Kit, stained for PE-anti-IFN-γ and analysed by FACS. For a detailed description see Loi et al. 2017 (Loi, et al. *submitted*).

5.10 Statistical analysis

Statistical tests applied are indicated in the respective figure legends and performed with GraphPad Prism v5.0a for Mac OSX (GraphPad Software, Inc). Unpaired, two-tailed student t test, Mann-Whitney U test and Pearson correlation coefficient were performed/calculated. A P-value <0.05 was considered statistically significant.

References

Ackerman, A. L., C. Kyritsis, et al. (2003). "Early phagosomes in dendritic cells form a cellular compartment sufficient for cross presentation of exogenous antigens." Proc Natl Acad Sci U S A **100**(22): 12889-12894.

Ahner, A. and J. L. Brodsky (2004). "Checkpoints in ER-associated degradation: excuse me, which way to the proteasome?" Trends Cell Biol **14**(9): 474-478.

Akram, A. and R. D. Inman (2012). "Immunodominance: a pivotal principle in host response to viral infections." Clin Immunol **143**(2): 99-115.

Alcami, A. and U. H. Koszinowski (2000). "Viral mechanisms of immune evasion." Trends Microbiol **8**(9): 410-418.

Alemu, E. A., T. Lamark, et al. (2012). "ATG8 family proteins act as scaffolds for assembly of the ULK complex: sequence requirements for LC3-interacting region (LIR) motifs." J Biol Chem **287**(47): 39275-39290.

Antsiferova, O., A. Muller, et al. (2014). "Adoptive transfer of EBV specific CD8+ T cell clones can transiently control EBV infection in humanized mice." PLoS Pathog **10**(8): e1004333.

Apcher, S., A. Komarova, et al. (2009). "mRNA translation regulation by the Gly-Ala repeat of Epstein-Barr virus nuclear antigen 1." J Virol **83**(3): 1289-1298.

Appay, V., D. F. Nixon, et al. (2000). "HIV-specific CD8(+) T cells produce antiviral cytokines but are impaired in cytolytic function." J Exp Med **192**(1): 63-75.

Auwaerter, P. G. (1999). "Infectious mononucleosis in middle age." JAMA **281**(5): 454-459.

Babcock, G. J., D. Hochberg, et al. (2000). "The expression pattern of Epstein-Barr virus latent genes in vivo is dependent upon the differentiation stage of the infected B cell." Immunity **13**(4): 497-506.

Baghdadi, M., A. Yoneda, et al. (2013). "TIM-4 glycoprotein-mediated degradation of dying tumor cells by autophagy leads to reduced antigen presentation and increased immune tolerance." Immunity **39**(6): 1070-1081.

Barlowe, C. K. and E. A. Miller (2013). "Secretory protein biogenesis and traffic in the early secretory pathway." Genetics **193**(2): 383-410.

Barouch, W., K. Prasad, et al. (1997). "Auxilin-induced interaction of the molecular chaperone Hsc70 with clathrin baskets." Biochemistry **36**(14): 4303-4308.

Barral, D. C., M. Cavallari, et al. (2008). "CD1a and MHC class I follow a similar endocytic recycling pathway." Traffic **9**(9): 1446-1457.

Bartee, E., M. Mansouri, et al. (2004). "Downregulation of major histocompatibility complex class I by human ubiquitin ligases related to viral immune evasion proteins." J Virol **78**(3): 1109-1120.

Basha, G., G. Lizee, et al. (2008). "MHC class I endosomal and lysosomal trafficking coincides with exogenous antigen loading in dendritic cells." PLoS One **3**(9): e3247.

Basha, G., K. Omilusik, et al. (2012). "A CD74-dependent MHC class I endolysosomal cross-presentation pathway." Nat Immunol **13**(3): 237-245.

Beale, R., H. Wise, et al. (2014). "A LC3-interacting motif in the influenza A virus M2 protein is required to subvert autophagy and maintain virion stability." Cell Host Microbe **15**(2): 239-247.

Belz, G. T., C. M. Smith, et al. (2004). "Distinct migrating and nonmigrating dendritic cell populations are involved in MHC class I-restricted antigen presentation after lung infection with virus." Proc Natl Acad Sci U S A **101**(23): 8670-8675.

Bender, B. S., T. Croghan, et al. (1992). "Transgenic mice lacking class I major histocompatibility complex-restricted T cells have delayed viral clearance and increased mortality after influenza virus challenge." J Exp Med **175**(4): 1143-1145.

Berg, T. O., M. Fengsrud, et al. (1998). "Isolation and characterization of rat liver amphisomes. Evidence for fusion of autophagosomes with both early and late endosomes." J Biol Chem **273**(34): 21883-21892.

Blake, N., T. Haigh, et al. (2000). "The importance of exogenous antigen in priming the human CD8+ T cell response: lessons from the EBV nuclear antigen EBNA1." J Immunol **165**(12): 7078-7087.

Blanchet, F. P., A. Moris, et al. (2010). "Human immunodeficiency virus-1 inhibition of immunoamphisomes in dendritic cells impairs early innate and adaptive immune responses." Immunity **32**(5): 654-669.

Bonifacino, J. S. and E. C. Dell'Angelica (1999). "Molecular bases for the recognition of tyrosine-based sorting signals." J Cell Biol **145**(5): 923-926.

Briken, V., R. M. Jackman, et al. (2002). "Intracellular trafficking pathway of newly synthesized CD1b molecules." EMBO J **21**(4): 825-834.

Brooks, J. M., H. M. Long, et al. (2016). "Early T Cell Recognition of B Cells following Epstein-Barr Virus Infection: Identifying Potential Targets for Prophylactic Vaccination." PLoS Pathog **12**(4): e1005549.

Byun, M., X. Wang, et al. (2007). "Cowpox virus exploits the endoplasmic reticulum retention pathway to inhibit MHC class I transport to the cell surface." Cell Host Microbe **2**(5): 306-315.

Campbell-Valois, F. X., M. Trost, et al. (2012). "Quantitative proteomics reveals that only a subset of the endoplasmic reticulum contributes to the phagosome." Mol Cell Proteomics **11**(7): M111 016378.

Capps, G. G., M. Van Kampen, et al. (1989). "Endocytosis of the class I major histocompatibility antigen via a phorbol myristate acetate-inducible pathway is a cell-specific phenomenon and requires the cytoplasmic domain." J Cell Biol **108**(4): 1317-1329.

Cebrian, I., C. Croce, et al. (2016). "Rab22a controls MHC-I intracellular trafficking and antigen cross-presentation by dendritic cells." EMBO Rep **17**(12): 1753-1765.

Cebrian, I., G. Visentin, et al. (2011). "Sec22b regulates phagosomal maturation and antigen crosspresentation by dendritic cells." Cell **147**(6): 1355-1368.

Cecconi, F. and B. Levine (2008). "The role of autophagy in mammalian development: cell makeover rather than cell death." Dev Cell **15**(3): 344-357.

Chhangani, D., S. Chinchwadkar, et al. (2014). "Autophagy coupling interplay: can improve cellular repair and aging?" Mol Neurobiol **49**(3): 1270-1281.

Cho, K. J. and P. A. Roche (2013). "Regulation of MHC Class II-Peptide Complex Expression by Ubiquitination." Front Immunol **4**: 369.

Coleman, C. B., J. E. McGraw, et al. (2014). "A gammaherpesvirus Bcl-2 ortholog blocks B cell receptor-mediated apoptosis and promotes the survival of developing B cells in vivo." PLoS Pathog **10**(2): e1003916.

Coscoy, L., D. J. Sanchez, et al. (2001). "A novel class of herpesvirus-encoded membrane-bound E3 ubiquitin ligases regulates endocytosis of proteins involved in immune recognition." J Cell Biol **155**(7): 1265-1273.

D'Souza-Schorey, C. and P. Chavrier (2006). "ARF proteins: roles in membrane traffic and beyond." Nat Rev Mol Cell Biol **7**(5): 347-358.

Dasari, V., S. Rehan, et al. (2016). "Autophagy and proteasome interconnect to coordinate cross-presentation through MHC class I pathway in B cells." Immunol Cell Biol **94**(10): 964-974.

Daskalogianni, C., S. Apcher, et al. (2008). "Gly-Ala repeats induce position- and substrate-specific regulation of 26 S proteasome-dependent partial processing." J Biol Chem **283**(44): 30090-30100.

De Angelis Rigotti, F., A. De Gassart, et al. (2017). "MARCH9-mediated ubiquitination regulates MHC I export from the TGN." Immunol Cell Biol **May 31**.

de la Salle, H., E. Houssaint, et al. (1997). "Human peptide transporter deficiency: importance of HLA-B in the presentation of TAP-independent EBV antigens." J Immunol **158**(10): 4555-4563.

De Leo, A., F. Colavita, et al. (2015). "Inhibition of autophagy in EBV-positive Burkitt's lymphoma cells enhances EBV lytic genes expression and replication." Cell Death Dis **6**: e1876.

De Luca, A., R. G. Iannitti, et al. (2012). "CD4(+) T cell vaccination overcomes defective cross-presentation of fungal antigens in a mouse model of chronic granulomatous disease." J Clin Invest **122**(5): 1816-1831.

Deegan, S., S. Saveljeva, et al. (2013). "Stress-induced self-cannibalism: on the regulation of autophagy by endoplasmic reticulum stress." Cell Mol Life Sci **70**(14): 2425-2441.

Dengjel, J., M. Hoyer-Hansen, et al. (2012). "Identification of autophagosome-associated proteins and regulators by quantitative proteomic analysis and genetic screens." Mol Cell Proteomics **11**(3): M111 014035.

Deretic, V. and B. Levine (2009). "Autophagy, immunity, and microbial adaptations." Cell Host Microbe **5**(6): 527-549.

Deter, R. L., P. Baudhuin, et al. (1967). "Participation of lysosomes in cellular autophagy induced in rat liver by glucagon." J Cell Biol **35**(2): C11-16.

Deter, R. L. and C. De Duve (1967). "Influence of glucagon, an inducer of cellular autophagy, on some physical properties of rat liver lysosomes." J Cell Biol **33**(2): 437-449.

Doherty, P. C., D. J. Topham, et al. (1996). "Establishment and persistence of virus-specific CD4+ and CD8+ T cell memory." Immunol Rev **150**: 23-44.

Doherty, P. C. and R. M. Zinkernagel (1975). "Enhanced immunological surveillance in mice heterozygous at the H-2 gene complex." Nature **256**(5512): 50-52.

Duncan, L. M., S. Piper, et al. (2006). "Lysine-63-linked ubiquitination is required for endolysosomal degradation of class I molecules." EMBO J **25**(8): 1635-1645.

English, L., M. Chemali, et al. (2009). "Autophagy enhances the presentation of endogenous viral antigens on MHC class I molecules during HSV-1 infection." Nat Immunol **10**(5): 480-487.

Farre, J. C. and S. Subramani (2016). "Mechanistic insights into selective autophagy pathways: lessons from yeast." Nat Rev Mol Cell Biol **17**(9): 537-552.

Feederle, R., M. Kost, et al. (2000). "The Epstein-Barr virus lytic program is controlled by the co-operative functions of two transactivators." EMBO J **19**(12): 3080-3089.

Fiegl, D., D. Kagebein, et al. (2013). "Amphisomal route of MHC class I cross-presentation in bacteria-infected dendritic cells." J Immunol **190**(6): 2791-2806.

Flomenberg, P., J. Szmulewicz, et al. (1992). "Role of the adenovirus E3-19k conserved region in binding major histocompatibility complex class I molecules." J Virol **66**(8): 4778-4783.

Florey, O., N. Gammoh, et al. (2015). "V-ATPase and osmotic imbalances activate endolysosomal LC3 lipidation." Autophagy **11**(1): 88-99.

Fotheringham, J. A. and N. Raab-Traub (2015). "Epstein-Barr virus latent membrane protein 2 induces autophagy to promote abnormal acinus formation." J Virol **89**(13): 6940-6944.

Fu, X., L. Tao, et al. (2010). "A short polypeptide from the herpes simplex virus type 2 ICP10 gene can induce antigen aggregation and autophagosomal degradation for enhanced immune presentation." Hum Gene Ther **21**(12): 1687-1696.

Fujita, N., T. Itoh, et al. (2008). "The Atg16L complex specifies the site of LC3 lipidation for membrane biogenesis in autophagy." Mol Biol Cell **19**(5): 2092-2100.

Galluzzi, L., E. H. Baehrecke, et al. (2017). "Molecular definitions of autophagy and related processes." EMBO J **36**(13): 1811-1836.

Gannage, M., D. Dormann, et al. (2009). "Matrix protein 2 of influenza A virus blocks autophagosome fusion with lysosomes." Cell Host Microbe **6**(4): 367-380.

Gewurz, B. E., E. W. Wang, et al. (2001). "Human cytomegalovirus US2 endoplasmic reticulum-lumenal domain dictates association with major histocompatibility complex class I in a locus-specific manner." J Virol **75**(11): 5197-5204.

Goepfert, P. A., A. Bansal, et al. (2000). "A significant number of human immunodeficiency virus epitope-specific cytotoxic T lymphocytes detected by tetramer binding do not produce gamma interferon." J Virol **74**(21): 10249-10255.

Goodall, M. L., T. Wang, et al. (2014). "Development of potent autophagy inhibitors that sensitize oncogenic BRAF V600E mutant melanoma tumor cells to vemurafenib." Autophagy **10**(6): 1120-1136.

Gordon, P. B. and P. O. Seglen (1988). "Prelysosomal convergence of autophagic and endocytic pathways." Biochem Biophys Res Commun **151**(1): 40-47.

Guermonprez, P., L. Saveanu, et al. (2003). "ER-phagosome fusion defines an MHC class I cross-presentation compartment in dendritic cells." Nature **425**(6956): 397-402.

Gupta-Rossi, N., S. Ortica, et al. (2011). "The adaptor-associated kinase 1, AAK1, is a positive regulator of the Notch pathway." J Biol Chem **286**(21): 18720-18730.

Hadinoto, V., M. Shapiro, et al. (2009). "The dynamics of EBV shedding implicate a central role for epithelial cells in amplifying viral output." PLoS Pathog **5**(7): e1000496.

Hampson, A. W. and J. S. Mackenzie (2006). "The influenza viruses." Med J Aust **185**(10 Suppl): S39-43.

Hara, T., K. Nakamura, et al. (2006). "Suppression of basal autophagy in neural cells causes neurodegenerative disease in mice." Nature **441**(7095): 885-889.

Hardie, D. G. (2011). "AMPK and autophagy get connected." EMBO J **30**(4): 634-635.

He, C. and D. J. Klionsky (2009). "Regulation mechanisms and signaling pathways of autophagy." Annu Rev Genet **43**: 67-93.

Henderson, D. M. and S. D. Conner (2007). "A novel AAK1 splice variant functions at multiple steps of the endocytic pathway." Mol Biol Cell **18**(7): 2698-2706.

Hislop, A. D., M. E. Ressing, et al. (2007). "A CD8+ T cell immune evasion protein specific to Epstein-Barr virus and its close relatives in Old World primates." J Exp Med **204**(8): 1863-1873.

Hislop, A. D. and G. S. Taylor (2015). "T-Cell Responses to EBV." Curr Top Microbiol Immunol **391**: 325-353.

Honing, S., D. Ricotta, et al. (2005). "Phosphatidylinositol-(4,5)-bisphosphate regulates sorting signal recognition by the clathrin-associated adaptor complex AP2." Mol Cell **18**(5): 519-531.

Houde, M., S. Bertholet, et al. (2003). "Phagosomes are competent organelles for antigen cross-presentation." Nature **425**(6956): 402-406.

Houssaint, E., X. Saulquin, et al. (2001). "Immunodominant CD8 T cell response to Epstein-Barr virus." Biomed Pharmacother **55**(7): 373-380.

Hubbard-Lucey, V. M., Y. Shono, et al. (2014). "Autophagy gene Atg16L1 prevents lethal T cell alloreactivity mediated by dendritic cells." Immunity **41**(4): 579-591.

Hutagalung, A. H. and P. J. Novick (2011). "Role of Rab GTPases in membrane traffic and cell physiology." Physiol Rev **91**(1): 119-149.

Jacomin, A. C. and I. P. Nezis (2016). "Using Fluorescent Reporters to Monitor Autophagy in the Female Germline Cells in Drosophila melanogaster." Methods Mol Biol **1457**: 69-78.

Jagannath, C., D. R. Lindsey, et al. (2009). "Autophagy enhances the efficacy of BCG vaccine by increasing peptide presentation in mouse dendritic cells." Nat Med **15**(3): 267-276.

Johnstone, C., M. Ramos, et al. (2012). "Exogenous, TAP-independent lysosomal presentation of a respiratory syncytial virus CTL epitope." Immunol Cell Biol **90**(10): 978-982.

Kaech, S. M., E. J. Wherry, et al. (2002). "Effector and memory T-cell differentiation: implications for vaccine development." Nat Rev Immunol **2**(4): 251-262.

Kalvari, I., S. Tsompanis, et al. (2014). "iLIR: A web resource for prediction of Atg8-family interacting proteins." Autophagy **10**(5): 913-925.

Karanasios, E., S. A. Walker, et al. (2016). "Autophagy initiation by ULK complex assembly on ER tubulovesicular regions marked by ATG9 vesicles." Nat Commun **7**: 12420.

Kasai, M., I. Tanida, et al. (2009). "Autophagic compartments gain access to the MHC class II compartments in thymic epithelium." J Immunol **183**(11): 7278-7285.

Keller, C. W., M. Loi, et al. (2017). "The autophagy machinery restrains iNKT cell activation through CD1D1 internalization." Autophagy **13**(6): 1025-1036.

Khaminets, A., C. Behl, et al. (2016). "Ubiquitin-Dependent And Independent Signals In Selective Autophagy." Trends Cell Biol **26**(1): 6-16.

Kimura, T., A. Jain, et al. (2015). "TRIM-mediated precision autophagy targets cytoplasmic regulators of innate immunity." J Cell Biol **210**(6): 973-989.

Kisselev, A. F., T. N. Akopian, et al. (1999). "The sizes of peptides generated from protein by mammalian 26 and 20 S proteasomes. Implications for understanding the degradative mechanism and antigen presentation." J Biol Chem **274**(6): 3363-3371.

Klionsky, D. J., E. L. Eskelinen, et al. (2014). "Autophagosomes, phagosomes, autolysosomes, phagolysosomes, autophagolysosomes... wait, I'm confused." Autophagy **10**(4): 549-551.

Ko, Y. H. (2015). "EBV and human cancer." Exp Mol Med **47**: e130.

Komatsu, M., S. Waguri, et al. (2005). "Impairment of starvation-induced and constitutive autophagy in Atg7-deficient mice." J Cell Biol **169**(3): 425-434.

Kulpa, D. A., N. Del Cid, et al. (2013). "Adaptor Protein 1 Promotes Cross-Presentation through the Same Tyrosine Signal in Major Histocompatibility Complex Class I as That Targeted by HIV-1." Journal of Virology **87**(14): 8085-8098.

Kumanovics, A., T. Takada, et al. (2003). "Genomic organization of the mammalian MHC." Annu Rev Immunol **21**: 629-657.

Kwun, H. J., S. R. da Silva, et al. (2007). "Kaposi's sarcoma-associated herpesvirus latency-associated nuclear antigen 1 mimics Epstein-Barr virus EBNA1 immune evasion through central repeat domain effects on protein processing." J Virol **81**(15): 8225-8235.

Lautscham, G., S. Mayrhofer, et al. (2001). "Processing of a multiple membrane spanning Epstein-Barr virus protein for CD8(+) T cell recognition reveals a proteasome-dependent, transporter associated with antigen processing-independent pathway." J Exp Med **194**(8): 1053-1068.

Lawton, A. P., T. I. Prigozy, et al. (2005). "The mouse CD1d cytoplasmic tail mediates CD1d trafficking and antigen presentation by adaptor protein 3-dependent and -independent mechanisms." J Immunol **174**(6): 3179-3186.

Lee, D. Y. and B. Sugden (2008). "The latent membrane protein 1 oncogene modifies B-cell physiology by regulating autophagy." Oncogene **27**(20): 2833-2842.

Lee, H. K., L. M. Mattei, et al. (2010). "In vivo requirement for Atg5 in antigen presentation by dendritic cells." Immunity **32**(2): 227-239.

Lee, J. S., Q. Li, et al. (2009). "FLIP-mediated autophagy regulation in cell death control." Nat Cell Biol **11**(11): 1355-1362.

Lehner, P. J., J. T. Karttunen, et al. (1997). "The human cytomegalovirus US6 glycoprotein inhibits transporter associated with antigen processing-dependent peptide translocation." Proc Natl Acad Sci U S A **94**(13): 6904-6909.

Leung, C. S., T. A. Haigh, et al. (2010). "Nuclear location of an endogenously expressed antigen, EBNA1, restricts access to macroautophagy and the range of CD4 epitope display." Proc Natl Acad Sci U S A **107**(5): 2165-2170.

Levine, B. and D. J. Klionsky (2017). "Autophagy wins the 2016 Nobel Prize in Physiology or Medicine: Breakthroughs in baker's yeast fuel advances in biomedical research." Proc Natl Acad Sci U S A **114**(2): 201-205.

Levine, B. and G. Kroemer (2008). "Autophagy in the pathogenesis of disease." Cell **132**(1): 27-42.

Levy, J., W. Cacheux, et al. (2015). "Intestinal inhibition of Atg7 prevents tumour initiation through a microbiome-influenced immune response and suppresses tumour growth." Nat Cell Biol **17**(8): 1062-1073.

Li, Y., L. X. Wang, et al. (2008). "Efficient cross-presentation depends on autophagy in tumor cells." Cancer Res **68**(17): 6889-6895.

Liepe, J., F. Marino, et al. (2016). "A large fraction of HLA class I ligands are proteasome-generated spliced peptides." Science **354**(6310): 354-358.

Lizee, G., G. Basha, et al. (2003). "Control of dendritic cell cross-presentation by the major histocompatibility complex class I cytoplasmic domain." Nat Immunol **4**(11): 1065-1073.

Longhi, M. P., C. Trumpfheller, et al. (2009). "Dendritic cells require a systemic type I interferon response to mature and induce CD4+ Th1 immunity with poly IC as adjuvant." J Exp Med **206**(7): 1589-1602.

Loos, B., A. du Toit, et al. (2014). "Defining and measuring autophagosome flux-concept and reality." Autophagy **10**(11): 2087-2096.

Lotteau, V., L. Teyton, et al. (1990). "Intracellular transport of class II MHC molecules directed by invariant chain." Nature **348**(6302): 600-605.

Lussignol, M., C. Queval, et al. (2013). "The herpes simplex virus 1 Us11 protein inhibits autophagy through its interaction with the protein kinase PKR." J Virol **87**(2): 859-871.

Mari, M., S. A. Tooze, et al. (2011). "The puzzling origin of the autophagosomal membrane." F1000 Biol Rep **3**: 25.

Marshall, R. S., F. Li, et al. (2015). "Autophagic Degradation of the 26S Proteasome Is Mediated by the Dual ATG8/Ubiquitin Receptor RPN10 in Arabidopsis." Mol Cell **58**(6): 1053-1066.

Martinez, J., R. K. Malireddi, et al. (2015). "Molecular characterization of LC3-associated phagocytosis reveals distinct roles for Rubicon, NOX2 and autophagy proteins." Nat Cell Biol **17**(7): 893-906.

Matloubian, M., R. J. Concepcion, et al. (1994). "CD4+ T cells are required to sustain CD8+ cytotoxic T-cell responses during chronic viral infection." J Virol **68**(12): 8056-8063.

Matsuki, Y., M. Ohmura-Hoshino, et al. (2007). "Novel regulation of MHC class II function in B cells." EMBO J **26**(3): 846-854.

McFadden, K., A. Y. Hafez, et al. (2016). "Metabolic stress is a barrier to Epstein-Barr virus-mediated B-cell immortalization." Proc Natl Acad Sci U S A **113**(6): E782-790.

Miller, G., A. El-Guindy, et al. (2007). "Lytic cycle switches of oncogenic human gammaherpesviruses." Advances in cancer research **97**: 81-109.

Mintern, J. D., S. Bedoui, et al. (2009). "Transience of MHC Class I-restricted antigen presentation after influenza A virus infection." Proc Natl Acad Sci U S A **106**(16): 6724-6729.

Mintern, J. D., C. Macri, et al. (2015). "Differential use of autophagy by primary dendritic cells specialized in cross-presentation." Autophagy **11**(6): 906-917.

Mizushima, N., A. Yamamoto, et al. (2001). "Dissection of autophagosome formation using Apg5-deficient mouse embryonic stem cells." J Cell Biol **152**(4): 657-668.

Mukherjee, A., B. Patel, et al. (2016). "Selective endosomal microautophagy is starvation-inducible in Drosophila." Autophagy **12**(11): 1984-1999.

Murali-Krishna, K., J. D. Altman, et al. (1998). "Counting antigen-specific CD8 T cells: a reevaluation of bystander activation during viral infection." Immunity **8**(2): 177-187.

Nair-Gupta, P., A. Baccarini, et al. (2014). "TLR signals induce phagosomal MHC-I delivery from the endosomal recycling compartment to allow cross-presentation." Cell **158**(3): 506-521.

Nakatogawa, H., K. Suzuki, et al. (2009). "Dynamics and diversity in autophagy mechanisms: lessons from yeast." Nat Rev Mol Cell Biol **10**(7): 458-467.

Naslavsky, N., R. Weigert, et al. (2004). "Characterization of a nonclathrin endocytic pathway: membrane cargo and lipid requirements." Mol Biol Cell **15**(8): 3542-3552.

Nathan, J. A. and P. J. Lehner (2009). "The trafficking and regulation of membrane receptors by the RING-CH ubiquitin E3 ligases." Exp Cell Res **315**(9): 1593-1600.

Nedjic, J., M. Aichinger, et al. (2008). "A novel role for autophagy in T cell education." Autophagy **4**(8): 1090-1092.

Neumann, L., W. Kraas, et al. (1997). "The active domain of the herpes simplex virus protein ICP47: a potent inhibitor of the transporter associated with antigen processing." J Mol Biol **272**(4): 484-492.

Nguyen, T. N., B. S. Padman, et al. (2016). "Atg8 family LC3/GABARAP proteins are crucial for autophagosome-lysosome fusion but not autophagosome formation during PINK1/Parkin mitophagy and starvation." J Cell Biol **215**(6): 857-874.

Nishida, Y., S. Arakawa, et al. (2009). "Discovery of Atg5/Atg7-independent alternative macroautophagy." Nature **461**(7264): 654-658.

Nowag, H., B. Guhl, et al. (2014). "Macroautophagy Proteins Assist Epstein Barr Virus Production and Get Incorporated Into the Virus Particles." EBioMedicine **1**(2-3): 116-125.

Ohsumi, Y. (2001). "Molecular dissection of autophagy: two ubiquitin-like systems." Nat Rev Mol Cell Biol **2**(3): 211-216.

Orvedahl, A., D. Alexander, et al. (2007). "HSV-1 ICP34.5 confers neurovirulence by targeting the Beclin 1 autophagy protein." Cell Host Microbe **1**(1): 23-35.

Paludan, C., D. Schmid, et al. (2005). "Endogenous MHC class II processing of a viral nuclear antigen after autophagy." Science **307**(5709): 593-596.

Park, B., Y. Kim, et al. (2004). "Human cytomegalovirus inhibits tapasin-dependent peptide loading and optimization of the MHC class I peptide cargo for immune evasion." Immunity **20**(1): 71-85.

Paul, P. and C. Munz (2016). "Autophagy and Mammalian Viruses: Roles in Immune Response, Viral Replication, and Beyond." Adv Virus Res **95**: 149-195.

Prod'homme, V., C. Griffin, et al. (2007). "The human cytomegalovirus MHC class I homolog UL18 inhibits LIR-1+ but activates LIR-1- NK cells." J Immunol **178**(7): 4473-4481.

Proikas-Cezanne, T., Z. Takacs, et al. (2015). "WIPI proteins: essential PtdIns3P effectors at the nascent autophagosome." J Cell Sci **128**(2): 207-217.

Pryor, P. R. and J. P. Luzio (2009). "Delivery of endocytosed membrane proteins to the lysosome." Biochim Biophys Acta **1793**(4): 615-624.

Qu, X., Z. Zou, et al. (2007). "Autophagy gene-dependent clearance of apoptotic cells during embryonic development." Cell **128**(5): 931-946.

Ravikumar, B., K. Moreau, et al. (2010). "Plasma membrane contributes to the formation of pre-autophagosomal structures." Nat Cell Biol **12**(8): 747-757.

Reid, P. A. and C. Watts (1990). "Cycling of cell-surface MHC glycoproteins through primaquine-sensitive intracellular compartments." Nature **346**(6285): 655-657.

Reusch, U., W. Muranyi, et al. (1999). "A cytomegalovirus glycoprotein re-routes MHC class I complexes to lysosomes for degradation." EMBO J **18**(4): 1081-1091.

Ricotta, D., S. D. Conner, et al. (2002). "Phosphorylation of the AP2 mu subunit by AAK1 mediates high affinity binding to membrane protein sorting signals." J Cell Biol **156**(5): 791-795.

Rogov, V. V., H. Suzuki, et al. (2017). "Phosphorylation of the mitochondrial autophagy receptor Nix enhances its interaction with LC3 proteins." Sci Rep **7**(1): 1131.

Romao, S., N. Gasser, et al. (2013). "Autophagy proteins stabilize pathogen-containing phagosomes for prolonged MHC II antigen processing." J Cell Biol **203**(5): 757-766.

Rubinsztein, D. C. (2006). "The roles of intracellular protein-degradation pathways in neurodegeneration." Nature **443**(7113): 780-786.

Saitoh, T., N. Fujita, et al. (2008). "[Autophagy and innate immunity]." Tanpakushitsu Kakusan Koso **53**(16 Suppl): 2279-2285.

Sanjuan, M. A., C. P. Dillon, et al. (2007). "Toll-like receptor signalling in macrophages links the autophagy pathway to phagocytosis." Nature **450**(7173): 1253-1257.

Schaefer, M. R., E. R. Wonderlich, et al. (2008). "HIV-1 Nef targets MHC-I and CD4 for degradation via a final common beta-COP-dependent pathway in T cells." PLoS Pathog **4**(8): e1000131.

Schirmbeck, R., W. Bohm, et al. (1997). "Stress protein (hsp73)-mediated, TAP-independent processing of endogenous, truncated SV40 large T antigen for Db-restricted peptide presentation." Eur J Immunol **27**(8): 2016-2023.

Schmid, D., M. Pypaert, et al. (2007). "Antigen-loading compartments for major histocompatibility complex class II molecules continuously receive input from autophagosomes." Immunity **26**(1): 79-92.

Sridhar, S., S. Begom, et al. (2013). "Cellular immune correlates of protection against symptomatic pandemic influenza." Nat Med **19**(10): 1305-1312.

Sugita, M., R. M. Jackman, et al. (1996). "Cytoplasmic tail-dependent localization of CD1b antigen-presenting molecules to MIICs." Science **273**(5273): 349-352.

Tangye, S. G., U. Palendira, et al. (2017). "Human immunity against EBV-lessons from the clinic." J Exp Med **214**(2): 269-283.

Tattevin, P., Y. Le Tulzo, et al. (2006). "Increasing incidence of severe Epstein-Barr virus-related infectious mononucleosis: surveillance study." J Clin Microbiol **44**(5): 1873-1874.

Tellam, J., M. Sherritt, et al. (2001). "Targeting of EBNA1 for rapid intracellular degradation overrides the inhibitory effects of the Gly-Ala repeat domain and restores CD8+ T cell recognition." J Biol Chem **276**(36): 33353-33360.

Tey, S. K. and R. Khanna (2012). "Autophagy mediates transporter associated with antigen processing-independent presentation of viral epitopes through MHC class I pathway." Blood **120**(5): 994-1004.

Thorley-Lawson, D. A. (2001). "Epstein-Barr virus: exploiting the immune system." Nat Rev Immunol **1**(1): 75-82.

Tian, S., J. Lin, et al. (2010). "Beclin 1-independent autophagy induced by a Bcl-XL/Bcl-2 targeting compound, Z18." Autophagy **6**(8): 1032-1041.

Tian, Y., J. C. Chang, et al. (2013). "Adaptor complex AP2/PICALM, through interaction with LC3, targets Alzheimer's APP-CTF for terminal degradation via autophagy." Proc Natl Acad Sci U S A **110**(42): 17071-17076.

Tooze, S. A. and T. Yoshimori (2010). "The origin of the autophagosomal membrane." Nat Cell Biol **12**(9): 831-835.

Tsuboyama, K., I. Koyama-Honda, et al. (2016). "The ATG conjugation systems are important for degradation of the inner autophagosomal membrane." Science **354**(6315): 1036-1041.

Uebel, S. and R. Tampe (1999). "Specificity of the proteasome and the TAP transporter." Curr Opin Immunol **11**(2): 203-208.

Uhl, M., O. Kepp, et al. (2009). "Autophagy within the antigen donor cell facilitates efficient antigen cross-priming of virus-specific CD8+ T cells." Cell Death Differ **16**(7): 991-1005.

van Endert, P. M., L. Saveanu, et al. (2002). "Powering the peptide pump: TAP crosstalk with energetic nucleotides." Trends Biochem Sci **27**(9): 454-461.

Vega, M. A. and J. L. Strominger (1989). "Constitutive endocytosis of HLA class I antigens requires a specific portion of the intracytoplasmic tail that shares structural features with other endocytosed molecules." Proc Natl Acad Sci U S A **86**(8): 2688-2692.

Verlhac, P., I. P. Gregoire, et al. (2015). "Autophagy receptor NDP52 regulates pathogen-containing autophagosome maturation." Cell Host Microbe **17**(4): 515-525.

Voigt, V., C. A. Forbes, et al. (2003). "Murine cytomegalovirus m157 mutation and variation leads to immune evasion of natural killer cells." Proc Natl Acad Sci U S A **100**(23): 13483-13488.

von Muhlinen, N., M. Akutsu, et al. (2012). "LC3C, bound selectively by a noncanonical LIR motif in NDP52, is required for antibacterial autophagy." Mol Cell **48**(3): 329-342.

Walseng, E., O. Bakke, et al. (2008). "Major histocompatibility complex class II-peptide complexes internalize using a clathrin- and dynamin-independent endocytosis pathway." J Biol Chem **283**(21): 14717-14727.

Wang, Z., Y. Wan, et al. (2015). "Recovery from severe H7N9 disease is associated with diverse response mechanisms dominated by CD8(+) T cells." Nat Commun **6**: 6833.

Weigert, R., A. C. Yeung, et al. (2004). "Rab22a regulates the recycling of membrane proteins internalized independently of clathrin." Mol Biol Cell **15**(8): 3758-3770.

Wenger, T., S. Terawaki, et al. (2012). "Autophagy inhibition promotes defective neosynthesized proteins storage in ALIS, and induces redirection toward proteasome processing and MHCI-restricted presentation." Autophagy **8**(3): 350-363.

Wherry, E. J., J. N. Blattman, et al. (2003). "Viral persistence alters CD8 T-cell immunodominance and tissue distribution and results in distinct stages of functional impairment." J Virol **77**(8): 4911-4927.

Wiertz, E. J., T. R. Jones, et al. (1996). "The human cytomegalovirus US11 gene product dislocates MHC class I heavy chains from the endoplasmic reticulum to the cytosol." Cell **84**(5): 769-779.

Xie, Z. and D. J. Klionsky (2007). "Autophagosome formation: core machinery and adaptations." Nat Cell Biol **9**(10): 1102-1109.

Yang, Z. and D. J. Klionsky (2010). "Eaten alive: a history of macroautophagy." Nat Cell Biol **12**(9): 814-822.

Yewdell, J. W., L. C. Anton, et al. (1996). "Defective ribosomal products (DRiPs): a major source of antigenic peptides for MHC class I molecules?" J Immunol **157**(5): 1823-1826.

Yin, Y., B. Manoury, et al. (2003). "Self-inhibition of synthesis and antigen presentation by Epstein-Barr virus-encoded EBNA1." Science **301**(5638): 1371-1374.

Yoon, H., K. L. Legge, et al. (2007). "Sequential activation of CD8+ T cells in the draining lymph nodes in response to pulmonary virus infection." J Immunol **179**(1): 391-399.

Young, L. S. and A. B. Rickinson (2004). "Epstein-Barr virus: 40 years on." Nature reviews. Cancer **4**(10): 757-768.

Abbreviations

Abbreviation	full name
AAK1	Adaptor protein-Associated Kinase
AMPK	AMP-activated Protein Kinase
AP	Adaptor Protein
APC	AlloPhycoCyanin
APC-Cy7	AlloPhycoCyanin-Cyanin7
ATG	Autophagy-related protein
Atg	Autophagy-related gene
ATP	Adenosine TriPhosphate
Bcl-2	B-cell lymphoma 2
BM-DC	Bone Marrow-Derived DC
BSA	Bovine Serum Albumine
CD	Cluster of Differentiation
CFSE	CarboxyFluorescein Succinimidyl Ester
CMA	Chaperone-Mediated Autophagy
CQ	Chloroquine
Cre	Cyclization (or causes) recombination enzyme
DAPI	4',6-DiAmidino-2-PhenylIndole
DC	Dendritic Cell
DEC-205	Dendritic and Epithelial Cells, 205 kDa
DNA	DeoxyriboNucleic Acid
DNase	DeoxyriboNuclease
dNTP	deoxyNucleotide TriPhosphates
DRiP	Deferctive Ribosomal Product
EBNA	EBV Nuclear Antigen
EBV	Epstein Barr Virus
EDTA	Ethylenediaminetetraacetic acid
EGFR	Enhanced Green Fluorescent Protein
ELISA	enzyme-linked immunosorbent assay
ER	Endoplasmatic Recticulum
ERC	Endosomal Recycling Compartment
ERGIC	ER-Golgi Intermediate Compartment
FLICE	Fas-associated death domain-like interleukin-1β-converting enzyme
Fl or flox	DNA sequence that is flanked by two loxP sites
GABARAP	GABA Type A Receptor-Associated Protein
GABARAPL	GABA Type A Receptor-Associated Protein Like
GAr	Glycine Alanine Repeat
GDP	Guanosine DiPhosphate
GFP	Green Fluorescent Protein
GM-CSF	Granulocyte-Macrophage Colony-Stimulating Factor
GP	GlycoProtein
GTP	Guanosine TriPhosphate
HA	Haemagglutinin
HAU	hemagglutination Unit
HLA	Human leukocyte antigen
HRP	Horseradish peroxidase
IAV	Inflenza A Virus
IFN	Interferon

Abbreviation	full name
IL	InterLeukin
IRES	Internal Ribosome Entry Site
kb	KiloBase
kDa	Kilo Dalton
LAMP2	Lysosome-Associated Membrane Protein 2
LAP	LC3-associated phagocytosi
LC3	Microtubule-associated protein 1A/1B-light chain 3
LCL	Lymphoblastoid cells
LIR	LC3-Associated Region
LMCV	LyMphocytic Choriomeningitis Virus
LMP	Latent Membrane Proteins
MACS	Magnetic Cell Separation
MARCH	Membrane-Associated RING-CH
MEF	Murine Embronic Fibroblast
MFI	Mean Fluorescence Intensity
MHC	Major Histocompatibility Complex
MIIC	MHC-II loading compartment
min	minute
MS	Mass Spectrometry
mTOR	mammalian Target Of Rapamycin
MVB	Multi Vesiculr Body
NA	Neuraminidase
NK	Natural Killer
NADPH	Nicotinamide adenine dinucleotide phosphate
NP	NucleoProtein
PAGE	PolyAcrylamide Gel Electrophoresis
PB	Pacific Blue
PBS	Phospate Buffer Saline
PBS-T	PBS 0.2% Tween20
PCR	Polimerase Chain Reaction
PE	phosphatidylethanolamine
PE	Phycoeritrin
PE-Cy7	Phycoeritrin cyanin7
PFU	Plaque forming Unit
qRT-PCR	quantitative real-time reverse transcription polymerase chain reaction
RPMI	Roswell Park Memorial Institute
R10	RPMI 10% FCS
RALBP1	RalA Binding Protein 1
RNA	RiboNucleic Acid
ROS	Reactive-Oxygen Species
SDS	Sodium Dodecyl Sulphate
SIGLEC	Sialic Acid binding Ig-like lectin
SNARE	Soluble NSF Attachment Receptors
SQSTM1/p62	Sequestrosome
sec	second

Abbreviation	full name
T1.B35	HLA-B*3501 trasfected 721.45 T1
T2.B35	HLA-B*3501 trasfected CEMx174 T2
TAP	Transporter-Associated with antigen Presentation
VAMP	Vesicle-Associated Membrane Proteins
VPS	Vacuolar Protein Sorting
β2m	Beta2-microglobulin

Declaration

I declare that I have written this thesis myself and have only used the aforementioned references.

Additionally, I declare that I performed all the experiment by myself. Monique Gannagé, who started the project, together with Anne Müller, Assunta Caruso and Jennifer Niven performed experiments for figures 3.1, 3.2, 3.5A, 3.5C, D, 3.6, 3.9, 3.11D, 3.13, 3.14, 3.16, 3.17, 3.20. Petra Paul and Laure-Anne Ligeon, as unbiased eyes, quantified the intracellular MHC-I staining of figure 3.8. Julia Rühl took care of $CD8^+$T cell clone culture. Finally, mass spectrometry analysis has been conducted by the lab of Jörn Dengjel.

Zürich 20 09.2017

Monica Loi, Zurich, Switzerland

Curriculum Vitae

Personal Data

Monica Loi
Born in San Gavino Monreale (CA), November 3, 1983
Citizenship: Italian
Private Address: Niederlenzer Kirchweg 5b, 5600 Lenzburg (AG)
Mobile: +41 789494538
E-mail: monicaloi83@gmail.com

Academic qualification

09.2013 (scheduled PhD defence 09.11.2017) PhD student enrolled in the Microbiology and Immunology Program at the Institute of Experimental Immunology, University of Zürich. Thesis supervisor, Professor Dr. Christian Münz. Title of the project: Macroautophagy in MHC class I restricted antigen presentation.

07.2007 M.Sc. in Molecular Biotechnology (110/110 cum laudae), University of Sassari, Italy, focused on "Targeting liposomal chemotherapy via both tumor cell-specific and tumor vasculature-specific ligands potentiates therapeutic efficacy".

07.2005 B.S. in Biotechnology (110/110 cum laudae), University of Sassari, Italy, focused on "Antiproliferative and pro-apoptotic activity of eugenol-related biphenyls on malignant melanoma cells".

Professional Experience

09.2007- 08.2013 Assistant researcher at the Experimental Therapy Unit (Head, Dr. Mirco Ponzoni) of the Laboratory of Oncology (Head, Dr. Vito Pistoia), IRCCS, Istituto G. Gaslini, in Genoa, involved in the following projects:

- Phage display technology for novel tumour and vascular targeted therapies against Neuroblastoma
- New Immunotherapeutic approaches to Neuroblastoma;
- Tissue–penetrating phage display-derived peptides for the design of novel anticancer drugs-loaded nanocarriers.

01-07.2007 Graduating student at the Experimental Therapy Unit of the Laboratory of Oncology, IRCCS, Istituto Gaslini in Genoa.

01.2005-12.2006 Graduating student at the Biomolecular Chemistry Institute (Head, Dr. Giuseppe Palmieri), National Research Council, Sassari.

Trasferable skills/Continuing Education

08.2016 Personalized practical medicine, organized by Ecole Polytechnique Federale de Lausanne (EPFL) and Eidgenössische Technische Hochschule (ETH)

09.2015 Project management for research organized by the University of Zurich

09.2015 Leadership skills for doctoral candidates organized by the University of Zurich

02.2014 Felasa accreditation, Category B, ID LTK2364 organized by the University of Zurich

Awards

06.2017 MIM travel grant for the EMBO workshop on Antigen processing and presentation

09.2015 EFIS-Biolegend Bright Sparks Award for a presentation judged outstanding.

09.2015 EFIS Travel Grant for the European Conference of Immunology.

06.2012 "Premio Vincenzo Secondo e Luigi Gallo" of the Rotary Club Genova.

08.2011 "2010 CRS Jorge Heller Journal of Controlled Release Outstanding Paper Award"

Achievements:

2017 Responsible for the organization of the Institute day

2016 Successfully organised 3 days PhD retreat in Grindelwald

2016 Successfully organized a seminar series at the University of Zurich

2015-2016 Lesson and exam assistant of Genetic and Immunology Courses for graduating students

2015-2016 Forschungskredit recipient from University of Zurich.

Languages

Italian	mother tongue
English	fluent
German	basic
French	basic

Selected oral presentations

2015 "Regulation of MHC class I endocytosis by the macroautophagy machinery" presented within a 'Bright Sparks in Immunology' Workshop at the European Conference of Immunology.

Scientific publications

Loi M, Ligeon L, Münz C. MHC class I internalization via autophagy proteins. Methods in Molecular Biology. 2017 *submitted*

Keller CW, **Loi M**, Ewert S, Quast I, Theiler M, Gannagé M, Münz C, De Libero G, Freigang S, and Lünemann JD. The autophagy machinery restrains iNKT cell activation through CD1d internalization. Autophagy. 2017 Jun 3;13(6):1025-1036

Loi M, Gannagé M, Münz C. ATGs help MHC class II, but inhibit MHC class I antigen presentation. Autophagy. 2016 Sep;12(9):1681-2

Loi M, Müller A, Steinbach K, Niven J, Barreira da Silva R, Paul P, Ligeon L, Caruso A, Albrecht RA, Becker A, Annaheim N, Nowag H, Dengjel J, García-Sastre A, Merkler D, Münz C and Gannagé M. Macroautophagy controls MHC class I levels on dendritic cells and shapes the anti-viral $CD8^+$ T cell response. Cell Rep. 2016 May 3;15(5):1076-87

Piaggio F, Kondylis V, Pastorino F, Di Paolo D, Perri P, Cossu I, Schorn F Marinaccio C, Murgia D, Daga A, **Loi M**, Emionite L, Ognio E, Pasparakis M, Ribatti D, Ponzoni M, Brignole C. A novel liposomal Clodronate depletes tumor associated macrophages in primary and metastatic melanoma: anti-angiogenic and anti-tumor effects. J Control Release. 2016 Feb 10;223:165-77

Cossu I, Bottoni G, **Loi M**, Emionite L, Bartolini A, Di Paolo D, Brignole C, Piaggio F, Perri P, Sacchi A, Curnis F, Gagliani MC, Bruno S, Marini C, Gori A, Longhi R, Murgia D, Sementa AR, Cilli M, Tacchetti C, Corti A, Sambuceti G, Marchiò S, Ponzoni M, Pastorino F. Neuroblastoma-targeted nanocarriers improve drug delivery and penetration, delay tumor growth and abrogate metastatic diffusion. Biomaterials 2015 Nov; 68:89-99.

Zuccari G, Milelli A, Pastorino F, **Loi M**, Petretto A, Parise A, Marchetti C, Minarini A, Cilli M, Emionite L, Di Paolo D, Brignole C, Piaggio F, Perri P, Tumiatti V, Pistoia V, Pagnan G, Ponzoni M.Tumor vascular targeted liposomal-bortezomib minimizes side effects and increases therapeutic activity in human Neuroblastoma. Journal of Controlled Release 2015 May 29; pii: S0168-3659(15)00595-7.

Loi M, Becherini P, Emionite L, Giacomini A, Cossu I, Destefanis E, Brignole C, Di Paolo D, Piaggio F, Perri P, Cilli M, Pastorino F, Ponzoni M. sTRAIL coupled to liposomes improves its pharmacokinetic profile and overcomes neuroblastoma tumour resistance in combination with Bortezomib. J Control Release. 2014 Jul 17;19C:157-166.

Pastorino F, Brignole C, **Loi M**, Di Paolo D, Di Fiore A, Perri P, Pagnan G, Ponzoni M. Nanocarrier-mediated targeting of tumor and tumor vascular cells improves uptake and penetration of drugs into neuroblastoma. Front Oncol. 2013 Aug 5; 3:190.

Di Paolo D, Pastorino F, Zuccari G, Caffa I, **Loi M**, Marimpietri D, Brignole C, Perri P, Cilli M, Nico B, Ribatti D, Pistoia V, Ponzoni M, Pagnan G. Enhanced anti-tumor and anti-angiogenic efficacy of a novel liposomal fenretinide on human neuroblastoma. J Control Release. 2013 Jun 19;170(3):445-451.

Loi M, Di Paolo D, Soster M, Brignole C, Bartolini A, Emionite L, Sun J, Becherini P, Curnis F, Petretto A, Sani M, Gori A, Milanese M, Gambini C, Longhi R, Cilli M, Allen TM, Bussolino F, Arap W, Pasqualini R, Corti A, Ponzoni M, Marchiò S, Pastorino F. Novel phage display-derived neuroblastoma-targeting peptides potentiate the effect of drug nanocarriers in preclinical settings. J Control Release. 2013 Sep 10;170(2):233-41.

Di Paolo D, Ambrogio C, Pastorino F, Brignole C, Martinengo C, Carosio R, **Loi M**, Pagnan G, Emionite L, Cilli M, Ribatti D, Allen TM, Chiarle R, Ponzoni M, Perri P. Selective therapeutic targeting of the Anaplastic Lymphoma Kinase with Liposomal siRNA induces Apoptosis and inhibits angiogenesis in Neuroblastoma. Mol Ther. 2011 Dec;19(12):2201-12

Loi M, Di Paolo D, Becherini P, Zorzoli A, Perri P, Carosio R, Cilli M, Ribatti D, Brignole C, Pagnan G, Ponzoni M, Pastorino F. The use of orthotopic model to validate antivascular terapies for cancer. Int J Dev Biol. 2011;55(4-5):547-55.

Di Paolo D, Brignole C, Pastorino F, Carosio R, Zorzoli A, Rossi M, **Loi M**, Pagnan G, Emionite L, Cilli M, Bruno S, Chiarle R, Allen TM, Ponzoni M, Perri P. Neuroblastoma-targeted nanoparticles entrapping siRNA specifically knockdown ALK. Mol Ther. 2011 Jun; 19(6): 1131-40.

Brignole C, Marimpietri D, Di Paolo D, Perri P, Morandi F, Pastorino F, Zorzoli A, Pagnan G **Loi M**, Caffa I, Erminio G, Haupt R, Gambini C, Pistoia V, Ponzoni M. Therapeutic targeting of TLR9 inhibits cell growth and induces apoptosis in neuroblastoma. Cancer Res. 2010 Dec 1; 70(23): 9816-26

Pastorino F, **Loi M**, Sapra P, Becherini P, Cilli M, Emionite L, Ribatti D, Greenberger LM, Horak ID, Ponzoni M. Tumor regression and curability of preclinical neuroblastoma models by PEGylated SN38 (EZN-2208), a novel topoisomerase I inhibitor. Clin Cancer Res. 2010 Oct 1; 16(19): 4809-21.

Loi M, Marchiò S, Becherini P, Di Paolo D, Soster M, Curnis F, Brignole C, Pagnan G, Perri P, Longhi R, Nico B, Bussolino F, Ribatti D, Cilli M, Arap W, Pasqualini R, Corti A, Allen TM, Ponzoni M and Pastorino F. Combined targeting of perivascular and endothelial tumor cells enhances the anti-tumor effectiveness of liposomal chemotherapy in neuroblastoma. J Control Release. 2010 Jul 1; 145(1): 66-73.

Loi M, Di Paolo D, Pastorino F, Brignole C, Marimpietri D, Beccherini P, Caffa I, Zorzoli A, Longhi R, Gagliani C, Tacchetti C, Corti A, Allen TM, Ponzoni M and Pagnan G. Liposomes-mediated therapy of neuroblastoma. Methods in Enzymology. 2009; 465:225-49.

Pastorino F, Di Paolo D, **Loi M**, Becherini P, Caffa I, Zorzoli A, Marimpietri D, Carosio R, Perri P, Montaldo PG, Brignole C, Pagnan G, Ribatti D, Allen TM, Ponzoni M. Recent Advances in Targeted Anti-Vasculature Therapy: The Neuroblastoma Model. Curr Drug Targets. 2009 Oct; 10(10): 1021-7.

Brignole C, Marimpietri D, Pastorino F, Di Paolo D, Pagnan G, **Loi M**, Piccardi F, Cilli M, Tradori-Cappai A, Arrigoni G, Pistoia V, Ponzoni M. Anti-IL-10R antibody improves the therapeutic efficacy of targeted liposomal oligonucleotides. J Control Release. 2009 Sep 1; 138(2): 122-7.

Pagnan G, Di Paolo D, Carosio R, Pastorino F, Marimpietri D, Brignole C, Pezzolo A, **Loi M**, Galietta LJ, Piccardi F, Cilli M, Nico B, Ribatti D, Pistoia V, Ponzoni M. The combined therapeutic effects of bortezomib and fenretinide on neuroblastoma cells involve endoplasmic reticulum stress response. Clin Cancer Res. 2009 Feb 15; 15(4): 1199-209.

Pastorino F, Di Paolo D, Piccardi F, Nico B, Ribatti D, Daga A, Baio G, Neumaier CE, Brignole C, **Loi M**, Marimpietri D, Pagnan G, Cilli M, Lepekhin EA, Garde SV, Longhi R, Corti A, Allen TM, Wu JJ, Ponzoni M. Enhanced antitumor efficacy of clinical-grade vasculature-targeted liposomal doxorubicin. Clin Cancer Res. 2008 Nov 15; 14(22): 7320-9.

Di Paolo D, Pastorino F, Brignole C, Marimpietri D, **Loi M**, Ponzoni M, Pagnan G. Drug delivery systems: application of liposomal anti-tumor agents to neuroectodermal cancer treatment. Tumori. 2008 Mar-Apr; 94(2): 246-53.

Pisano M, Pagnan G, **Loi M**, Mura ME, Tilocca MG, Palmieri G, Fabbri D, Dettori MA, Delogu G, Ponzoni M, Rozzo C. Antiproliferative and pro-apoptotic activity of eugenol-related biphenyls on malignant melanoma cells. Mol Cancer. 2007 Jan 18;6:8.